Biofouling and cleaning of Microchannels

by

J.Ponmozhi

Dissertation submitted to

UNIVERSIDADE DO PORTO

For the degree of Doctor in Chemical and Biological Engineering

Supervised by:

Dr. João Mario Miranda

Co-Supervised by:

Prof. João M. Campos

Prof. Filipe Mergulhão

Universidade do Porto

Faculdade de Engenharia

FEUP

Centro de Estudos de Fenómenos de Transporte

Departmento de Engenharia Química

Faculdade de Engenharia da Universidade do Porto

Portugal

January, 2016

FCT Fundação para a Ciência e a Tecnologia

MINISTÉRIO DA EDUCAÇÃO E CIÊNCIA

Abstract

Biofouling in microdevices is not as visible as biofouling seen in macroscale scale devices. There is a necessity to monitor and amplify the microscopic events that human eye cannot see, into the visual scale, in order to have an efficient and continuous functioning of the microdevices. The main objective of the present thesis is to investigate the biofouling in microchannels, with emphasis on the initial adhesion step. A cell suspension of *Escherichia coli* flows through the microchannel and cell adhesion is monitored by visualization along the experiment. The channels used comprise a set of diverse designs, from simple rectangular straight microchannels, to microchannels with multiple constrictions, all belonging to different microfluidic devices. The flow parameters and temperature used for the biofouling study mimic real human body *in vivo* conditions.

The microchannels used in the experiments were produced in polydimethylsiloxane (PDMS) polymer by soft lithography technique using molds manufactured by two methods, namely xurography and photolithography (SU-8 molds). A new in-house technique was developed to enable the insertion of a polymeric surface into one of the walls of the microchannel. The developed technique has a simple protocol to follow, without the need for costly apparatus and also without any constrain in the fabrication process. The adhesion of *E. coli* over the inserted bottom wall surface was visualized through the microscope and the images captured at different time intervals were processed in order to find the adhesion rate.

Experiments on biofouling to understand initial adhesion phenomenon were carried following three guiding vectors: 1- range of wall shear stresses that occur in the human body; 2 - different biomedical polymer surfaces; 3 - microchannel geometries incorporating constrictions as the main hot spot adhesion region. A small region of interest, out of the whole length of the microchannel, was monitored to find the adhesion rate for a particular wall shear stress, surface or geometry. Biofouling on six different polymeric surfaces were studied along with glass (used as reference) surface for two different shear stresses to correlate the adhesion rate with surface properties (hydrophobicity and zeta potential). The adhesion rates on polymeric surfaces on micro and macro scales were compared. When similar wall shear stresses are used in both scales, similar adhesion rates are obtained whatever the surface

enabling the use of different scales for adhesion tests, depending on expertise and equipment availability. In the adhesion studies on different microchannel geometries, the whole length of the microchannel was analyzed to quantify the adhesion before, in and after the constriction regions. The results obtained were stimulating and they can be applied in different microfluidic devices and application fields.

The cleaning of microchannels with the help of antibiotics was also investigated. The conjugate effects of wall shear stress and antibiotics contribute to the removal of adhered cells. Data on dead and live cells removed using antibiotics were obtained.

To clarify the stability and predictability of the flow patterns near the observation region, numerical simulations were made with the commercial code ANSYS Fluent CFD package (version 14.5) by solving Navier–Stokes equations. In straight channels, the wall shear stress was found to be constant along the flow direction. With the new in-house technique developed to incorporate the polymer patch in the microchannel, a lowered surface is attained near the region of interest. In this region, the wall shear stress suffers a small transition, which the experimental results demonstrate to have a negligible effect on adhesion.

Keywords: Cell adhesion; Biofouling; Biomedical coatings; Biomicrofabrication; Computational fluid dynamics; Microfluidics; *Escherichia. Coli*; Antibiotic cleaning; Constrictions; Multiple constrictions channel; Converging channel; Biofouling hot spots

Resumo

A incrustação biológica em microdispositivos não é tão visível como visto a incrustação biológica em dispositivos escala macro-escala. Há uma necessidade de monitorar e amplificar os eventos microscópicos que o olho humano não pode ver, na escala visual, a fim de ter um funcionamento eficiente e contínua dos microdispositivos. O principal objetivo do presente trabalho é investigar o estágio inicial do processo de formação de biofilmes, a adesão inicial de bactérias a superficies, em microcanais. Durante as experiências, de adesão inicial de bactérias realizadas uma suspensão de células de *Escherichia coli* flui através do microcanal e a adesão de bactérias é monitorizada através da visualização por microscopia. Foram estudados vários designs de canais, em diferentes dispositivos microfluídicos, desde canais reactangulares simples a canais com múltiplas constrições. Os parâmetros de escoamento e temperatura utilizadas para o estudo foram seleccionados para mimetizar as condições *in vivo* do corpo humano.

Os microcanais utilizados nas experiências foram produzidas em polidimetilsiloxano (PDMS) por litrografia suave a partir de moldes fabricados por dois métodos alternativos, nomeadamente a fotolitografia (moldes de SU-8) e a xurografia. Uma nova técnica de fabricação de microcanais foi desenvolvida para permitir a inserção de uma superfície polimérica numa das paredes do microcanal. Foi desenvolvido um protocolo simples de seguir, sem a necessidade de equipamentos dispendiosos. A adesão de E. coli à superfície inserida foi visualizada através do microscópio e as imagens captadas ao longo do tempo foram processadas para determinar a taxa de adesão em diferentes materiais.

As experiências para compreender fenómeno de adesão inicial foram realizados de acordo com três linhas orientadoras: 1- a gama de tensões de corte na parede foi selecionada para ser idêntica à que ocorre no corpo humano; 2 – os materiais selecionados foram consideradas superfícies de polímeros com aplicação biomédica; 3 – as geometrias estudadas têm relevância para microdispositivos de análises clínicas.. Duante as experiências, uma pequena região do microcanal foi monitorizada para determinar a taxa de adesão para cada taxa de corte, geometria ou superfície. A adesão em vidro (referência) e em seis superfícies poliméricas diferentes foi estudada para duas taxas de corte diferentes com o objectivo de tentar correlacionar a taxa de

adesão com as propriedades das superfícies (hidrofobicidade e potenciais zeta). As taxas de adesão em superfícies poliméricas à micro e à macro escalas foram comparadas. Quando são usadas tensões de corte na parede semelhantes em ambas as escalas, são obstidas taxas de adesão semelhantes, qualquer que seja a superfície. Este resultado sugere que as experiências de adesão inicial podem ser feitas a qualquer das escalas estudadas, sendo que a escolha do procedimento experimental e da escala utilizada depende da experiência da equipa de investigação e da disponibilidade de equipamento. Nos estudos de adesão em diferentes geometrias, foi determinada a adesão ao longo do microcanal sendo possível identificar o efeito de constrições e variação da secção recta do canal. Os resultados obtidos são estimulantes e eles podem ser aplicados em diferentes microdispositivos e campos de aplicação.

A limpeza de microcanais com o auxílio de antibióticos também foi investigada. Os efeitos conjugados de tensão de corte e antibióticos contribuem para a remoção de células aderentes.

Para esclarecer a estabilidade e previsibilidade dos padrões de escoamento junto da região de observação, foram feitas simulações numéricas com o código comercial ANSYS Fluent (versão 14.5), o qual resolve as equações de Navier-Stokes. Em canais simples, de secção recta constante, a tensão de corte de corte é constante ao longo da direcção do escoamento. Com a nova técnica in-house desenvolvido para incorporar uma superfície polimérica no microcanal, forma-se uma região rebaixada na vizinhança da região de interesse. Nesta região, a tensão de corte na parede sofre um pequeno decréscimo, que os resultados experimentais demonstram que têm um efeito desprezável sobre a adesão celular.

Palavras-chave: Adesão celular; Biosujamento biológico; Biomicrofabricação; Mecânica dos Fluidos Computacional; Microfluidica; *Escherichia. Coli;* Limpeza por antibiotico; Constrições; Canal com multiplas constrições; Canal convergente; Biosujamento em pontos críticos.

To My life partner Shanmugam Dhinakaran, and Kids D.Ganesh and D. Shanmugam who always helped me, in every aspect of life.

Acknowledgements

This thesis is the result of the plentiful knowledge acquired in FEUP, Portugal, specifically in CEFT laboratory, where I spent most of the time seeing the *E. coli* through a microscope for hours. My experience at FEUP has been nothing short of learning amazing technical aspects in microfluidics. I would like to express my sincere gratitude to everyone who I have encountered these years during the progress and completion of this thesis.

First and foremost I wish to thank my supervisor, Professor **João Mario Miranda** for his ideas, guidance and immense academical support through the rough road to finish this thesis. He is humble, honest and has flexible attitude towards new initial ideas in research. With deep gratitude, I acknowledge the great debt I owe to him, whose valuable guidance and constructive criticism has always helped me in shaping my experimental work. He encouraged me with enthusiasm, to stay in the lab throughout the research period, with the freedom I needed to move on. He listened carefully to what I said and gave me constructive comments. He is a splendid Professor who inspired me in many ways and combines the role of the supervisor along with being the mentor.

I wish to give special thanks to Professor **João M. Campos** head of Centro de Estudos de Fenómenos de Transporte **(**CEFT) group because he was the sole reason to be here in FEUP doing this research work, as he selected me for this research topic. He is fair and open and mostly accessible in and around to all my academic and research needs and queries and I got all my e-mails answered. His physical insight guidance, generous support and encouragement have been the impetus for me to keep working hard to succeed.

I would like to express a great deal of appreciation for my third supervisor Prof. **Filipe Mergulhão** for his amazing source of support in planning the work, giving me clear work instructions, praising me whenever I deserve it, motivating me in gaining technical knowledge and making me to acquire consistent standards of performance in research work. He is a humble, non-struck up Professor while

understanding my experimental problems and giving appropriate and valuable suggestions to proceed. He advised his students in providing the cell suspension assay whenever I needed and because of this help, I could conduct numerous trials in the lab to finish my truly interesting work.

All the three professors were accessible, read my work quickly, made sensible comments and inspired me to write. They have proven to be very considerate and patient advisors, who served as a role model for professional excellence and integrity. I adore all my three supervisors, who will be reflected in my nature through out my life in terms of teaching, guiding and dealing with scientific ideas.

A special thanks to my friend and colleague **Erica Doutel**. We began to be friends ever since we began to share an office in 2011. Erica is an amazing person in too many ways. I would like to thank Joana Moreira for her enthusiasm, intensity and willingness to do frequent *E. coli* assay preparations for my whole research work. I almost visualized everyday this *E. coli* produced by her through the microscope flowing in the microchannel and also thank Luciana for providing the samples in Joana's absence.

I would also like to thank my fellow students Patrícia Catarina Saraiva de Sousa, João Carneiro, Samir Sadek, Vera Ribeiro, Joana Cruz, Andreia, Tania and all those in CEFT group who all shared the microfluidics lab space together in a friendly manner.

I would like to thank in silence to my Life partner, my two sons, father, mother, father-in-law, mother-in-law, brother, sister and sister-in-law to make everything work in proper manner for me with their unconditional love. And, behind all of these activities, God was with me and made me to encounter with numerous good people in Portugal (my professors, colleagues, friends, family) in this part of life.

Finally, I would like also to thank to Fundação para a Ciência e a Tecnologia (FCT), Portugal for the financial support through the project PTDC/EQU-FTT/105535/2008 and PEst- OE/EME/UI0532/2013

Table of contents

List of Figures

List of Tables

Nomenclature

Greek

θ_w	Surface contact angle of water
$(\theta_{\alpha-B})$	Surface contact angle for Bromonafthalene
(θ_F)	Surface contact angle for formamide
ρ	Density
τ	Shear stress
τ_{ls}	Shear stress of lowered surface
τ_w	Shear stress at the wall
μ	Viscosity of the fluid

Acronyms

PDMS	Polydimethylsiloxane
PA	Polyamide
PLLA	Poly-l-lactide acid
PS	Polystyrene
PEO	Polyethylene oxide
PEI	Polyethyleneimine
POC	Point of care
MEMS	Microeletromechanical systems
LOC	Lab-on-a-chip
DCM	Dichloromethane

Roman

Re	Reynolds number
x, y, z	Cartesian coordinates
Q	flow rate

L_e	Entrance length
L_c	Constriction length
L_{in}	Length of the inlet section
L_{out}	Length of outlet section
H	Height of the microchannel
H_{ls}	Height of the lowered surface
L_w	Length of the wide section of the multiple constriction section.
L_{conv}	Length of the converging channel
W_c	Width of the constriction
W	Width of the microchannel

CHAPTER 1

Introduction

1.1 Background

Biofouling is a general problem found in day-to-day life. Adhesion and growth of microorganisms that can multiply and form colonies and later develop to biofilms have a whole of negative effects from homes to industrial sectors. Biofouling can be easily visualized by naked eye in homes where water is flowing through the pipes and locations exposed to water [1] (kitchen sinks and bathroom drain pipes, showers, strainers, toothbrush bristles, etc.) and in human body on teeth as pictorially represented in Figure 1.1. If these biofilms are not noticed in time they will reduce the draining efficiency of kitchen sink and will affect the tooth with decay causing pain and removal of the teeth. The very first study on biofouling was made on teeth by van Leeuwenhoek [2] in 1684.

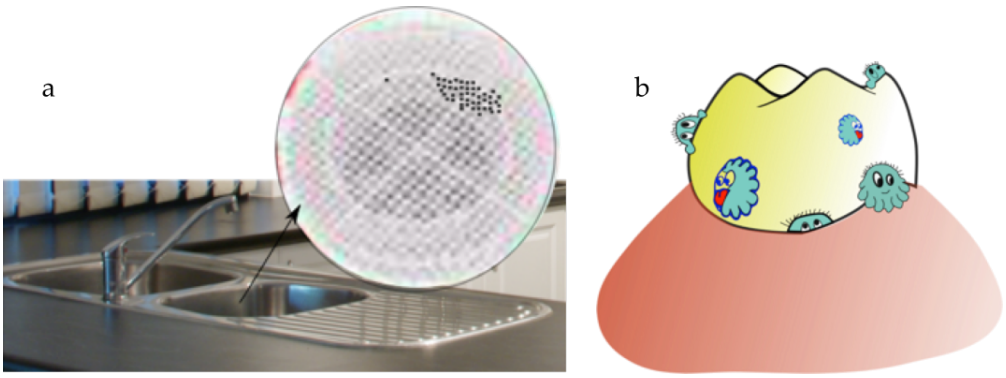

Figure 1.1. Visible biofouling in day-to-day life: (a) Biofouling in kitchen sink; (b) Biofouling in teeth.

Apart from the household fouling, biofouling is responsible for financial losses and health risks as biofouling exist in both macro and micro scale. For instance, industries face many problems due to biofouling [3, 4], such as frictional losses in flow systems, contamination of fluids, reduced efficiency, food contamination, etc. Marine biofouling leads to too much fuel wastage, as ship hull will be fouled with macro sea organisms (macroorganisms such as plant, algae, animals, etc.) along with

biocorrosion as shown in Figure 1.2 (a) [5]. There are cases where microorganisms foul macroscale objects such as heat exchangers Figure 1.2 (b). Considerable funds are spent in industrial and marine sectors due to macroscale biofouling.

Figure 1.2. Macroscale biofouling: (a) Ship hull with macro organisms; (b) Condenser tubes with microorganisms

Microscale biofouling is generally noticed in biomedical field, Point-of-care devices, Lab-on-a-chip devices and modern biosensors. Worst scenarios are encountered in medical field where numerous orthopedic implant [6, 7] removal cases have been reported. Usage of contact lenses develops corneal infection increasing the risk of potential pathogenicity [8]. Catheter-associated urinary tract infections (CA-UTI) [9, 10] leads to heavy damage to kidney or bladder, in many cases. In regard to the medical devices and utilities, biofouling reduces the sensitivity of the equipment and also its lifetime and, contaminates syringe walls [11, 12]. Malfunction of biosensors occurs causing faulty measurements and wastage of the sensors. Biofouling in microdevices are shown in Figure 1.3.

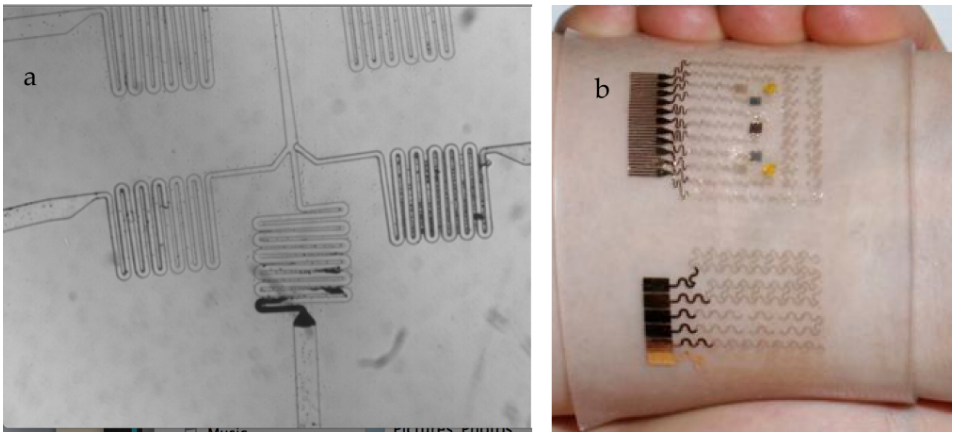

Figure 1.3. Microscale biofouling: (a) Fouled and clogged microchannel used for cell encapsulation (LOC device); (b) Fouled point-of-care device that can both monitor blood glucose levels and deliver medication that reduces high sugar levels.

Several microdevices are used in chemical and biological engineering fields [13]. There is a lack of knowledge of biofouling in microdevices due to the limited studies made; biofouling is visible in these microdevices only with the help of the microscope and not with the naked eye. The microdevices are used for different applications such as: micromixers for multiphase mixing [14] and continuous flow chemical reactors [15], among others.

1.2 Initial adhesion and biofouling

Biofouling ranges from macro-organisms to microorganisms. There are a variety of microorganisms that affects different microstructures and medical devices. The microorganisms responsible for the biofouling and infection of central venous catheters are *Staphylococcus epidermidis, S. aureus, Candida albicans, Pseudomonas aeruginosa, Klebsiella pneumoniae,* and *Enterococcus faecalis* [16, 17]. The microorganisms that are responsible for infecting urinary catheters are *Escherichia coli, Enterococci, P. aeruginosa, K. pneumoniae, C. albicans, Enterobacter, Proteus mirabilis and coagulase-negative Staphylococci* [18, 19].

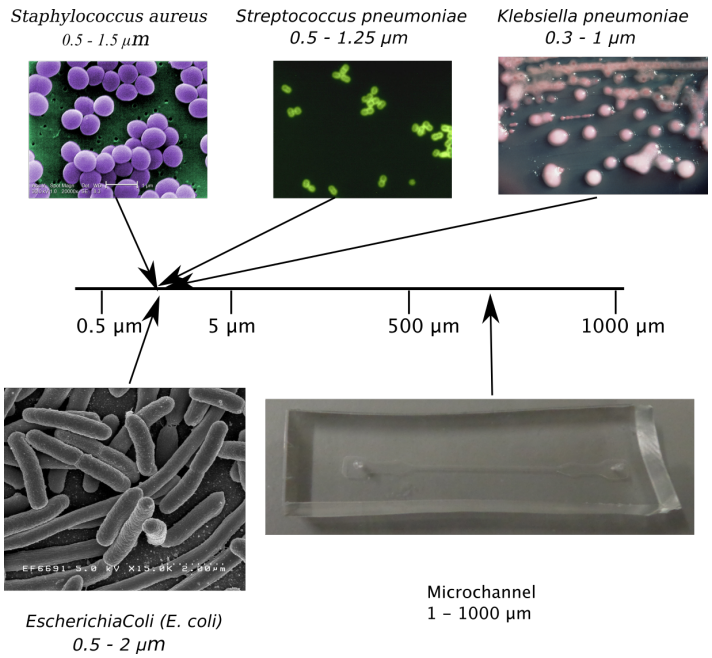

Figure 1.4. Size scale representation of the *E. coli* bacterium and microchannel used for fouling studies in microchannels

Staphylococcus infections are found in orthopedic implants [20]. *Acanthamoeba*, *P. aeruginosa*, *negative staphylococci* are found in contact lenses [8]. These microorganisms are a threat to human health. They enter the infected site from the surrounding skin and other devices nearby. It is almost impossible to completely remove these microorganisms from the device and infected site.

A pictorial representation of the range of dimensions in adhesion in microchannels is shown in Figure 1.4. A microchannel width normally ranges from 1 to 1000 μm and the bacteria that are responsible for human disease are in the range between 0.5 to 5 μm. In the figure, microchannel dimension range and the bacterium that was used for the biofouling study in this thesis are represented.

Biofouling starts with initial adhesion of motile and non-motile microorganisms. Even after adhesion, some migrate due to many factors. Those that are permanently adhered form the base for clusters. Proliferation also occurs to form clusters or colonies. After primary stabilization of individual microorganisms, secondary stabilization continues and slowly clogging and later plugging of microstructure devices occur [21].

Initial adhesion is a stage that occurs prior to biofilm formation. The cells in the surrounding bulk fluid adhere to the substrate depending on the favourable conditions and non-favourable conditions. The favourable conditions are determined by the following parameters: thermal energy; pH [22]; nutrients [23]; density of cells and physiological state of the cells in the surrounding fluid wall, shear stresses (laminar or turbulent regimes) and temperature of the surroundings. The cell surface properties, having fimbriae, flagella and specialized structures [24] (appendages) also affect the adhesion phenomenon. The surface contribution towards adhesion depends on chemical nature of the surface, its hydrophobicity [25] and roughness (in case of macro scale).

1.3. Background and motivation.

1.3.1 Biofouling due to adhesion phenomenon in small size equipment

Biofouling is an important source of losses in medical industry and, in general, in chemical and biological processes in mini and micro-sized equipment such as high throughput screening of catalysts and synthesis of fine chemicals and of biomolecules.

The advantages of small-sized equipment come mainly from the easier prediction and control of fluid flow (often in laminar regime), from its flexibility (distribution of flow in hundreds or thousands of small channels and production parts) and from its large surface area-to-volume ratio. This enhances heat and mass transfer coefficients and, also mixing efficiencies, thereby optimizing heat and mass transfer operations, allowing better control and flexibility of reaction processes and providing higher safety levels in risk-prone processes. On the other hand, these advantageous characteristics also bear important operational problems, a very crucial one being the increased fouling [26]. Therefore, the science of fouling is facing new challenges in these scales, resulting mainly from much lower fouling allowances in the design and operation of mini/micro sized equipment. Even a very thin deposit can cause plugging, severely reducing heat and mass transfer, increasing pressure drop, decreasing the hydraulic diameter and producing secondary flow patterns near the fouled layer. These drawbacks are reasons for the present fouling study.

In the context of adhesion, surface properties play an important role, as they are responsible for the conditions provided for initial attachment and subsequent development of the fouling layer. To have a strong antifouling outcome, different surfaces and even modified surfaces were developed [27-29] and studied. However, some questions are still without adequate answer:

a. What is the effect to fouling of constrictions, which are associated with a sudden change in the wall shear stress (WSS)?

b. Does fouling depend on the scale on which it operates viz. micro scale and macro scales?
c. If the deposits are thick, will it be easier, or more difficult, to clean them?

So far, many types of measures were developed to combat biofilms, like using antibiotics to kill or using modified surfaces to inhibit initial adhesion of cells. The process of biofilm formation starts with initial adhesion [30]. If there is clear understanding of the initial adhesion mechanism, biomaterials that are less colonized by bacteria can be developed by material science engineers and researchers [31]. So there arises a need to quantify and understand the initial adhesion phenomenon over different surfaces with respect to time.

In the last few years there has been a large improvement in the optical techniques to measure velocity profiles, record the initial adhesion and biofilm formation by monitoring them online. So, optical techniques can be relied on as capable tools to study the fouling phenomena.

1.3.2 Advantages of microfluidics

Microfluidics is a versatile multidisciplinary field that is attractive for a wide range of applications [32]. Pertaining to the advantages of microfluidics made use in initial adhesion studies, they are remarkable. The study made with microfluidics for the initial adhesion is almost the same as the study made for biofilm development where the biofilm formation platform is continuously monitored to know the response of *C. albicans* and *P. pastoris* biofilms to different shear stress conditions [33]. It is possible to have a real time monitoring in a hydrodynamic environment in high throughput devices in chemical and biological engineering fields. It is also possible to mimic the human *in vivo* condition. With the automation of the microfluidic devices, it is possible to have good repeatability and reproducibility with increased selectivity and sensitivity in the experiments when compared to their macro counterparts.

The microfluidic devices can be manufactured with fine details applying developed microfabrication techniques and in an inexpensive way applying xurography microfabrication method. The microfabrication techniques that developed in 1980's has driven MicroElectroMechanical Systems (MEMS) that has more commercial values in mechanical, chemical, biomedical domains [34-36], supports other domains such as Automotive (active suspension, vehicle security systems, automatic door locks), Space exploration field (pressure sensors, micro-power sources and turbines), etc. Xurography introduced by Bartholomeusz et al. [37] can produce the micromolds, bypassing the expensive photolithography technique for areas where precision in microchannels construction is not required. With the help of the microfabrication techniques, the microchannel width with respect to the bacterium characteristic dimension can be easily manipulated. Very small volumes of reagents are enough, since surface effects are dominating over volume effects in the biofouling study. Due to the compact size of the microchannel, the inertial forces become negligible and the viscous force is prevalent resulting in low Reynolds numbers. At same hydrodynamic conditions, microchannels encounters low Reynolds number while turbulent flows are often encountered in macro flow systems.

The real time monitoring is made with transparent microchannel; the monitoring was made at the same location for a period of time and also scanned through out the length of the channel. A range of shear stress can be used in a microfluidic-closed system, where outside disturbances and infections could be avoided making it beneficial for initial adhesion study. The temperature of the very small flow volumes assays can be maintained at the in vivo body temperature.

The advantages of microfluidics pertaining to the initial biofouling study implemented in this thesis are listed in Figure 1.5. The microfluidic approach developed in this thesis has the capacity further elucidate the so far unknown mechanism of adhesion, which would surely subsides fouling related problems in many fields.

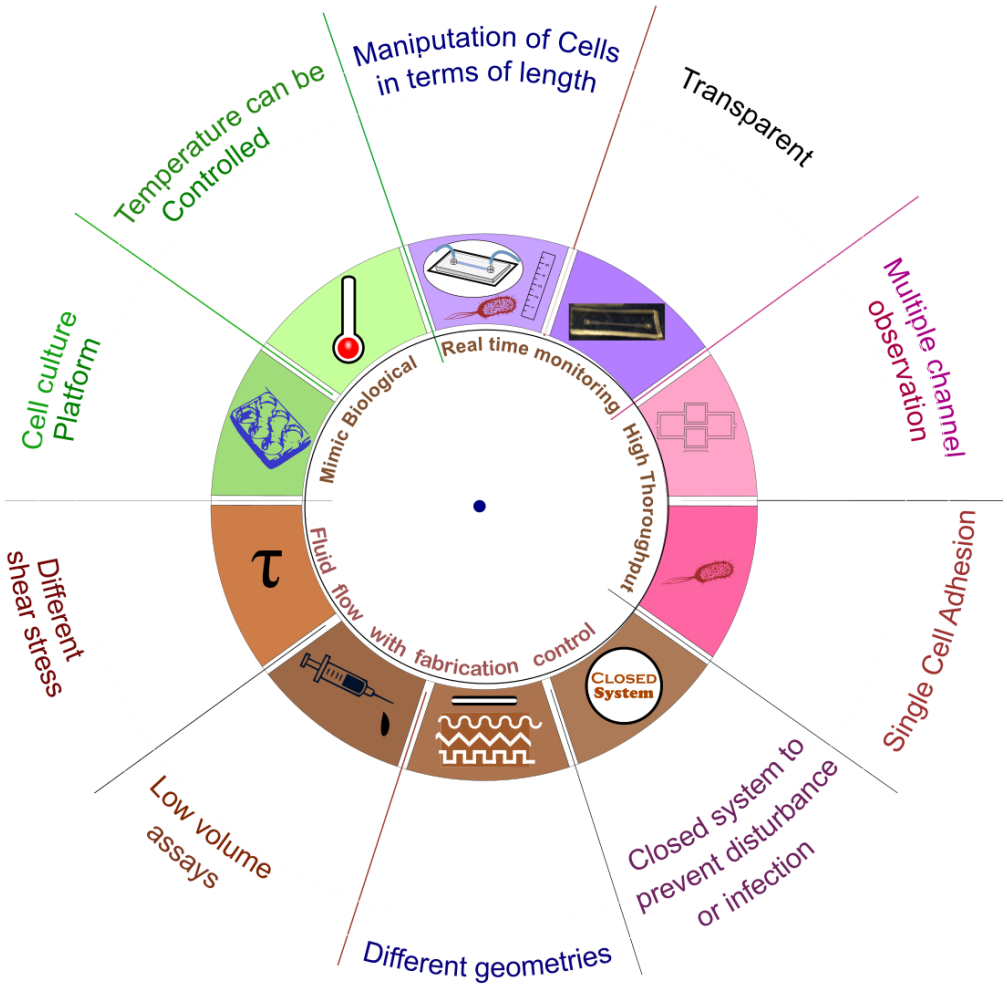

Figure 1.5. Advantages if microfluidics related to initial adhesion

1.4 Objectives

The biofouling study is made in a microscale basically for creating new research tools for determining the efficiency of developing and developed microscale biomedical devices. The main objectives of this thesis are summarised as follows:

a. Develop a microfluidic set up that could mimic the biomedical scenario based on *in vivo* temperature and wall shear stress;
b. Analyse, establish and finalize different polymers, with biomedical applications, to be used as microchannel walls, based on their durability, spincoatability and ease of fabrication;

c. Develop fabrication methods to produce microchannels with polymeric walls, adequate for adhesion research in polymers with biomedical applications;
d. Perform an initial adhesion study, to understand the biofouling phenomenon that happens *in vivo* implant surfaces or catheters, lab-on-chips (LOC) and point of care diagnostics (POC) microfluidic systems;
e. In all the microscale equipment (POC, LOC, etc.) constrictions are the hot spot zones where blockage occurs due to biofouling. Different geometries will be developed, compared, analysed and the adhesion results will be identified taking in account their relevance in different biomedical applications;
f. Analyse the difference between micro and macro scales adhesion with different polymeric surfaces that are commonly employed in biomedical devices. Compare the difference in the results obtained between micro and macro scales platforms to determine whether the dimensions of the real systems do not need to be mimicked and the experiments can be performed either at the micro as at the macro scales;
g. Investigate the cleaning phenomenon of fouled microchannels by antibiotics as an aid the shear stress cleaning.

1.5. Methods

The biofouling study was made in PDMS microchannels with very small volume of *E. coli* suspension, which was prepared with overnight cell cultures by conventional microbiology methods. The polymeric surfaces were prepared in-house with well-established methods, available in the literature, and they were characterized through hydrophobicity studies, before and after the biofouling experiment, to test the durability of their properties. A Zeta potential study was also made to characterize the polymer and the *E. coli* cell property surfaces. The biofouling study was made varying different parameters: wall shear stress, surface properties, geometries with and without constrictions, along with comparison of biofouling in micro and macro scales. The cleaning of biofouled microchannels was done with two antibiotics to understand its killing and removal properties.

The images of the biofouling process during the experiments (30 minutes) were used for counting adhered *E. coli* on the bottom wall of the microchannel. Through out the thesis work, all the initial adhesion studies were carried out at human body temperature of 37 °C and for a time period of 30 mins.

The experimental methods, necessary for the biofouling study, microfabrication and microscopy methods, were available in our research group, Centro de Estudos de Fenómenos de Transporte (CEFT). Microbiology methods for preparing the cell culture and surface characterization methods were available in Laboratório de Processos de Engenharia, Ambiente, Biotecnologia e Energia (LEPABE) group. With the facilities available (CEFT), xurography technique was used to prepare microchannels for certain experiments. A new in-house method was developed for obtaining a polymeric wall in the microchannel. The SU-8 molds were purchased.

1.5.1 Microfabrication methods

Microchannels were produced in CEFT laboratory with the help of soft lithography technique. SU-8 molds, produced by photolithography process were purchased and used for producing microchannels.

Molds were prepared by xurography, which is a novel and rapid technique recently introduced for producing microchannels in different films. A normal cutter plotter was used for making negative features of a microchannel of 100 μm in films that could be easily transported on to a Petridish with a transport sheet, as the cutter plotter can cut films with thickness ranging from 25 to 1000 μm [37]. The films used for the molds are normal adhesive vinyl films that are used in sign industry for cutting graphics [38]. Major reasons for choosing xurography technique are:

- Easy to produce microchannels with molds prepared from adhesive vinyl films of different geometries in a very short time;
- The whole mold production can be recreated if the adhesion experiments need design changes.
- It does not have any time consuming process using chemicals for mold production as photolithographic process;

- The production cost is inexpressible, making it extremely fit for any basic and infant research operation study.

The few disadvantages that can be overlooked for basic research are the resolution, it is not as high as in the standard lithographic techniques, and only the materials cut by the cutter blade can be used for making microchannels.

A new in-house microfabrication technique to insert a polymeric wall in the microchannel was developed in the present thesis.

1.5.2 Microbiology methods

E. coli was prepared in LEPABE group following conventional microbiology methods for culture preparation. This strain was used because it had already demonstrated a good biofilm formation capacity [39].

1.5.3 Microscopy

The adhesion of *E. coli* was monitored using a fluorescence inverted microscope, along 30 minutes. The images were captured with a CCD camera in consecutive time intervals. The captured images were used for counting the adhered cells. All the microchannels produced were transparent, one of the criteria in developing microchannels by different techniques in the laboratory. The images captured were stored in tiff format by Leica application suite software. The images stored were processed and the number of *E. coli* cells was counted with Image J software, a versatile tool for quantifying the fouling.

1.5.4 Characterization of materials and cells

The prepared polymeric surfaces were characterized for hydrophobicity, durability (adherence to the channel wall throughout the biofouling study) and zeta potential, with the facilities available in LEPABE laboratory. The hydrophobicity was determined by the contact angle between the surface and polar and apolar liquid drops.

The contact angles were determined automatically by the sessile drop method in a contact angle meter. The surface charges of the polymers and of the *E. coli* were characterized through the zeta potential.

1.5.5 Computational Fluid Dynamics (CFD)

The flow in the microchannel was simulated by numerical methods to clarify the stability and predictability of the flow patterns near the observation region. The main drawback while developing the new in-house technique for insertion of the polymer wall in the microchannel was a lowered surface level of approximately 10 μm. This region was analysed with numerical flow simulation to understand whether this lowered surface affects the WSS and velocity fields. Numerical simulations were made with the commercial code Ansys Fluent CFD package (version 14.5) by solving Navier-stokes equations.

1.6. Summary of the thesis

The thesis is summarised as follows with a brief description along with the pictorial representation Figure 1.6.

The present chapter (Chapter 1) is the introduction and section that provides the overall information about the thesis work and structure.

Chapter 2 is the literature review section, where the literature on the topics relevant to the thesis is reviewed. This chapter is focused on the influence of surface properties, wall shear stress and geometrical configuration on initial adhesion, with particular emphasis on works developed in microfluidic devices.

Chapter 3 is devoted to describe the microchannel fabrication methods. The approaches used to produce the microchannels to study initial adhesion are described. Two types of methods were used to fabricate microchannels in this thesis: soft lithography from SU-8 molds and by combining xurographically-produced molds and

soft lithography. A method was also developed to add a polymer patch to the wall of the channel to be used in adhesion tests of different polymeric surfaces.

Chapter 4 relates the study performed about initial adhesion on different polymeric surfaces. A relation between zeta potential, hydrophobicity and adhesion rate is discussed for different polymeric surfaces. The adhesion rate for a range of wall shear stress, based on applications, is studied for polydimethyl siloxane (PDMS) transparent polymer.

Chapter 5 deals with initial adhesion of cells in different locations of microchannels. Here, initial adhesion is quantified on different types of geometries, trying to understand the effect of geometries on cell adhesion, in particular the effect of wall shear stress changes along the channel. The aim of the study is to find the critical points prone to fouling and clogging in microchannel networks as it is mostly relevant to applications such as Micro Electro-Mechanical Systems (MEMS), Lab on Chip Devices (LOC) and Point of Care Systems (POC).

Chapter 6 is devoted to study one of the cleaning strategies based on wall shear stress and antibiotics. Ampicillin and ciprofloxacin were prepared in LEPABE group. The adhesion process and detachment process were observed for five hours with a Y shaped xurographically-fabricated microchannel. The detaching influence of two antibiotics over the *E. coli* that had adhered at a particular wall shear stress was compared. The wall shear stress is kept constant for both fouling and cleaning mechanisms. Unlike other studies, here fouling and cleaning were observed both during two and a half hours.

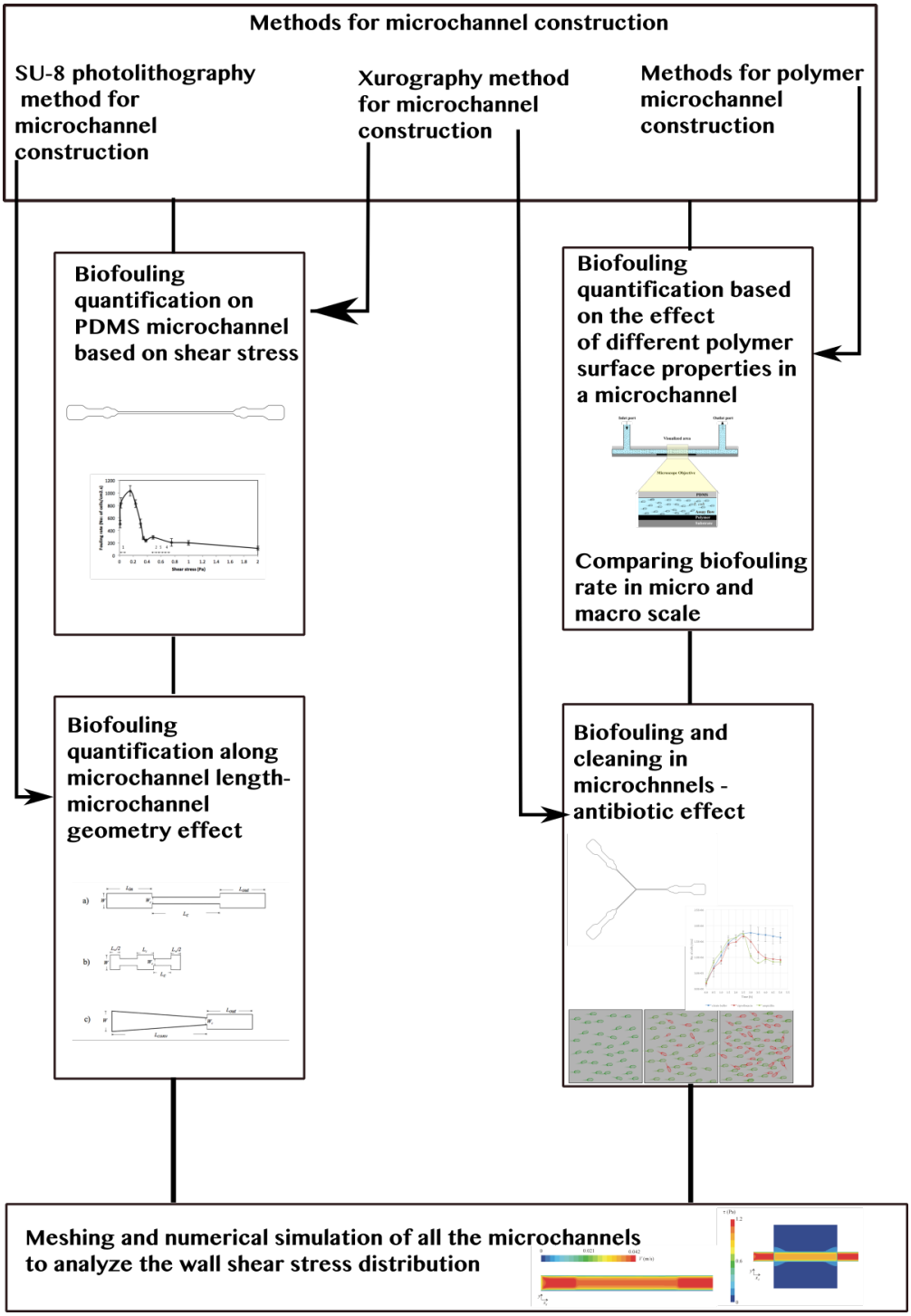

Figure 1.6. Pictorial presentation of the thesis outline.

The principal results of the thesis are summarised in the conclusion chapter (Chapter 7). The future prospective works, regarding this biofouling work, are discussed in the future work chapter (Chapter 8).

References

[1] J. Rayner, R. Veeh, J. Flood, Prevalence of microbial biofilms on selected fresh produce and household surfaces, Int J Food Microbiol, 95 (2004) 29-39.

[2] v.L. A., Microscopical observations about animals in the scurf of the teeth., Philos Trans R Soc Lond B Biol Sci, 14 (1684) 568-574.

[3] S.E. Coetser, T.E. Cloete, Biofouling and biocorrosion in industrial water systems, Critical reviews in microbiology, 31 (2005) 213-232.

[4] T.R. Bott, Industrial Biofouling: Occurrence and Control, Elsevier Science, 2011.

[5] M.E. Callow, J.E. Callow, Marine biofouling: a sticky problem, Biologist (London), 49 (2002) 10-14.

[6] Z. Song, L. Borgwardt, N. Hoiby, H. Wu, T.S. Sorensen, A. Borgwardt, Prosthesis infections after orthopedic joint replacement: the possible role of bacterial biofilms, Orthop Rev (Pavia), 5 (2013) 65-71.

[7] P. Stoodley, G.D. Ehrlich, P.P. Sedghizadeh, L. Hall-Stoodley, M.E. Baratz, D.T. Altman, N.G. Sotereanos, J.W. Costerton, P. Demeo, Orthopaedic biofilm infections, Curr Orthop Pract, 22 (2011) 558-563.

[8] L. McLaughlin-Borlace, F. Stapleton, M. Matheson, J.K. Dart, Bacterial biofilm on contact lenses and lens storage cases in wearers with microbial keratitis, J Appl Microbiol, 84 (1998) 827-838.

[9] G.G. Anderson, J.J. Palermo, J.D. Schilling, R. Roth, J. Heuser, S.J. Hultgren, Intracellular bacterial biofilm-like pods in urinary tract infections, Science, 301 (2003) 105-107.

[10] S. Saint, C.E. Chenoweth, Biofilms and catheter-associated urinary tract infections, Infect Dis Clin North Am, 17 (2003) 411-432.

[11] D. Mack, H. Rohde, L.G. Harris, A.P. Davies, M.A. Horstkotte, J.K. Knobloch, Biofilm formation in medical device-related infection, Int J Artif Organs, 29 (2006) 343-359.

[12] R.M. Donlan, Biofilms and device-associated infections, Emerg Infect Dis, 7 (2001) 277-281.

[13] M. Schoenitz, L. Grundemann, W. Augustin, S. Scholl, Fouling in microstructured devices: a review, Chem Commun (Camb), 51 (2015) 8213-8228.

[14] V. Hessel, H. Lowe, F. Schonfeld, Micromixers - a review on passive and active mixing principles, Chemical Engineering Science, 60 (2005) 2479-2501.

[15] C. Erbacher, F.G. Bessoth, M. Busch, E. Verpoorte, A. Manz, Towards integrated continuous-flow chemical reactors, Mikrochimica Acta, 131 (1999) 19-24.

[16] C. Jeske, C. Raedler, A. von Goedecke, A. Mayr, G. Hinterberger, C. Aspoeck, C. Lass-Floerl, A. Benzer, Early identification of bacteria leading to central venous catheter contamination, Anesth Analg, 97 (2003) 940-943, table of contents.

[17] C.G. Esmanhoto, M. Taminato, D.S. Fram, A.G.S. Belasco, D.A. Barbosa, Microorganisms isolated from patients on hemodialysis by central venous catheter and related clinical evolution, Acta Paulista De Enfermagem, 26 (2013) 413-420.

[18] J.C. Nickel, J.W. Costerton, Bacterial biofilms and catheters: A key to understanding bacterial strategies in catheter-associated urinary tract infection, Can J Infect Dis, 3 (1992) 261-267.

[19] M.A.R. Amalaradjou, K. Venkitanarayanan, Role of bacterial biofilms in catheter-associated urinary tract infections (CAUTI) and strategies for their control, Recent Advances in the Field of Urinary Tract Infections, InTech, Rijeka, (2013) 1-31.

[20] A. Trampuz, A.F. Widmer, Infections associated with orthopedic implants, Curr Opin Infect Dis, 19 (2006) 349-356.

[21] T. Bjarnsholt, The role of bacterial biofilms in chronic infections, APMIS, 121 (2013) 1-58.

[22] K.G. Beaumont, M. Mrksich, The mechanostability of isolated focal adhesions is strongly dependent on pH, Chem Biol, 19 (2012) 711-720.

[23] B.A. Cowell, M.D. Willcox, B. Herbert, R.P. Schneider, Effect of nutrient limitation on adhesion characteristics of Pseudomonas aeruginosa, J Appl Microbiol, 86 (1999) 944-954.

[24] S. Kleta, M. Nordhoff, K. Tedin, L.H. Wieler, R. Kolenda, S. Oswald, T.A. Oelschlaeger, W. Bleiß, P. Schierack, Role of F1C Fimbriae, Flagella, and Secreted Bacterial Components in the Inhibitory Effect of Probiotic Escherichia coli Nissle 1917 on Atypical Enteropathogenic E. coli Infection, Infection and Immunity, 82 (2014) 1801-1812.

[25] M.C. van Loosdrecht, J. Lyklema, W. Norde, G. Schraa, A.J. Zehnder, The role of bacterial cell wall hydrophobicity in adhesion, Appl Environ Microbiol, 53 (1987) 1893-1897.

[26] M. R., When microfluidic devices go bad. How does fouling occur in microfluidic devices, and what can be done about it?, Anal Chem., 77 (2005) 429A-432A.

[27] F. Zhou, Antifouling Surfaces and Materials: From Land to Marine Environment, Springer Berlin Heidelberg, 2014.

[28] K.L. Mittal, Polymer Surface Modification: Relevance to Adhesion, Taylor & Francis, 2009.

[29] J.L. Dalsin, P.B. Messersmith, Bioinspired antifouling polymers, Materials Today, 8 (2005) 38-46.

[30] N.I. Abu-Lail, H. Beyenal, Chapter 5.2 - Characterization of Bacteria–Biomaterial Interactions, from a Single Cell to Biofilms, in: A. Bandyopadhyay, S. Bose (Eds.) Characterization of Biomaterials, Academic Press, Oxford, 2013, pp. 207-253.

[31] A.K. Dillow, M. Tirrell, Targeted cellular adhesion at biomaterial interfaces, Current Opinion in Solid State and Materials Science, 3 (1998) 252-259.

[32] A.M. Streets, Y. Huang, Chip in a lab: Microfluidics for next generation life science research, Biomicrofluidics, 7 (2013) 011302.

[33] L. Richter, C. Stepper, A. Mak, A. Reinthaler, R. Heer, M. Kast, H. Bruckl, P. Ertl, Development of a microfluidic biochip for online monitoring of fungal biofilm dynamics, Lab Chip, 7 (2007) 1723-1731.

[34] R. Zaouk, B. Park, M. Madou, Introduction to Microfabrication Techniques, in: S. Minteer (Ed.) Microfluidic Techniques, Humana Press, 2006, pp. 5-15.

[35] S.J.J. Lee, N. Sundararajan, Microfabrication for Microfluidics, Artech House, 2010.

[36] D. Qin, Y. Xia, J.A. Rogers, R.J. Jackman, X.-M. Zhao, G.M. Whitesides, Microfabrication, microstructures and microsystems, in: Microsystem technology in chemistry and life science, Springer, 1998, pp. 1-20.

[37] D.A. Bartholomeusz, R.W. Boutte, J.D. Andrade, Xurography: rapid prototyping of microstructures using a cutting plotter, Journal of Microelectromechanical Systems, 14 (2005) 1364-1374.

[38] P.P. de Santana, I.M.F. de Oliveira, E. Piccin, Evaluation of using xurography as a new technique for the fabrication of disposable gold electrodes with highly reproducible areas, Electrochemistry Communications, 16 (2012) 96-99.

[39] J.S. Teodosio, M. Simoes, L.F. Melo, F.J. Mergulhao, Flow cell hydrodynamics and their effects on *E. coli* biofilm formation under different nutrient conditions and turbulent flow, Biofouling, 27 (2011) 1-11.

CHAPTER 2

State of the art

Abstract

Persistent chronic infections develop in competition with acute infections, most of the times, due to the development of biofilms, which are resilient to numerous infection regulation practices, just like antibiotics and vaccines. When trying to analyse the root cause of any infection, there is a need to understand the formation of biofilms through initial adhesion mechanisms [1]. This comprehension will help, in the future, the restoring of any surface without chronic infection or non-removable biofilms. A firm attachment between cells or any microorganism to a biomedical surface, either to maintain the mechanical integrity of the tissue or to infect the surface, is known as adhesion. If the adhesion is unwanted we will address it as fouling. The root cause for any infection or microdevice failure starts with initial adhesion of single cells on to the surface, so this review was done to identify the so far available studies about initial adhesion in biofilms. The relevance of geometry, surface material and wall shear stresses are going to be highlighted. This review will contribute to the scientific community in understanding the studies made so far on biofouling phenomenon occurring on surfaces of implants or microdevices with the available and recently developed new techniques.

In spite of the large amount of research carried out on biofilms formation, this review focuses on microfluidic platforms where, until now, it is not clear, the reason for the accumulation of cells on infected spots.

2.1 Introduction

The term ‘biofilm’ was coined in 1981 [2] and refers to an assemblage of microbial cells, which are irreversibly associated with a surface, and enclosed in a self-produced

exopolymeric matrix mainly composed of polysaccharide material [3]. Biofilm formation starts with cell adhesion to a pre-conditioned surface. The development of biofilms in medical devices is a common problem, which can lead to hospitalization, revision surgery or mortality.

Recent reviews provide a source of evidence to the undesirable biofilm formation in medical devices [4-10] as shown in Figure 2.1. These biofilms pose a challenge to the health care community. Currently, there is a spurring development of smart polymers that are used for coating biomedical implants, artificial organs, lab on chip surfaces, implantable drug delivery systems [11], in order to reduce biofouling. They will give way for the development of a next generation of biomedical devices, which are less prone to fouling.

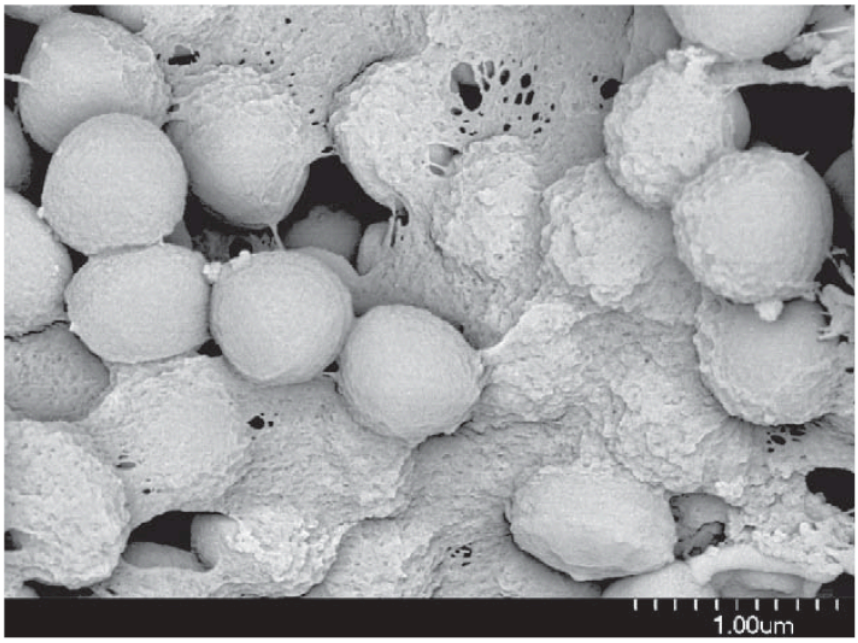

Figure 2.1. Scanning Electron Microscopic image of a staphylococcal biofilm [5]

Initial adhesion is a largely unexplored research area, since full-formed biofilms have been attracting most of the researchers. The majority of the initial adhesion studies so far are based on different surfaces; different bacterial strains and different environmental conditions and they were performed using different experimental procedures. Only a handful amount of research was done with the help of microfluidic

devices. But keeping in mind the advantages of microfluidics [12] and the need for point-of-care devices (POC), it is expected that more research on biofilms will be carried out on these platforms. There is plenty of scope relating adhesion studies to microfluidic devices, since, in a near future, the likely trend is that every individual will be using POC and lab-on-a-chip (LOC) tools for safety and security reasons.

Cell micro-processing devices have been developed to deal with biological fluids containing cells. Flow cytometry [13] allows for the continuous measurement and discrimination of individual cells flowing across a sensor. Moreover, microdevices have been developed for blood fractionation [14], cell trapping and analysis [15, 16], removal of pathogens from blood [17] and transformation of bacteria using plasmids [18].

2.2 Historical review on adhesion in microchannels

Adhesion of microorganisms exists everywhere, from teeth to ship hulls. This phenomenon just needs a surface and water to materialize. The earliest studies about adhesion of microorganisms were performed at the macroscale, where the event can be visualized by naked eye. Research on macrofouling has received significant funding [19-22], as it was realised that fouling control was very expensive in different scenarios. Research on biofilm formation in smaller (micro) scales has started to develop [23, 24], but studies on initial adhesion in microchannels are scarce. Although initial adhesion and detachment can be studied under a microscope by different means and methods [25] and despite the advantages of microfluidics, the research on initial adhesion in microchannels is still in its infancy.

Earlier in 1995, platelet aggregation in patients with Behcet's disease was studied using silicon microchannels [26]. In order to reduce adhesion, PVC was tested with strains of *Pseudomonas aeruginosa* by Triandafillu et al. [27]. These authors concluded that oxygen plasma treated surfaces yields a hydrophilic surface and reduces the number of adhering bacteria up to 70%. A study on attachment and detachment with four types of living cells namely T47D, U937, CaCo2 and NCTC 2544 was made by Zhang et al. [28] who concluded that applying an optimal range of

wall shear stresses can enhance adhesion. In a microfluidic study, it was concluded that adhesion depends on the shape of the adhering cell/particle [29]. Tousi et al. [30] reported that adhesion does not depend on cell deformation, cell signalling nor heterogeneous distribution of adhesion molecules, but primarily depends on the hemodynamic forces. They made both *in vivo* and *in vitro* studies (with a PDMS based microvascular device) to confirm their findings. In 2012, a numerical study of the lateral migration and deformation of leukocytes in a microchannel was investigated, to open up the possibility of deploying microchannels for deformability-based flow cytometry studies [31]. Recently, in 2013, a study was made to analyse the random motion of mammalian cells in a continuous microchannel, in order to aid in the design of scaffolds for tissue engineering (Young-Gwang et al. [32]). Additionally, Hojin Ha and Sang-Joon Lee [33] studied platelet aggregation and stenosis in a microchannel, whereas Schnegas et al. [34] investigated, by 3D modelling and computational fluid dynamics simulations (CFD), the force required to detach a eukaryotic cell from a microchannel. Other adhesion studies in microfluidic devices, without any analysis of the shear flow field, were made by several researchers [35, 36], which are of less importance to this thesis.

2.3 How do cells adhere?

In a channel, the cells start to flow freely, but depending on the shear stresses field, they progressively transit from free flow to dragging flow or rolling flow to reversible adhesion and then irreversible adhesion. This concept is explained and supported by most of the published studies [37]. However, a recent work by Wang et al. [38] claims that, when the cell size is lower than 1 μm, adhesion is not influenced by the hydrodynamic flow.

In the present thesis, the bacteria used are the Gram negative *Escherichia coli*. The characteristic dimensions of this bacteria range between 1 and 3 μm. In most of the studies addressing biofouling, researchers aimed at developing strategies to inhibit biofilm growth. An alternative strategy consists on delaying initial adhesion so that the onset of a biofilm can be retarded. For this purpose, a lot more information must

be gathered regarding the first phases of biofilm formation and for that purpose it is of paramount importance to monitor the adhesion process from the beginning.

2.4 Current techniques used to observe and quantify initial adhesion

The cell adhesion process was studied by different methodologies [39] since the 1960's. These techniques include:

- Internal reflection techniques [40];
- Total internal reflection microscopy (TIRM) which was initially developed to observe single particles [41];
- Total internal reflection fluorescence microscopy (TIRFM) [42];
- Infrared spectroscopy techniques [43];
- Quartz crystal microbalance analysis [44];
- Centrifugation techniques [45] including measurements based on gravity [46] and other spinning disc techniques [47];
- Cytodetacher technique [48] to measure the detachment forces;
- Atomic force microscopy (AFM) [49].

All of these techniques have their relative advantages and disadvantages but most of them are sophisticated, require a complex experimental set up, and must be applied without any disturbance during the experimental execution.

2.5 Initial adhesion studies based on applied wall shear stresses

Different cell adhesion studies have been performed based on applied shear stress. An interesting study was made by Wesley et al. [50] who captured cells (using a low flowrate of 1μL/min) in a microchannel. They tried to quantify two types of cells, namely, HL-60 and U-937 at a given wall shear stress. A review study was made by Bianchi et al. [51] about leukocyte adhesion on a microchannel surface based on applied wall shear stresses featuring several high-throughput solutions for adhesion

monitoring. A PDMS multi shear microchannel design was used to quantify the cell adhesion on various protein-coated surfaces, varying the applied wall shear stress [52]. Different wall shear stresses in the same microchannel were achieved by varying the width along the length of the microchannel. A large range of wall shear stresses, from 0 to 200 Pa, was achieved with this multi-shear microchannel device. Another study to isolate tumour cells using microsystems was performed with two types of cells (BT-20 and MDA-MB-231) at different flowrates up to 3 ml/min [53]. It was reported that the detachment rate of BT-20 was higher and the attachment rate lower when compared to MDA-MB-231 cells at a constant flowrate of 0.3 ml/min. Further, the cell dynamics of cancer cells in free motion, rolling adhesion and firm adhesion were studied in microchannels [37]. Cheung et al. [54] used epithelial-cell-adhesion-molecule (EpCAM) functionalized microchannels to separate two types of cancer cells, namely breast cancer cells (MDA-MB-231) and prostate cancer cells (PC3N). They concluded that: 1- higher hydrodynamic loading decreased cell adhesion along the channel length; 2 - the distance travelled by the cells before the adhesion is linearly proportional to the rolling velocity; and 3 - the capture efficiency of the cancer cells is smaller for high wall shear stresses. Cell rolling behaviour was monitored in real time for wall shear stresses ranging from 0.05 to 0.3 Pa, in a microsystem that mimics the endothelial microvasculature of a bone marrow [55].

The adhesion and detachment processes of different mutant strains of *P. aeruginosa* [matrix (*pelA*), type I (*cupA 1*), type IV pili (*pilC*) and flagellum defective (*flgK*)] were influenced by the intensity of the applied wall shear stresses. The *pilC* mutation negatively affected bacterial adhesion when wall shear stress was increased [56]. Other works have reported different parameters affecting cellular adhesion such as culture time and surface geometry [57, 58].

2.6 Effects of the surface material on the initial adhesion.

The review on bacterial biofilms by Hall-Stoodley et al. [59, 60] gives a better understanding about biofilms in different surface materials and the need to prevent them. The physicochemical properties of the polymer surface have a strong influence in cell attachment and detachment. Research based on different polymer coatings,

with three medically relevant bacteria, namely, *P. aeruginosa*, *Staphylococcus epidermidis*, and *Staphylococcus aureus,* was made. The results show that cell adhesion can decrease up to 50% according to the type of polymer coating used [61].
In a study in microchannels using three different surfaces, namely SiO_2 uncoated surface and octadecyltrimethoxysilane (OTMS) or N-(triethoxysilylpropyl)-O-polyethylene oxide urethane (TESP) coated on SiO_2, the microchannel with uncoated surface was clogged rapidly due to cell adhesion [62]. The OTMS coated surface had a 75% decrease in the flowrate whereas the TESP coated surface experienced a 20% decrease. Although there are numerous publications addressing cell adhesion in polymeric surfaces [63-65], as shown in Figure 2.2. where adhesion of rat neuronal cells are tested with polyethyleneimine (PEI) biocompatible polymer.
The research on adhesion in polymer surfaces in microchannels is scarce. The reason may be due to the expensive microfabrication techniques and problems associated with cell visualization in these systems.

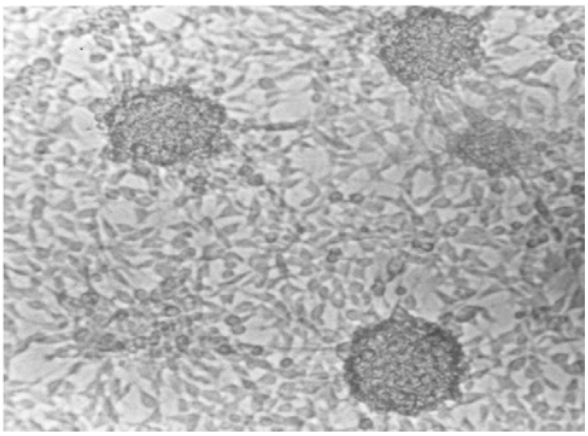

Figure 2.2. Images obtained with an inverted phase contrast microscope of cells (300∗250 μm) cultivated on PEI polymeric films after 90 h. [65]

2.7 Effects of the geometry on the initial adhesion.

The effect of the geometry of the microchannel on the initial adhesion was the least studied topic. The impact of channel geometry is important as outlined in a patent by Manalis et al. [66] using a microchannel to capture diseased blood cells for high throughput diagnosis. Chang et al. [50] attempted to capture particular type of cells (HL-60 and U-937) with the help of different types of microstructures, like pillars arranged in different manners in a microchannel. Two types of pillar structures were

designed to quantify the cells, as shown in Figure 2.1. They reported that the offset pillar structures were able to capture more cells in the first minutes than the square pillar structures. From the third minute on, the capture efficiency was more or less the same for both types of geometries. Liu et al. [57], performed another interesting work with four different microchambers with identical surface area, placed in circle, in a polygon with 8 sides, 12 sides and 16 sides. This study was made to demonstrate that the geometry is responsible for adhesion changes. It was observed that fouling was more effective in complex geometries than in simple geometries. Cox et al. [62] made a cell adhesion test section using hexagonal microstructures to create restricted flows in the microchannels. They studied the flow rate changes over time due to adhesion. Yan et al. [67] fabricated U-shaped microsieves inside a microfluidic chip for the adhesion of tumor cell-targeted microbubbles and breast cancer cells at a wall shear stress of 0.05 Pa. They concluded that accumulation of targeted microbubbles was strongly influenced by flow velocity and that higher retention of microbubbles on cell surfaces was attained at flow velocities lower than 0.03 cm/s.

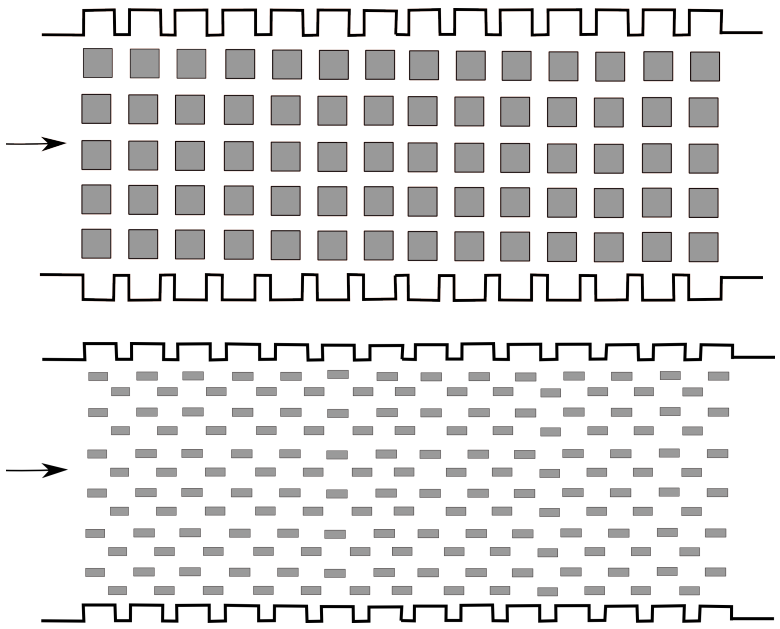

Figure 2.1. Microstructured flow channels, square and offset patterned, for adhesion studies [50].

2.8 Cleaning studies based on antibiotics

Cleaning or removal of cells is essential for chemical and biological engineering applications [68-71]. Until now, there are vague cleaning methods of the unnecessary cells or particles adhered onto a surface. Due to this scenario, the most advantageous lab-on-chip devices cannot be appropriately used by most of the companies. Industrially, the most commonly addressed and understood problem has been the fabrication cost, which was in part solved by Whiteside's work [72-74]. However, PDMS fabrication explained by Whiteside would not reduce the cost when it comes to mass production as PDMS fabrication methods do not scale-up. Another problem has been the fouling in lab-on-chip devices and this remains to be solved [75]. A very recent paper by Schoenitz et al. [76] concluded that particulate flows could be controlled in micro devices, resulting in intensified processes involving solid suspensions. In the present thesis, the cleaning of microchannels using antibiotics is explored.

2.9 Conclusions

The literature on adhesion of cells in micro devices was reviewed taking into account the main topics: wall shear stress effects, surface properties and geometries at the microscale. There are few studies about initial adhesion at the microscale and so there is plenty of scope for these studies. This review gives also relevant information about recent insights. Accordingly, the initial adhesion on microfluidic platforms depends on a variety of chemical and physical parameters, which differ from surface to surface, from geometry to geometry and from flow to flow.

Due to the complexity of the phenomena, any adhesion should be monitored in real time to give more insights according to its own specificity. *In vivo* conditions, where the surface hydrophobicity of the cell changes to a greater extent due to different grown conditions, should be mimicked in microfluidic platforms to get accuracy in the adhesion quantification. The future work is to create microfluidic platforms through which the real environment can be mimicked and the phenomena (adhesion,

cell removal, and cell quantification) monitored in real time. The present thesis tries to contribute to this challenge.

Two important and critical points are the effect of the geometry at the microscale, because different shapes and constrictions are prone to different adhesions, and also to effective cleaning methods. The present thesis focuses in particular on these two themes.

References

[1] M. Saadatian-Elahi, R. Teyssou, P. Vanhems, Staphylococcus aureus, the major pathogen in orthopaedic and cardiac surgical site infections: a literature review, Int J Surg, 6 (2008) 238-245.

[2] W.F. McCoy, J.D. Bryers, J. Robbins, J.W. Costerton, Observations of fouling biofilm formation, Can J Microbiol, 27 (1981) 910-917.

[3] R.M. Donlan, Biofilms: Microbial Life on Surfaces, Emerg Infect Dis, 8 (2002) 881-890.

[4] J.W. Costerton, P.S. Stewart, E.P. Greenberg, Bacterial Biofilms: A Common Cause of Persistent Infections, Science, 284 (1999) 1318-1322.

[5] L.G. Harris, R.G. Richards, Staphylococci and implant surfaces: a review, Injury, 37 Suppl 2 (2006) S3-14.

[6] K.F. Kong, C. Vuong, M. Otto, Staphylococcus quorum sensing in biofilm formation and infection, Int J Med Microbiol, 296 (2006) 133-139.

[7] C.R. Arciola, D. Campoccia, P. Speziale, L. Montanaro, J.W. Costerton, Biofilm formation in Staphylococcus implant infections. A review of molecular mechanisms and implications for biofilm-resistant materials, Biomaterials, 33 (2012) 5967-5982.

[8] T. Bjarnsholt, M. Alhede, M. Alhede, S.R. Eickhardt-Sorensen, C. Moser, M. Kuhl, P.O. Jensen, N. Hoiby, The in vivo biofilm, Trends Microbiol, 21 (2013) 466-474.

[9] A.K. Seth, M.R. Geringer, S.J. Hong, K.P. Leung, T.A. Mustoe, R.D. Galiano, In vivo modeling of biofilm-infected wounds: a review, J Surg Res, 178 (2012) 330-338.

[10] S. Esposito, S.M. Purrello, E. Bonnet, A. Novelli, F. Tripodi, R. Pascale, S. Unal, G. Milkovich, Central venous catheter-related biofilm infections: An up-to-date focus on meticillin-resistant Staphylococcus aureus, Journal of Global Antimicrobial Resistance, 1 (2013) 71-78.

[11] J.C. Middleton, A.J. Tipton, Synthetic biodegradable polymers as orthopedic devices, Biomaterials, 21 (2000) 2335-2346.

[12] D. Li, Encyclopedia of Microfluidics and Nanofluidics, Springer, 2008.

[13] D. Huh, W. Gu, Y. Kamotani, J.B. Grotberg, S. Takayama, Microfluidics for flow cytometric analysis of cells and particles, Physiological measurement, 26 (2005) R73-98.

[14] E. Sollier, M. Cubizolles, Y. Fouillet, J.-L. Achard, Fast and continuous plasma extraction from whole human blood based on expanding cell-free layer devices, Biomed Microdevices, 12 (2010) 485-497.

[15] W.-H. Tan, S. Takeuchi, A trap-and-release integrated microfluidic system for dynamic microarray applications, Proceedings of the National Academy of Sciences, 104 (2007) 1146-1151.

[16] Q. Zhang, L. Zhu, H. Feng, S. Ang, F.S. Chau, W.-T. Liu, Microbial detection in microfluidic devices through dual staining of quantum dots-labeled immunoassay and RNA hybridization, Analytica Chimica Acta, 556 (2006) 171-177.

[17] H.W. Hou, H.Y. Gan, A.A.S. Bhagat, L.D. Li, C.T. Lim, J. Han, A microfluidics approach towards high-throughput pathogen removal from blood using margination, Biomicrofluidics, 6 (2012) 024115.

[18] J. Sha, Y. Wang, J. Wang, L. Ren, Q. Tu, W. Liu, X. Wang, A. Liu, L. Wang, J. Wang, Capillary-composited microfluidic device for heat shock transformation of< i> Escherichia coli</i>, Journal of bioscience and bioengineering, 112 (2011) 373-378.

[19] G. Relini, F. Tixi, M. Relini, G. Torchia, The macrofouling on offshore platforms at Ravenna, International Biodeterioration & Biodegradation, 41 (1998) 41-55.

[20] M.D. Richmond, R. Seed, A review of marine macrofouling communities with special reference to animal fouling, Biofouling, 3 (1991) 151-168.

[21] M. Xu, G. Darrigran, Z. Wang, N. Zhao, C.C. Lin, B. Pan, Experimental study on control of Limnoperna fortunei biofouling in water transfer tunnels, Journal of Hydro-environment Research, 9 (2015) 248-258.

[22] K. Becker, Attachment strength and colonization patterns of two macrofouling species on substrata with different surface tension (in situ studies), Marine Biology, 117 (1993) 301-309.

[23] X. Shi, G. Tal, N.P. Hankins, V. Gitis, Fouling and cleaning of ultrafiltration membranes: A review, Journal of Water Process Engineering, 1 (2014) 121-138.

[24] T.J. Tan, D. Wang, C.I. Moraru, A physicochemical investigation of membrane fouling in cold microfiltration of skim milk, Journal of Dairy Science, 97 (2014) 4759-4771.

[25] D.C. Giliberti, K.A. Anderson, K.C. Dee, A jet impingement investigation of osteoblastic cell adhesion, J Biomed Mater Res, 62 (2002) 422-429.

[26] M. Ikeda, M. Yokogawa, Y. Yamamoto, H. Kodama, 160 Expression of leukocyte adhesion molecules on vascular endothelial cells by xanthoma

tissuemodified low density lipoprotein, Journal of Dermatological Science, 10 (1995) 89.

[27] K. Triandafillu, D. Balazs, B.-O. Aronsson, P. Descouts, P. Tu Quoc, C. van Delden, H. Mathieu, H. Harms, Adhesion of< i> Pseudomonas aeruginosa</i> strains to untreated and oxygen-plasma treated poly (vinyl chloride)(PVC) from endotracheal intubation devices, Biomaterials, 24 (2003) 1507-1518.

[28] X. Zhang, P. Jones, S. Haswell, Attachment and detachment of living cells on modified microchannel surfaces in a microfluidic-based lab-on-a-chip system, Chemical Engineering Journal, 135 (2008) S82-S88.

[29] N. Doshi, B. Prabhakarpandian, A. Rea-Ramsey, K. Pant, S. Sundaram, S. Mitragotri, Flow and adhesion of drug carriers in blood vessels depend on their shape: a study using model synthetic microvascular networks, Journal of Controlled Release, 146 (2010) 196-200.

[30] N. Tousi, B. Wang, K. Pant, M.F. Kiani, B. Prabhakarpandian, Preferential adhesion of leukocytes near bifurcations is endothelium independent, Microvascular Research, 80 (2010) 384-388.

[31] H.Z. Lan, D.B. Khismatullin, A numerical study of the lateral migration and deformation of drops and leukocytes in a rectangular microchannel, International Journal of Multiphase Flow, 47 (2012) 73-84.

[32] Y.G. Ko, C.C. Co, C.C. Ho, Directing cell migration in continuous microchannels by topographical amplification of natural directional persistence, Biomaterials, 34 (2013) 353-360.

[33] H. Ha, S.J. Lee, Hemodynamic features and platelet aggregation in a stenosed microchannel, Microvasc Res, 90 (2013) 96-105.

[34] S. Schnegas, S. Antonyuk, S. Heinrich, 3D modeling and Computational Fluid Dynamics simulations of surface-attached CHO-K1 cells going to detach from a microchannel wall, Powder Technology, 237 (2013) 529-536.

[35] Z.L. Zhang, C. Crozatier, M. Le Berre, Y. Chen, In situ bio-functionalization and cell adhesion in microfluidic devices, Microelectronic Engineering, 78-79 (2005) 556-562.

[36] S. Patel, R.G. Thakar, J. Wong, S.D. McLeod, S. Li, Control of cell adhesion on poly(methyl methacrylate), Biomaterials, 27 (2006) 2890-2897.

[37] X.J. Zheng, L.S.L. Cheung, L. Jiang, J.A. Schroeder, R.L. Heimark, J.C. Baygents, R. Guzman, Y. Zohar, Dynamic states of adhering cancer cells under shear flow in an antibody-functionalized microchannel, in: Micro Electro Mechanical Systems (MEMS), 2011 IEEE 24th International Conference on, 2011, pp. 849-852.

[38] X.-Y. Wang, C. Pichl, F. Gabor, M. Wirth, A novel cell-based microfluidic multichannel setup—impact of hydrodynamics and surface characteristics on the bioadhesion of polystyrene microspheres, Colloids and Surfaces B: Biointerfaces, 102 (2013) 849-856.

[39] H.E. Abaci, G. Drazer, S. Gerecht, Recapitulating the Vascular Microenvironment in Microfluidic Platforms, Nano LIFE, 03 (2013) 1340001.

[40] N.J. Harrick, Internal reflection spectroscopy, Harrick Scientific Corp., 1967.

[41] D.C. Prieve, Measurement of colloidal forces with TIRM., Advances in Colloid and Interface Science, 82 (1999) 93-125.

[42] J.B. Manneville, Use of TIRF microscopy to visualize actin and microtubules in migrating cells, Methods in enzymology, 406 (2006) 520-532.

[43] D. Naumann, D. Helm, H. Labischinski, P. Giesbrecht, The characterization of microorganisms by Fourier-transform infrared spectroscopy (FT-IR), Modern techniques for rapid microbiological analysis, (1991) 43-96.

[44] J. Wegener, A. Janshoff, H.-J. Galla, Cell adhesion monitoring using a quartz crystal microbalance: comparative analysis of different mammalian cell lines, Eur Biophys J, 28 (1998) 26-37.

[45] C.D. Reyes, A.J. Garcia, A centrifugation cell adhesion assay for high-throughput screening of biomaterial surfaces, Journal of biomedical materials research. Part A, 67 (2003) 328-333.

[46] L.S. Channavajjala, A. Eidsath, W.C. Saxinger, A simple method for measurement of cell-substrate attachment forces: application to HIV-1 Tat, J Cell Sci, 110 (Pt 2) (1997) 249-256.

[47] G. Skarja, R. Kinlough-Rathbone, D. Perry, F. Rubens, J. Brash, A cone-and-plate device for the investigation of platelet biomaterial interactions, Journal of biomedical materials research, 34 (1997) 427-438.

[48] K. Athanasiou, B. Thoma, D. Lanctot, D. Shin, C. Agrawal, R. LeBaron, Development of the cytodetachment technique to quantify mechanical adhesiveness of the single cell, Biomaterials, 20 (1999) 2405-2415.

[49] W.R. Bowen, N. Hilal, R.W. Lovitt, C.J. Wright, Direct measurement of the force of adhesion of a single biological cell using an atomic force microscope, Colloids and Surfaces A: Physicochemical and Engineering Aspects, 136 (1998) 231-234.

[50] W.C. Chang, L.P. Lee, D. Liepmann, Biomimetic technique for adhesion-based collection and separation of cells in a microfluidic channel, Lab Chip, 5 (2005) 64-73.

[51] E. Bianchi, R. Molteni, R. Pardi, G. Dubini, Microfluidics for in vitro biomimetic shear stress-dependent leukocyte adhesion assays, J Biomech, 46 (2013) 276-283.

[52] H. Lu, L.Y. Koo, W.M. Wang, D.A. Lauffenburger, L.G. Griffith, K.F. Jensen, Microfluidic shear devices for quantitative analysis of cell adhesion, Anal Chem, 76 (2004) 5257-5264.

[53] X. Zheng, L.S.-L. Cheung, J.A. Schroeder, L. Jiang, Y. Zohar, A high-performance microsystem for isolating circulating tumor cells, Lab Chip, 11 (2011) 3269-3276.

[54] L.S. Cheung, Z. Xiangjun, W. Lian, R. Guzman, J.A. Schroeder, R.L. Heimark, J.C. Baygents, Y. Zohar, Kinematics of Specifically Captured Circulating Tumor Cells in Bio-Functionalized Microchannels, Microelectromechanical Systems, Journal of, 19 (2010) 752-763.

[55] J.-W. Hsu, S. Yasmin-Karim, M.R. King, J.C. Wojciechowski, D. Mickelsen, M.L. Blair, H.-J. Ting, W.-L. Ma, Y.-F. Lee, Suppression of Prostate Cancer Cell Rolling and Adhesion to Endothelium by 1α, 25-Dihydroxyvitamin D< sub> 3</sub>, The American journal of pathology, 178 (2011) 872-880.

[56] S. Lecuyer, R. Rusconi, Y. Shen, A. Forsyth, H. Vlamakis, R. Kolter, H.A. Stone, Shear Stress Increases the Residence Time of Adhesion of< i> Pseudomonas aeruginosa</i>, Biophysical Journal, 100 (2011) 341-350.

[57] Y. Liu, J.-C. Wang, L. Ren, Q. Tu, W.-M. Liu, X.-Q. Wang, R. Liu, Y.-R. Zhang, J.-Y. Wang, Microfluidics-based assay on the effects of microenvironmental geometry and aqueous flow on bacterial adhesion behaviors, Journal of Pharmaceutical Analysis, 1 (2011) 175-183.

[58] C. Christophis, I. Taubert, G.R. Meseck, M. Schubert, M. Grunze, A.D. Ho, A. Rosenhahn, Shear stress regulates adhesion and rolling of CD44+ leukemic and hematopoietic progenitor cells on hyaluronan, Biophys J, 101 (2011) 585-593.

[59] L. Hall-Stoodley, J.W. Costerton, P. Stoodley, Bacterial biofilms: from the natural environment to infectious diseases, Nat Rev Microbiol, 2 (2004) 95-108.

[60] M.C. van Loosdrecht, J. Lyklema, W. Norde, G. Schraa, A.J. Zehnder, The role of bacterial cell wall hydrophobicity in adhesion, Appl Environ Microbiol, 53 (1987) 1893-1897.

[61] H.T. Badawy, P. Pasetto, J.L. Mouget, J.F. Pilard, T.J. Cutright, A. Milsted, Bacterial adhesion and growth reduction by novel rubber-derived oligomers, Biochem Biophys Res Commun, 438 (2013) 691-696.

[62] J.D. Cox, M.S. Curry, S.K. Skirboll, P.L. Gourley, D.Y. Sasaki, Surface passivation of a microfluidic device to glial cell adhesion: a comparison of hydrophobic and hydrophilic SAM coatings, Biomaterials, 23 (2002) 929-935.

[63] W.M. Saltzman, T.R. Kyriakides, Chapter 20 - Cell Interactions with Polymers, in: R.L.L. Vacanti (Ed.) Principles of Tissue Engineering (Fourth Edition), Academic Press, Boston, 2014, pp. 385-406.

[64] Y. Tamada, Y. Ikada, Cell-Adhesion to Plasma-Treated Polymer Surfaces, Polymer, 34 (1993) 2208-2212.

[65] S. Lakard, G. Herlem, A. Propper, A. Kastner, G. Michel, N. Valles-Villarreal, T. Gharbi, B. Fahys, Adhesion and proliferation of cells on new polymers modified biomaterials, Bioelectrochemistry, 62 (2004) 19-27.

[66] S. Manalis, T. Burg, S. Suresh, K. Babcock, Method and apparatus for high throughput diagnosis of diseased cells with microchannel devices, in, Google Patents, 2015.

[67] F. Yan, X. Li, C. Jiang, Q. Jin, Z. Zhang, R. Shandas, J. Wu, X. Liu, H. Zheng, A Novel Microfluidic Chip for Assessing Dynamic Adhesion Behavior of Cell-Targeting Microbubbles, Ultrasound in Medicine & Biology, 40 (2014) 148-157.

[68] H. Muhlberger, W. Hwang, A.E. Guber, V. Saile, W. Hoffmann, Polymer Lab-on-a-Chip system with electrical detection, Ieee Sensors Journal, 8 (2008) 572-579.

[69] T.A. Crowley, V. Pizziconi, Isolation of plasma from whole blood using planar microfilters for lab-on-a-chip applications, Lab Chip, 5 (2005) 922-929.

[70] L. Nyholm, Electrochemical techniques for lab-on-a-chip applications, Analyst, 130 (2005) 599-605.

[71] P.K. Sorger, Microfluidics closes in on point-of-care assays, Nat Biotechnol, 26 (2008) 1345-1346.

[72] J.C. McDonald, D.C. Duffy, J.R. Anderson, D.T. Chiu, H.K. Wu, O.J.A. Schueller, G.M. Whitesides, Fabrication of microfluidic systems in poly(dimethylsiloxane), Electrophoresis, 21 (2000) 27-40.

[73] J.C. McDonald, G.M. Whitesides, Poly (dimethylsiloxane) as a material for fabricating microfluidic devices, Accounts of chemical research, 35 (2002) 491-499.

[74] S.K. Sia, G.M. Whitesides, Microfluidic devices fabricated in poly(dimethylsiloxane) for biological studies, Electrophoresis, 24 (2003) 3563-3576.

[75] M. R., When microfluidic devices go bad. How does fouling occur in microfluidic devices, and what can be done about it?, Anal Chem., 77 (2005) 429A-432A.

[76] M. Schoenitz, W. Augustin, S. Scholl, Challenges in cleaning microstructured devices, Food and Bioproducts Processing, 93 (2015) 283-288.

CHAPTER 3

Microchannel fabrication

Abstract

Polymer coated microchannels were fabricated using materials that are commonly used in biomedical implants. In order to mimic *in vivo* conditions during initial bacterial adhesion, studies were performed at a temperature of 37˚C. This chapter describes the unique in-house fabrication process developed to incorporate the polymer surface in the microchannel by a spin coating method. Using this technique, the implant surface was obtained inside the microchannel and a bacterial suspension of *Escherichia coli* JM109 (DE3) was pumped into the microchannel to assess the fouling rate of the implant-like surface. Microchannels were fabricated with xurographic technique and the polymers were spin coated over the slide and the microchannels produced so that a leak-tight system was obtained to perform the adhesion studies. The microchannel widths are 450 μm with channel aspect ratio of 4.5. The major drawback of the method is the location of the region of interest in a lowered surface. It was demonstrated by bacterial adhesion experiments and computational fluid dynamics (CFD) simulations that this drawback has a negligible effect on adhesion. It is also shown that shear stress in the region of interest can be calculated by numerical methods and by an analytical equation for rectangular channels.

3.1 Introduction

Cell adhesion is predominantly determined by the properties of the surface and by the flow characteristics [1]. The present thesis focuses on the study of cell adhesion and cleaning of materials used in biomedical applications, as well as in microdevices in general. Microdevices are considered in two perspectives, as tools for cell adhesion

research and as objects of research. For these reasons, the construction of the microchannels used to perform the experiments is of primordial importance.

Many recent reviews provide a source of evidence to the undesirable biofilm formation in medical devices [2-8]. These biofilms pose a challenge to the health care community. Until now, there are very few bio-adhesion studies to quantify fouling phenomenon on different biomedical surfaces at the micro scale, while there is a spurring development of smart polymers that are used for coating biomedical implants, artificial organs, lab on chip surfaces and implantable drug delivery systems [9], giving way for the development of a next generation of anti-fouling biomedical devices. Ramakrishna et al. [10] discussed different biocompatible polymers used for different types of implants. For example, poly-L-lactide (PLLA) is a biodegradable polymer, which degrades with time without creating harm inside the body [11, 12]. Different types of pin and screws are used for fixing the implants. Autografts namely suspensory fixation, hamstring fixation [13] are used as fixing agents for femoral implants to reduce operation failures. These grafts pins and screws are coated with PLLA.

There are several biofilm research studies [14-16] in microchannels, stressing the unique advantages of microfluidics:

- The different biological cells can be monitored in real time through visualization techniques;
- The assays and different expensive reagents are needed in microliters helping in cost cutting;
- The surface can be modified easily and the geometry can be designed according to the application;
- The flow remains laminar even at high shear stress values.

Rajendrani Mukhopadhyay [17] discussed the sources of fouling in microfluidic devices and advised to keep an eye on fouling at every step of the development process, from the materials to the design of the device.

The transmission of a designed pattern on to a substrate through optical means is called photolithography. The desired patterns are transferred to a photoresist liquid

layer. This layer is coated uniformly over a substrate, exposed and developed with the desired pattern for subsequent processing. The different processes involved in photolithography are expensive and tedious, as they require clean surface preparation, spin coating, alignment for precision output, soft and hard baking, exposure, development, preparing mask alignment with pattern on the wafer's surface, the photoresist is exposed through the pattern on the mask with high intensity ultraviolet light, developed SU-8 positive microstructures baking [18].

Besides the SU-8 molds prepared by photolithography technique, there are many rapid prototyping techniques (mold making techniques) developed for fabricating microchannels by soft lithography. Duffy et al. [19] implemented a method to produce PDMS channels (soft lithography), which can be used in microscale total analysis systems (μTAS), genetic analysis, clinical diagnostics, drug screening and environmental monitoring. The design, produced using CAD software, is printed in a transparency and used as a mask for making positive relief master molds. The master molds are produced with SU-8 polymer epoxy photoresist described in detail by Blanco et al. (2004) and Che et al. (2002) [20, 21]. The PDMS channels are casted in these molds, which are baked to get well irreversibly sealed channels. The other conventional methods that are commercially used for micromolding are micromilling [22], micropowder blasting [23], hot embossing [24], laser ablation [25] and stereo lithography [26].

Xurography is a technique developed by Bartholomeusz et al. [27], which requires a simple cutter plotter. The microchannels are cut on vinyl films or other type of films according to the application. Positive relief molds of thicknesses between 25 and 1000 μm are generated in the cutter plotter and made ready for casting PDMS microchannels (soft lithographic technique[28]) in less than 30 minutes. Aspect ratios up to 5.2 for positive features are possible in a 360 μm thick material applying this Xurography technique.

The foremost advantage of xurography technique is the reduced capital cost and fast mold fabrication technique. The alternative to xurography is photolithography and the other conventional techniques, both needing expensive machines and expensive clean rooms. Furthermore, in these conventional techniques, any design change in the microchannel geometry requires more than a day to be performed, with long chemical

procedures and pre and post baking steps. The main disadvantage of xurography is the low resolution, which limits the production of microchannels to dimensions greater than 200 μm.

In this thesis, biofouling was studied in rectangular PDMS microchannels to assess the initial adhesion of cells to a surface. Different biomedical polymer surfaces and different configurations of the microfluidic device were tested. The polymers were selected according to their biocompatibility, easy spin coatability on microscopic slides and durability over the experiment. Microchannels were constructed using soft lithographic technique with molds obtained from SU-8 photolithography and xurography techniques. The microchannels produced by xurography are the best for testing the initial adhesion on PDMS surface and also on polymeric surfaces. This technique consumes less time and enables the incorporation of different polymer surfaces in the PDMS microchannels. As already referred, xurography is limited to dimensions higher than 200 μm and so, to study adhesion on smaller micochannels, photolithography was also used to make the molds.

3.1.1 Motivation for fabrication microchannels with polymer coated surfaces

The motivation to fabricate and study different microchannel polymeric surfaces arises from the literature reviewed concerning failure of different implants due to infection [29] and failure of different implantable sensors [30]. According to this literature, with a better understanding of bacterial adhesion and biofilm formation within the human body may reduce health risks by stopping infections at an early stage, reducing the need for revision surgery, mortality and morbidity of the patients. There are numerous polymeric biomaterials commonly used in biomedical devices and there is a demand to test them under controlled conditions. Microfluidics is an excellent option to test these materials, because it requires small setups, enables controlled operating conditions and the experiments are easily replicated. So far, PDMS based microsystems have received tremendous attention and the review by Jinwen Zhou et al. (2010) focuses on PDMS surface modifications [31].

In this chapter, a new technique to incorporate a small wall patch into a PDMS microchannel, produced from molds easily made in-house by xurography, is proposed. The wall patch can be made of different polymers. The technique, adapted from a standard PDMS soft-lithography technique, is useful to produce channels for adhesion tests. The spin coating technique is exploited to coat a polymer surface over PDMS. Different polymers were tested taking in consideration the restrictions of the microchannel fabrication methods and also those of the visualization techniques. Only transparent polymers can be used in visualization studies by bright-field microscopy.

3.2 Microfabrication techniques

Three microfabrication techniques were used in this work: SU-8 photolithography, xurography and soft lithography. Additionally, the soft lithography technique was modified to insert polymeric materials in the microchannels walls. These methods are described in the following sections.

3.2.1 SU-8 Photolithography technique

SU-8 photolithography is a high precision technique to produce microchannels for fouling studies. The fabrication technique is discussed briefly in Sia and Whitesides [32] and in detail in Duffy et al. [19].

The desired microchannel geometries are drawn in AutoCAD drawing software. The AutoCAD drawing is printed on a quartz surface. Hard and durable chrome masks are obtained by sputtering chrome over a quartz substrate [33]. Chrome masks are used for getting microchannel features down to 8 μm as said by Desai et al. [34] and down to 500 nm, which was recently said by Lalanne and Chavel. [35]. The chrome masks are much more expensive than the transparency films [36, 37] (alternative printing substrate to chrome) and they take a much longer time to be fabricated.

The molds are produced by a photolithography technique, where light is used to pattern the substrate namely the photocurable epoxy SU-8, a material used for

producing integrated circuits and microelectronic components [38]. SU-8 is exposed to ultraviolet light through the photomask. The cross-linking process, activated during the exposure, makes SU-8 fully polymerized. The unexposed SU-8, i.e. the unpolymerized SU-8, will get dissolved leaving the coated microchannel design to serve as a positive relief mold for making replicate PDMS microchannels. The rapid prototyping techniques consume much time for producing the positive-relief on the mold surface. The SU-8 photolithography technique enables the production of microchannels with very small dimensions, widths down to 100 μm [39], but the time consumption and requirements of clean environmental room to produce the molds are clearly disadvantages. A pictorial representation of the process of producing molds to prepare microchannels is shown in Figure 3.1.

In the present work, the molds were purchased, as the facilities required to produce the SU-8 molds were not available.

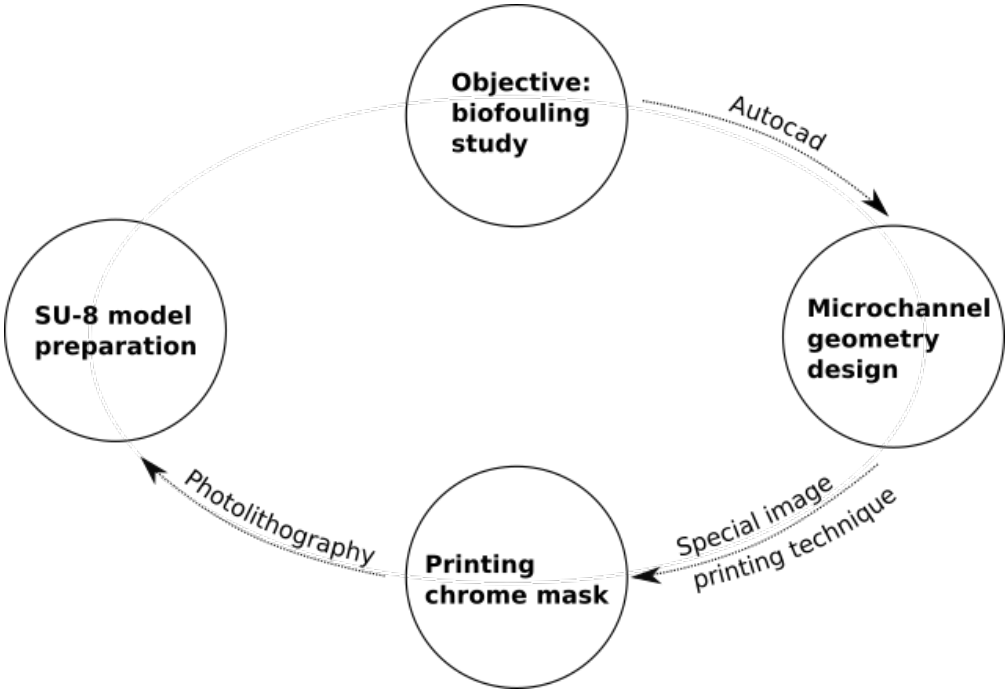

Figure 3.1. Procedure followed to make the mold for the production of microchannels

3.2.2 Xurography technique

Bartholomeusz et al. [27], developed a novel rapid prototyping technique for creating micromolds in various thin materials, ranging from 25-1000 μm in thickness, without

the need for photolithographic or chemical processes. The thin materials are nothing but adhesive films (e. g. vinyl films). The process of making film micromolds is pictorially described in Figure 3.2. After plotting the microchannel pattern over the film using a cutter plotter (GCC Expert 24 vinyl cutter plotter), the unwanted films are removed and the micromold structure is transferred to a Petri dish using a transport tape. This tape can be peeled off leaving the microchannel design in the Petri dish as shown in Figure 3.3.

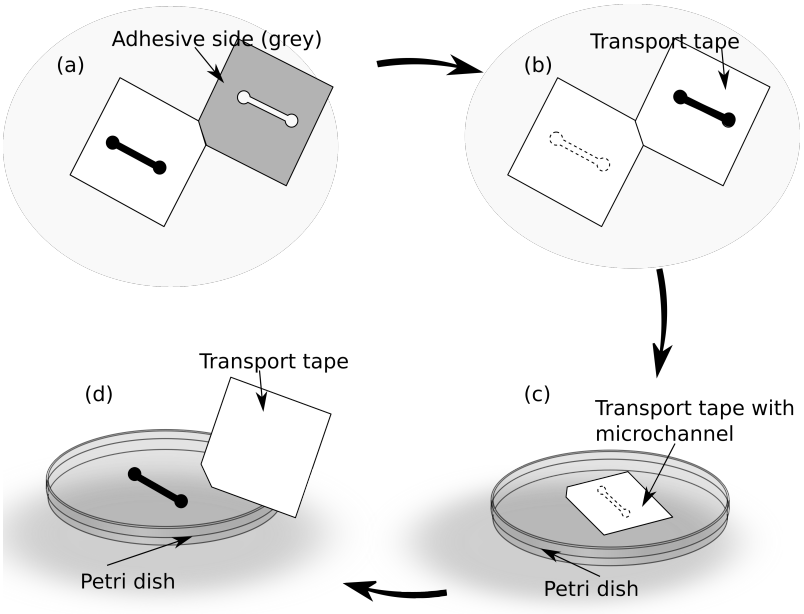

Figure 3.2. Process followed for making micromolds in various films: (a) Cut the microchannel in the vinyl film and peel off the unnecessary film area; (b) Peel off the microchannel mold pattern with a transport tape; (c) Press the microchannel pattern along with the transport tape in a Petri dish; (d) Peel off the transport tape leaving the micromold in the Petri dish.

Blue and red vinyl films [40] were tested with different cutter speeds (cutter speeds depends on the material and its width) using a GCC Expert 24 vinyl cutter plotter as shown in Figure 3.3 to produce microchannel micromolds were followed. The microchannel molds were used to make microchannels using a soft lithographic process. A PDMS microchannel casted from the mold is shown in Figure 3.4.

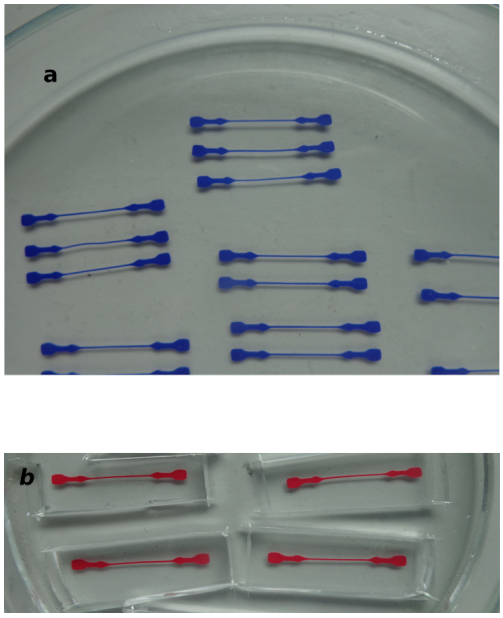

Figure 3.3. Micromolds created with Xurographic technique using: (a) a blue film; (b) a red film.

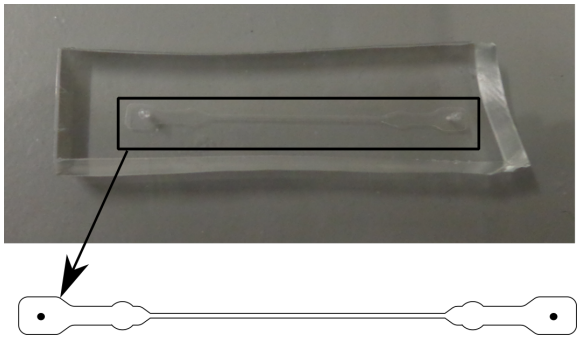

Figure 3.4. Rectangular PDMS microchannel developed from Xurography mold used for initial adhesion study

3.2.3 Soft lithography technique

The soft lithography technique was used to fabricate microchannels made from poly-dimethysiloxane (PDMS). The microchannels were fabricated with a homogenous mixture of PDMS (Sylgard 184, Dow Corning). Sylgard 184 is commercially available as a pre polymer kit composed of a PDMS oligomer and a crosslinking agent or curing agent in the ratio of 5:1. A desiccator connected to a vacuum pump was used to remove the air bubbles that formed during the mixing process. The PDMS was poured over the mold and kept in the oven for 20 mins at 80ºC. After curing, the PDMS microchannel was peeled off from the mold. Holes (1mm in diameter) were punched with the help of a syringe tip, through the PDMS replicas at

both ends of the channel to serve as the flow inlet and outlet. The PDMS microchannels were sealed with PDMS coated glass slide and kept in the oven for approximately 12 hours at 80ºC. The coated PDMS glass was prepared by spin coating, over a glass slide, using a mixture of PDMS and curing agent at a ratio of 20:1. An overview of the fabrication process is depicted in Figure 3.5.

This technique allows the construction of mini/micro channels with three walls in PDMS and another wall in PDMS coated on glass. The curing leads to the formation of an irreversible chemical bond between the 5:1 and 20:1 PDMS mixture, ensuring microchannels without leaks. The fabrication process shown in Figure 3.5 is also the general fabrication method for producing microchannels.

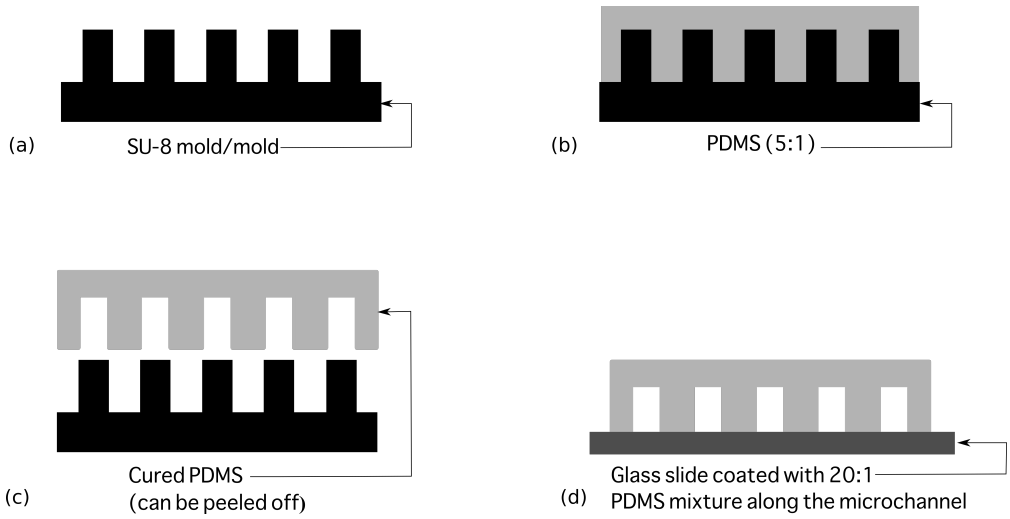

Figure 3.5. PDMS device fabrication procedure: (a) cross section of SU-8 mold / any mold with a positive relief; (b) mixture of PDMS and curing agent in a ratio of 5:1 is poured over the mold and kept in the oven; (c) cured PDMS is peeled off from the mold and access ports are created with the syringe tips; (d) PDMS layer containing the channel structure is bonded to the glass slide covered with the thin layer of PDMS and placed in the oven for 12 hours to seal the channels.

3.2.4. Insertion of polymer surface in the microchannel

The transparent and spincoatable polymer solutions were prepared as describe below. The polymer was mixed with the solvent in appropriate mass percentages as indicated in Table 3.1.

Table 3.1. Polymers and solvents used for preparing polymeric solutions

Polymer solution	Polymer	Solvent	Polymer mass percentage
cellulose acetate (CA)	CA	acetone	8%
polyethylene oxide, (PEO)	PEO	dichloromethane (DCM)	1.14%
poly-l-lactide acid (PLLA)	PLLA	dichloromethane (DCM)	5%
polyamide (PA)	PA	trichloroethanol	0.49%
polydimethylsiloxane (PDMS)	PDMS	curing agent (Sylgard 184)	10%

The PDMS was prepared with 10:1 of PDMS and curing agent and desiccated to remove air bubbles to get a homogenous mixture after mixing. The prepared polymers are spin coated over the microscopic slides via a Laurell Technologies spin coater (WS-650S-6NPP-Lite). The durability of the polymers presence over the surface was tested with a suspension in water, by making it flow over the slide for 30 minutes and checking the contact angle, with a contact angle meter, before and after the flow. The different spin coated polymer surfaces are shown in Figure 3.6.

Channels comprising six different wall materials were fabricated by manipulating different substrates. In one case, polystyrene cover was used as substrate to fabricate microchannels with polystyrene wall surfaces. In the other five cases, different polymers were spin coated over a glass substrate. The coated glass slides, used to seal the channel, were prepared by two-layer spin coating technique (Figure 3.7). Different volatile polymers and solvents were mixed in appropriate percentages (Table 3.1) and the polymer solution was spin coated over the substrate (Figure 3.7 b). After the formation of the polymeric film, by evaporation of the solvent, a scotch tape was pasted over the polymer surface (Figure 3.7 c) and the PDMS was spincoated for 50 s at 5000 rpm over both the polymer and the scotch tape (Figure 3.7 d). The scotch tape was then carefully peeled off (Figure 3.7 e) and the slide was baked for 5 minutes in the oven at 80°C. A lowered surface (3 x 3 mm^2) was left on the slide. The level of the lowered surface was determined from a relation between thickness, speed coating and time (Zhang et al. (2005) [41], koschwanez et al. (2009) [42]) and found to be approximately 10 μm. The PDMS slab and the slide were aligned to assure that the microchannel crosses the lowered surface.

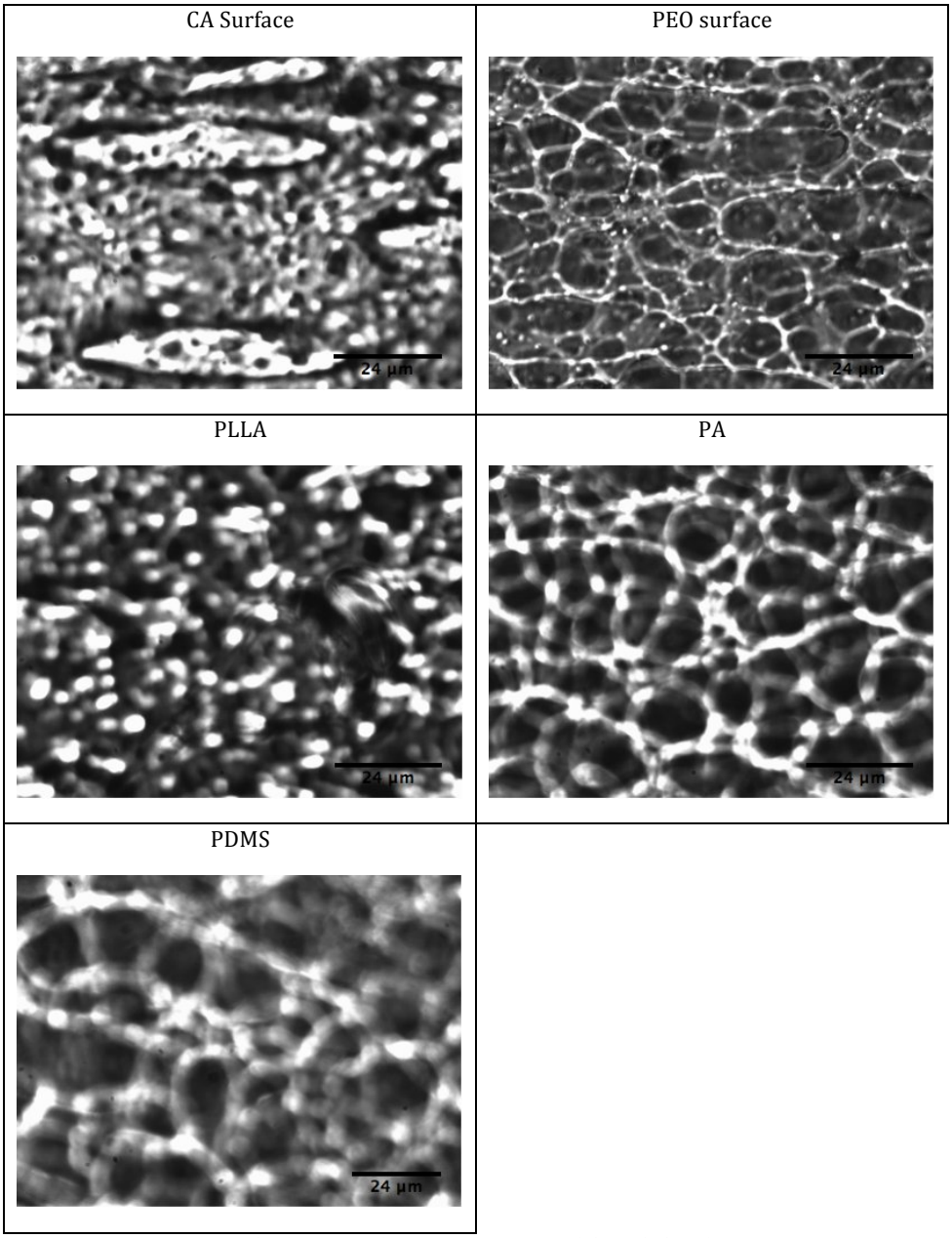

Figure 3.6. The different polymer surfaces captured through the microscopic camera.

The procedure can also be used to test the adhesion to the substrate (e.g. polystyrene surfaces) and in this case the first layer spin coating step (Figure 3.7 b) is skipped. This alternative procedure can be used to produce microchannels with other surfaces, such as glass, provided that a transparent thin slab is available.

The method described above produces microchannels with PDMS surface along most of its length and a small patch of a different material located in a lowered surface half-length from the inlet. To test the effect of the lowered surface on bacterial

cell adhesion, microchannels with PDMS walls along the full length of the microchannel were produced following the double layer technique, both layers made of PDMS.

As the polymer surface will be under the microscopic lens for monitoring the fouling and calculating the fouling rate, there arises a need to visualize it to process the cell counting in ImageJ software. Therefore, those polymer surfaces with imperfections creating spurious images, which disturb the cell count, were discarded. The surfaces passing this test were visualized and the images captured (Figure 3.6).

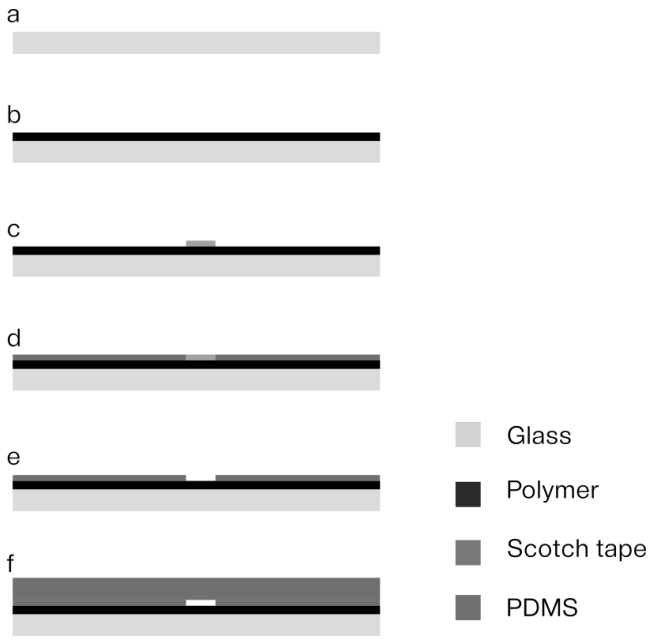

Figure 3.7. (a). Plain Glass slide or any substrate; (b). Polymer coated over the substrate; (c). Scotch tape pasted over polymer and PDMS coated over the tape; (d). The scotch tape removed and the PDMS with channel obtained by soft lithography is bonded.

3.2.5. Experimental set-up.

The cell suspension used in the fouling studies was prepared with Gram-negative bacteria Escherichia coli (*E. coli)*, used as a living cell (starving bacteria). This bacteria is the favored host for the recombinant protein production [43]. The suspensions were driven to the microchannels with dimensions of 0.45 × 15 × 0.10 mm (W × L × H) with the help of a syringe pump (Cetoni, neMESYS syringe pump) and the flow was observed through a microscope (Leica DMI 5000 M). White light shined through the transparent PDMS, so that the *E. coli* in the suspensions appears

dark. Microscopic images were recorded through a high resolution CCD camera (Leica DFC350 FX). The experimental set-up is illustrated in Figure 3.8.

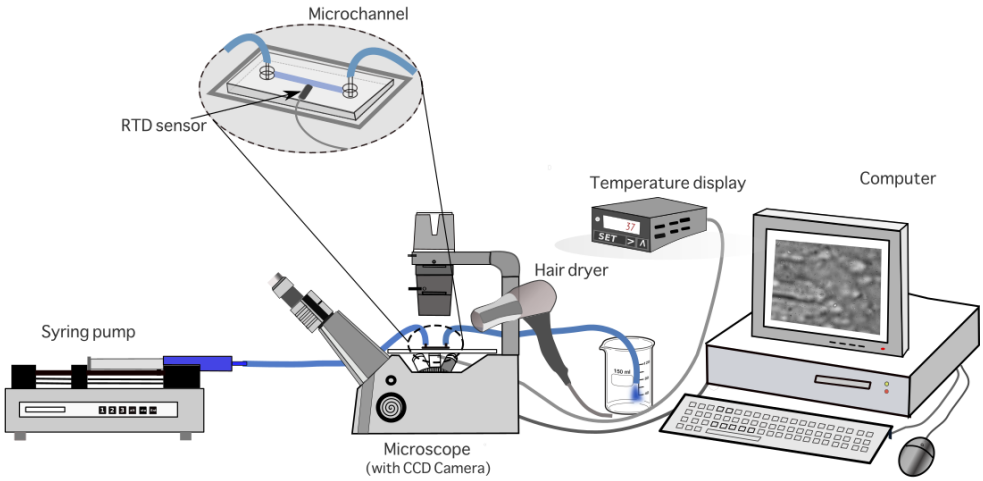

Figure 3.8. Experimental set up for fouling study

3.3. Polymer surface analysis

Merrett et al. (2002) [44] reviewed in detail the surface analysis techniques for characterizing polymeric biomaterials: microscopic, spectroscopic and surface contact angle measurement techniques. The degree of hydrophobicity of a polymer surface, with or without fouling, is expressed as the free energy of interaction (ΔG mJ.m^{-2}) between two entities, when the surface is immersed in a polar liquid (such as water).

There are three methods that are commonly used in lab to determine the surface contact angle: Wilhelmy plate method, sessile drop method and captive bubble method [45] (see Figure 3.9 a). Generally, the surface is considered hydrophilic or hydrophobic depending on the drop contact angle as shown in the Figure 3.9 b. In this work, the contact angles were determined by the sessile drop method in a contact angle meter (OCA 15 Plus; Dataphysics, Filderstadt, Germany) using water (θ_w), formamide (θ_F) and α-bromonaphtalene $(\theta_{\alpha-B})$ as reference liquids [46].

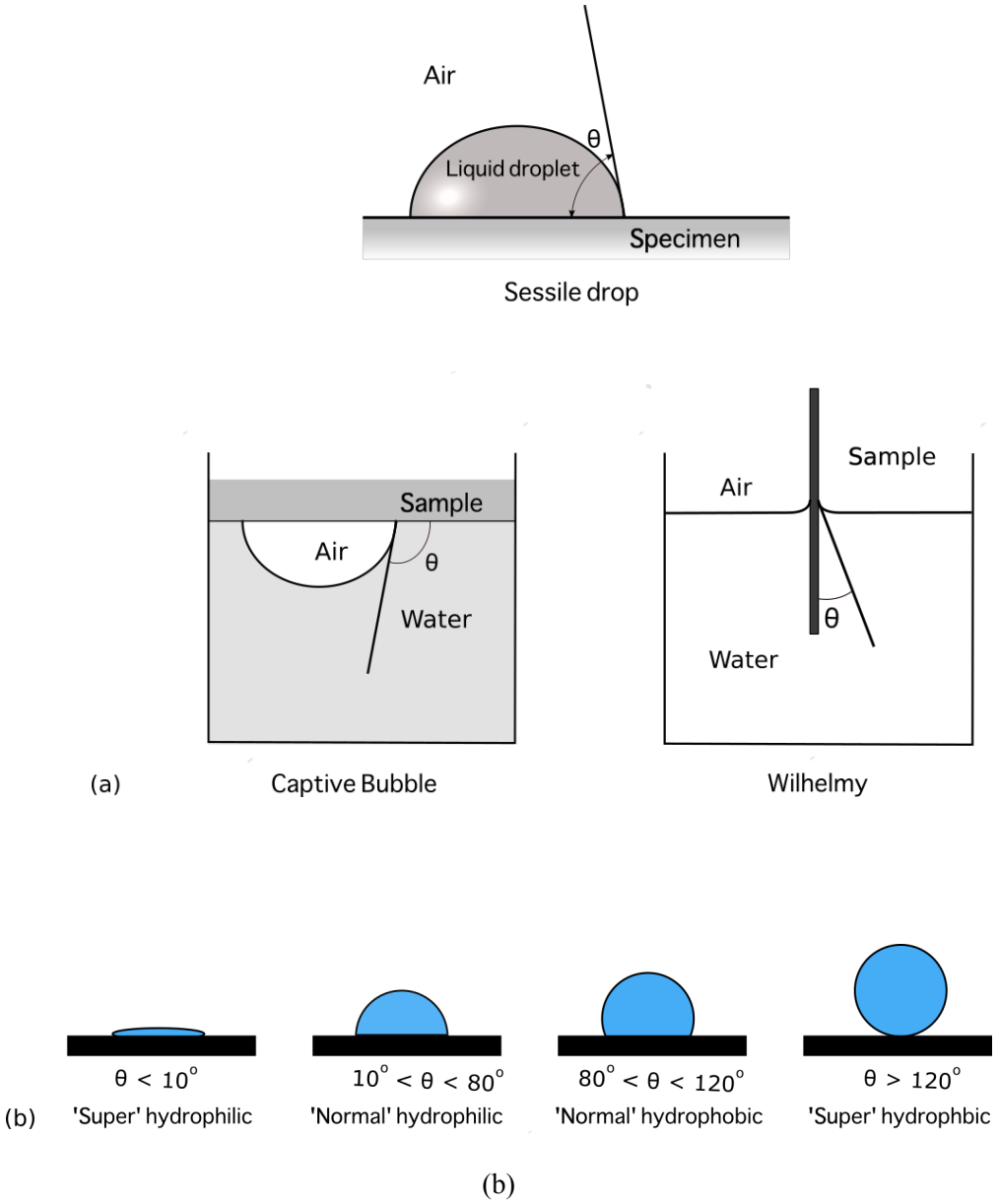

Figure 3.9. a) Schematic illustration of the static contact angle using sessile drop method, captive bubble method and Wilhelmy method; b) Surface characterization based on hydrophobicity and hydrophilicity.

According to van Oss [47], the total surface energy (γ) of a pure substance is the sum of the apolar Lifshitz-van der Waals components of the surface free energy (γ^{LW}) with the polar Lewis acid-base component (γ^{AB}):

$$\gamma = \gamma^{LW} + \gamma^{AB} \quad (1)$$

The polar γ^{AB} component comprises the electron acceptor $\left(\gamma^{+}\right)$ and the electron donor $\left(\gamma^{-}\right)$ parameters, and is given by:

$$\gamma^{AB} = 2\sqrt{\gamma^{+}\gamma^{-}} \quad (2)$$

The surface energy components of a solid surface (*s*) are obtained by measuring the contact angles (θ) with three different liquids (*1*), with known surface tension components, followed by the simultaneous resolution of three equations of the type:

$$(1+\cos\theta)\gamma_l = 2\left(\sqrt{\gamma_s^{LW}\gamma_l^{LW}} + \sqrt{\gamma_s^{+}\gamma_l^{-}} + \sqrt{\gamma_s^{-}\gamma_l^{+}}\right) \quad (3)$$

The degree of surface hydrophobicity is expressed as the free energy of interaction (ΔG mJ. m^{-2}) between two entities of that surface when immersed in a polar liquid (such as water (w) as a reference solvent). ΔG was calculated from the surface tension components of the interacting entities, using the equation:

$$\Delta G = -2\left(\sqrt{\gamma_s^{LW}} - \sqrt{\gamma_w^{LW}}\right)^2 + 4\left(\sqrt{\gamma_s^{+}\gamma_w^{-}} + \sqrt{\gamma_s^{-}\gamma_w^{+}} - \sqrt{\gamma_s^{+}\gamma_s^{-}} - \sqrt{\gamma_w^{+}\gamma_w^{-}}\right) \quad (4)$$

If the interaction between the two entities is stronger than the interaction of each entity with water, $\Delta G < 0$, the material is hydrophobic, in the counterpart if $\Delta G > 0$ the material is hydrophilic.

In the current work, for each surface, at least 10 measurements with each liquid were performed at 25 ± 2 ºC.

The polymer surfaces were also tested for its durability of adherence. The polymer surface was placed in a parallel plate flow chamber and the flow of a buffer solution without *E. coli* was promoted during 30 mins. The hydrophobicity results after these 30 mins were compared with those from fresh prepared polymer surfaces.

Additionally, the surface charge of each polymer was characterized through its zeta potential. Particle suspensions of each material [48] were prepared in order to measure the electrophoretic mobility, using a Nano Zetasizer (Malvern Instruments, UK). When the zeta potential is high, the repulsion force between similarly charged particles is strong and aggregation is avoided. When the zeta potential value is small,

the repulsion between similarly charged particles is weak. The zeta potential was calculated using Helmholtz–Smoluchowski equation.

3.4. Data analysis with ImageJ

Adhesion was followed using a fluorescence inverted microscope (DMI 5000M, Leica Microsystems GmbH) with a 40× objective. Microscopic images were captured during 30 mins with a CCD camera (Leica DFC350FX, Leica Microsystems GmbH) with a time interval of 60 s. The image sequence obtained is in tiff format as recorded by Leica Application Suite software.

Image processing to count cells over a surface during the experiment was performed using ImageJ, an open source software developed by Wayne Rasband at National Institute of Mental Health (NIH) during 1997. This software allows 8-bit, 16-bit and 32-bit grayscale images and supports a variety of file formats such as, TIFF, GIF, JPEG, BMP, DICOM, FITS and raw data using a URL. It can display a group of images in a single window, image sets are called stacks, and any sequence can be processed in a particular selected window. It uses the standard image processing functions such as contrast, sharpening, smoothing, edge detection and median filtering.

All the 30 images were imported to Image J software [49]. A low noise region was selected in the images using the crop tool. The images were converted from 8 bit to 32 bit to improve contrast. To set the scale for processing, the pixel aspect ratio was set to one. Depending on the images, they can be sharpened using mean filters with 1 pixel as radius. Then, the background was subtracted with rolling ball radius ranging from 1 to 18 pixels. A light background was obtained with the *E. coli* cells bright and visible. The brightness and contrast were fine-tuned to get more accurate cell count. The threshold was adjusted, for the stack of images, to generate a black and white image, black cells over a white background. Then the cells were automatically counted.

The cells counted with the help of the ImageJ software were confirmed with manual counting to establish the method developed for the cell counting as appropriate. The cell count result obtained was 99% exact to manual counting.

3.5. Bacteria and culture conditions

Escherichia coli JM109 (DE3) was used in the tests, since it has a good adhesion capacity [50]. A starter culture was prepared as described by [51] and incubated overnight. A volume of 60 mL from this culture was centrifuged (for 10 min at 3202 x g) and the cells were washed twice with citrate buffer 0.05 M [52], pH 5. The pellet was then resuspended and diluted in the same buffer to obtain a cell concentration of 7.6×10^{7} cells mL^{-1}.

3.6. Flow conditions

The flow conditions studied are indicated in Table 3.2. With these conditions, the shear stress ranges from 0.02 to 1 Pa, covering the majority of the shear stresses that can be found in the human body [53, 54].

Table 3.2. Hydrodynamic conditions

Flow rate(μL/min)	Mean Velocity (m/s)	Reynolds number	Nominal wall shear stress (Pa)
1.35	5.00×10^{-4}	0.12	0.02
15	5.56×10^{-3}	1.3	0.2
65.1	2.41×10^{-2}	5.65	1

3.7. Numerical simulations

The flow cell was simulated by numerical methods to clarify the stability and the predictability of the flow patterns near the observation region. The microchannel used, represented in Figure 3.10, has a rectangular cross section of 450 x 100 μm and a length of 15 mm. The inlet and outlet have a diameter of 0.44 mm.

A section of the microchannel, around the visualization region, was selected for simulation domain (Figure 3.10). This region includes the lowered surface, which results from the fabrication method, where the region of interest is located. The length of the domain is 5 mm. The lowered surface has a length of 3 mm and a width of 3mm. The lowered height is approximately 10 μm.

The flow regime was determined by the Reynolds number based on the equivalent diameter of the channel.

$$\mathrm{Re} = \frac{2\rho Q}{(W+H)\mu} \tag{5}$$

where ρ and μ are the density and viscosity of the fluid, respectively, Q the flow rate, W the width of the channel and H the depth of the channel.

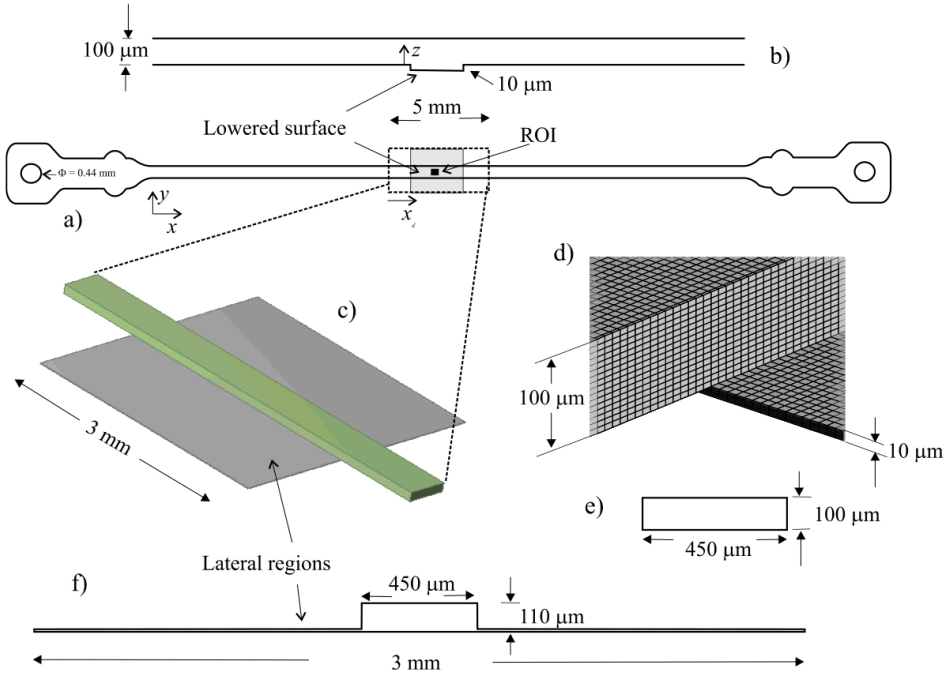

Figure 3.10. Microchannel representation and mesh details: a) Microchannel, showing the lowered surface in grey, the region of interest in black and domain limits; b) Profile representing the level of the upper and lower surfaces of the channel; c) 3D representation of the numerical domain; d) Lowered surface detail; e) Microchannel cross-section outside the lowered region; f) Cross-section available to the flow in the lowered surface region.

Numerical values of the wall shear stress (WSS) were compared with data from the analytical solution for the flow in a parallel plate channel [55]:

$$\tau = \mu \frac{3Q}{2\left(\frac{H}{2}\right)^2 w} \tag{6}$$

Nominal wall shear stress, used to distinguish the experiments, was calculated through the analytical equation 6. The real wall shear stress, as given by the numerical simulation, is slightly different.

The equation for the lowered surface was corrected by the following factor:

$$\tau_{ls} = \tau\left(\frac{H}{H_{ls}}\right)^2 \tag{7}$$

where τ is the wall shear stress in the straight channel (outside the lowered surface) and H_{ls} the depth of the channel in the lowered surface section.

Numerical simulations were made with the commercial code ANSYS Fluent CFD package (version 14.5) by solving Navier–Stokes equations. A model of the microchannel was built in Design Modeler 14.5 and was discretized into a grid of 278,000 cells by Meshing 14.5. The QUICK scheme [56] was used for the discretization of the momentum equations and the PRESTO! scheme for the discretization of the pressure terms.

The velocity–pressure coupled equations were solved by the PISO algorithm [57]. The no slip boundary condition was considered for all the walls. Simulations were made in steady state mode until convergence. The properties of water (density and viscosity) at 37◦C were used.

Corrected numerical results were calculated by applying equation (7). The value of τ used was the wall shear stress of a straight channel (without a lowered surface) previously obtained numerically.

3.8. Results

3.8.1. Numerical simulation

Wall shear stress (WSS) at the bottom wall and velocity field at the midplan are represented in Figure 3.11 and Figure 3.12, respectively. These figures show a small velocity decrease in the region of the channel crossing the lowered surface. The velocity at the lateral regions (see Figure 3.10) of the lowered surface is almost zero.

The wall shear stress is also small in the part of the channel that crosses the lowered surface region, where the region of interest is located.

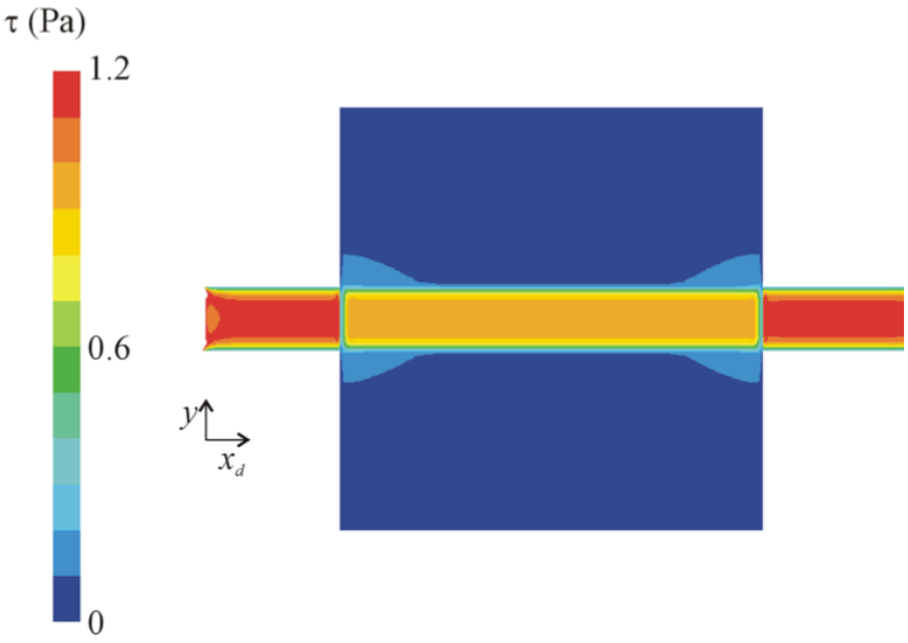

Figure 3.11. Wall shear stress (WSS) in the lowered surface region for a nominal wall shear stress of 1 Pa

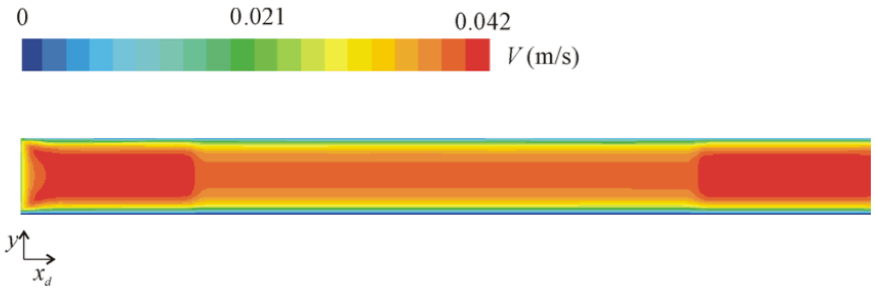

Figure 3.12. Velocity magnitude in the midplane in the lowered surface region for a nominal wall shear stress of 1 Pa.

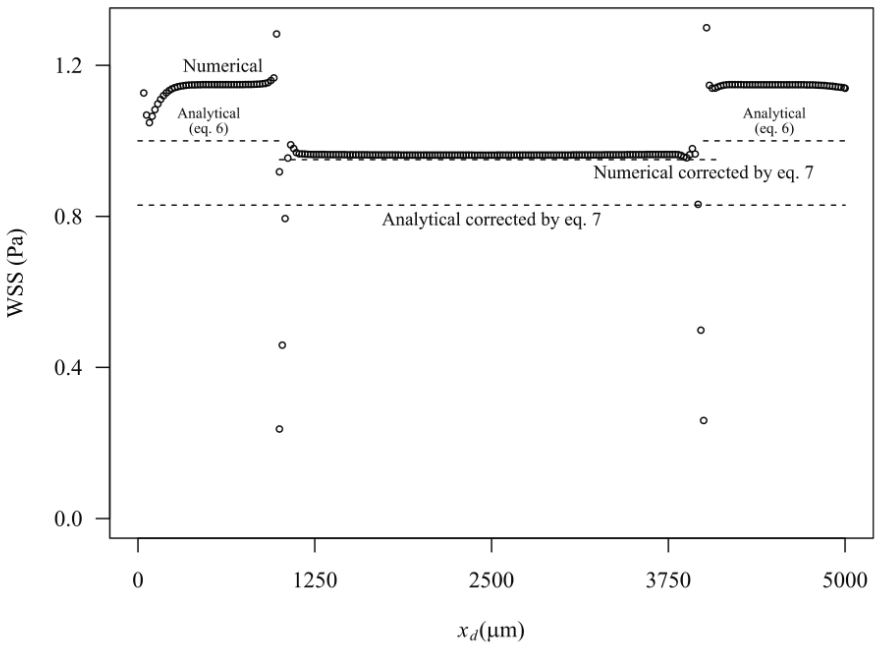

Figure 3.13. Wall shear stress along the centreline at the bottom surface in the lowered region for a nominal wall shear stress of 1 Pa. Figure show numerical predictions (symbols), predicted based on analytical equation 6 and predictions with corrections based on equation 7. Local domain coordinates are used to represent the distance from the domain inlet.

Figure 3.13 shows the wall shear stress along the centreline of the bottom wall of the channel. The figure is for the higher nominal WSS studies (1Pa), but results for the other wall shear stresses, not shown here, are similar. Some edge effects are observable, mainly due to the influence of the inlet and outlet boundary conditions. At the inlet, the edge effects are small, revealing that the flow develops in a short length, and enters fully developed in the lowered surface region. In the lowered region, the wall shear stress is smaller. A small transition exists of about 300 μm length.

The analytical equation 6 underpredicts the numerical WSS data in the channel outside the lowered region. This result is expected since the analytical equation is exact only for channels with an infinite width. In the present case the ratio between the width and the height of the channel is 4.5, which implies that the velocity is higher than what would be in a channel of infinite width.

The correction, equation 7, made on the analytical equation underpredicts the WSS in the lowered surface, while the correction applied to the numerical results predicts it correctly.

3.8.2. Surface characterization

The surface properties of the different materials fabricated are presented in Table 3.3. Exploring the results, it is observed that except for polyethylene oxide (PEO), the rest of the polymers are hydrophobic. PLLA, PDMS, CA, PA and PS are hydrophobic surfaces ($\Delta G < 0$ mJ.m^{-2}) whereas PEO is hydrophilic ($\Delta G > 0$ mJ.m^{-2}). Additionally, the zeta potential results showed that all the polymers surfaces have a negative charge. The range of surface characteristics assures that the procedure can be used to study a large range of surface parameters.

Table 3.3. Surface characterization with Hydrophobicity and Zeta potential

	Water (θ_w) (degree)	Bromonafthalene $(\theta_{\alpha-B})$ (degree)	Formamide (θ_F) (degree)	Hydrophobicity ΔG (mJ m^{-2})	Zeta potential (mV)
PDMS	113.56 ± 0.62	87.61 ± 1.77	111.18 ± 0.61	-61.82	-29.3
PLLA	88.03 ± 1.01	25.58 ± 1.55	68.49 ± 0.95	-65.32	-27.9
PS	80.81 ± 0.82	24.64 ± 0.89	64.32 ± 0.99	-49.56	-29.8
CA	65.24 ± 0.50	22.47 ± 1.05	36.63 ± 2.05	-36.04	-23.4
PA	69.36 ± 0.43	23.63 ± 0.53	48.02 ± 1.24	-37.58	-28.0
PEO	55.54 ± 3.11	34.17 ± 1.28	64.33 ± 0.99	0.35	-11.0

3.8.3. Image processing examples

Images were processed with ImageJ, as described in section 3.5, and the number of cells attached to the surface was obtained for every minute. Examples of images from adhesion experiments in PDMS, PLLA and PS are shown in Figure 3.14. In the first row it is possible to see images captured at the first minute of the fouling experiment while the second row contains images captured at the end of the fouling experiment (after 30 mins). In the third row are the processed images of those in the second row. Zoomed views of the images presented in Figure 3.14 are in Figure 3.15. A zoomed of the processed image of fouling in PDMS (third row, first column of Figure 3.15 is

shown in Figure 3.16. It shows bacteria attached and also noise and PDMS surface disturbances. The procedure developed for counting the cells attached eliminates these noise and surface disturbances.

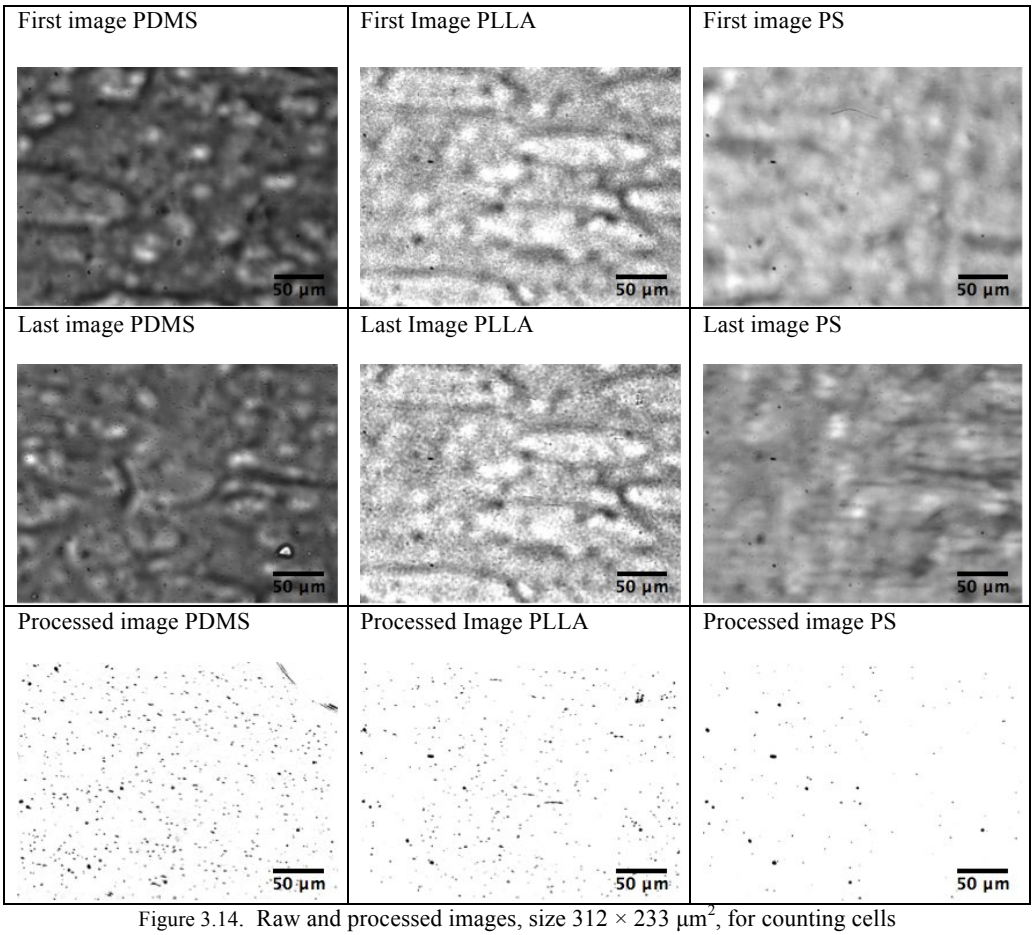

Figure 3.14. Raw and processed images, size 312 × 233 µm^2, for counting cells

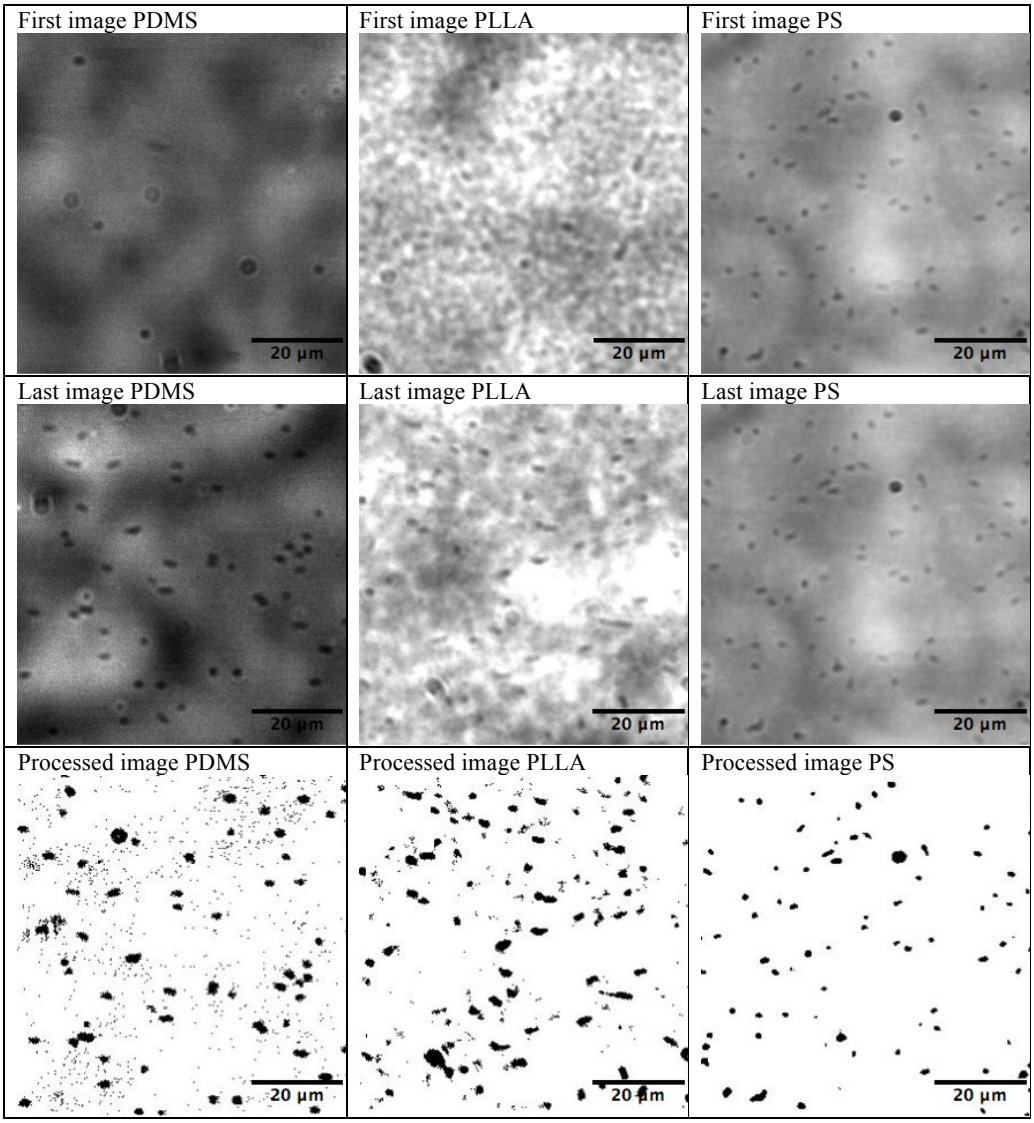

Figure 3.15. Zoomed view of the images of size 92.38 × 73.41 µm^{2}from Figure 3.14

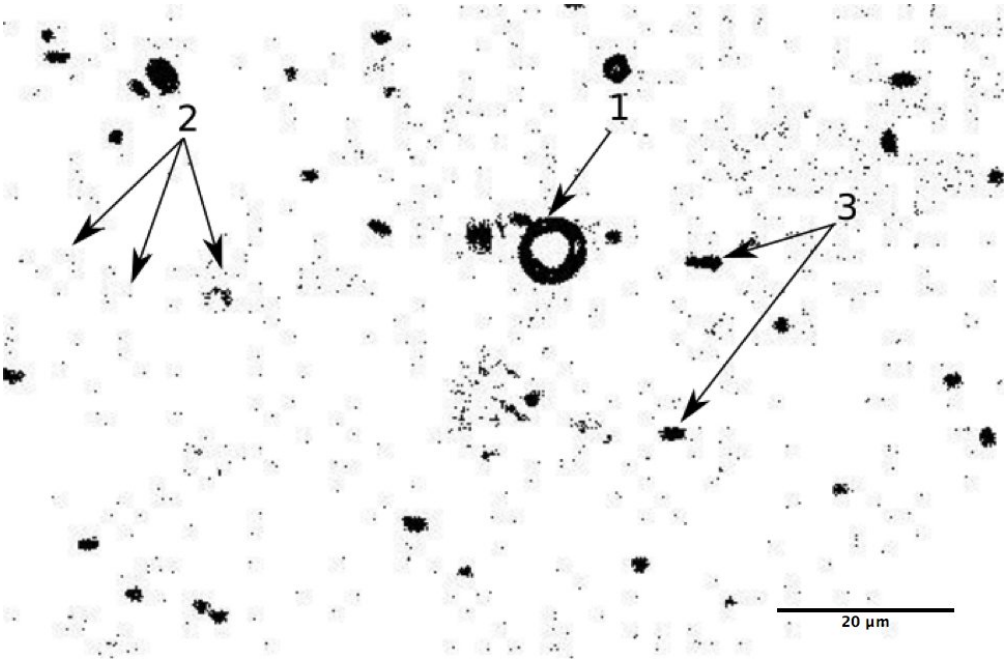

Figure 3.16. Zoomed view of the processed PDMS image of size 92.38 × 73.41 μm^2, including cells (3), PDMS surface disturbance (1) and noise (2).

3.8.4. Adhesion results

The adhesion of *E.coli* over each polymer surface for 30 minutes was carried out. The data shows that the materials have distinct adhesion behaviour. PS is the material with less adhesion, Figure 3.17, while PDMS has the highest. Additionally, it was observed that bacterial adhesion increases linearly with time. Standard deviations were calculated and plotted as error bars.

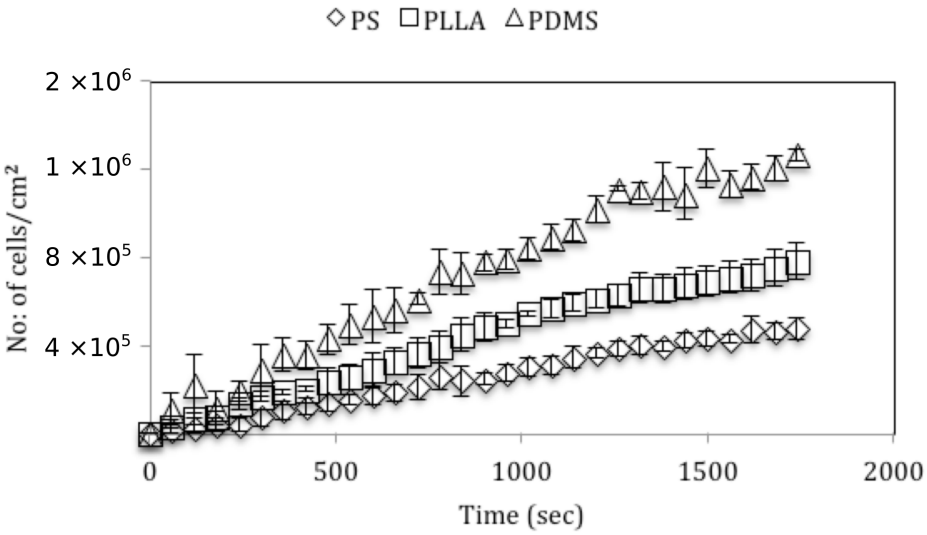

Figure 3.17. *E. coli* adhesion on PLLA, PS and PDMS over time.

An experiment was performed to test if an irregularity (lowered surface region) in the channel can change significantly the adhesion rate. To achieve this goal, experiments were performed in a PDMS channel produced by the same fabrication method. First, a layer of PDMS was spincoated over a glass slide. Then, a scotch tape was used to protect a small region, as described, and afterwards, a second layer of PDMS was spincoated over the first one. The slide was then used to produce the channels. Figure 3.18 shows the bacterial cell density along the channel after 1800 s for three different shear stresses (0.02, 0.2 and 1 Pa.). As can be seen in the figure, the presence of a lowered surface in the scotch tape location is not perceptible. The variability of adhesion along the channel is much higher than any possible effect produced by the lowered surface.

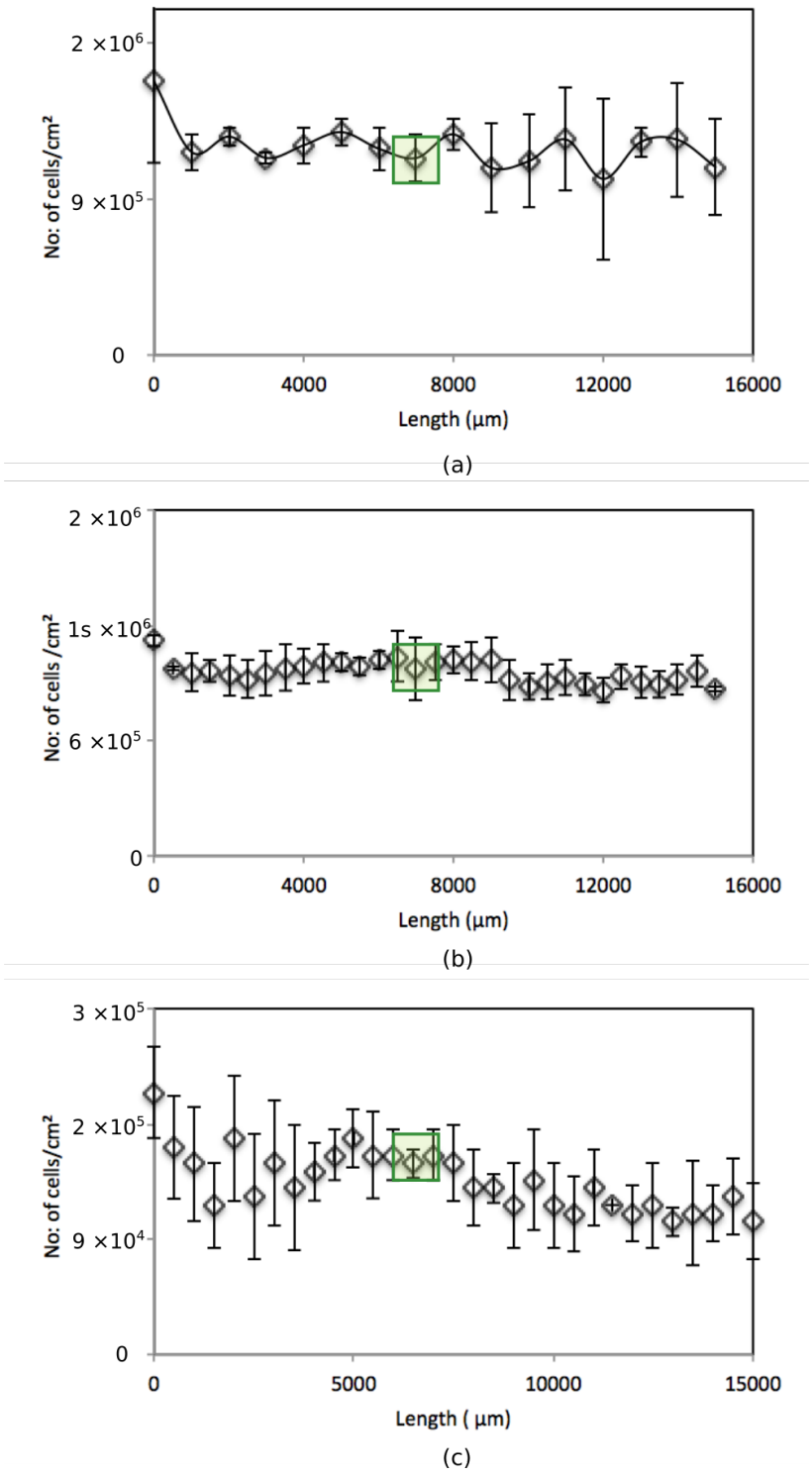

Figure 3.18. Cell density after 1800 s of adhesion for three different shear stresses (a) 0.02 Pa, (b) 0.2 Pa and (c) 1 Pa. The square represents the lowered region in the microchannel.

3.9. Conclusions

A new low-cost method that can be applied in a laboratory with low resources was proposed to fabricate microchannels with polymeric surfaces. The most expensive equipment used in the procedure is a spin coater. The method is suitable to produce microchannels to test bacterial adhesion in different materials in laboratories without sophisticated equipment provided that the material is available as a transparent substrate or that the material is a spincoatable transparent polymer that can be casted by solvent evaporation. This method can be used to leverage an efficient design and optimization of microsystems. The section of the channel containing the region of interest with the polymer is lowered. However, this lowered surface has a predictable effect on the wall shear stress and a negligible one on bacterial adhesion, as shown by adhesion tests and CFD.

The channels obtained can be used to perform bacterial adhesion test under relevant shear stresses. This work contributes to increase the options for experimenters to perform adhesion test in microfluidic devices, with advantages related to reactant consumption and parallelization.

References

[1] A. Skovager, K. Whitehead, H. Siegumfeldt, H. Ingmer, J. Verran, N. Arneborg, Influence of flow direction and flow rate on the initial adhesion of seven Listeria monocytogenes strains to fine polished stainless steel, Int J Food Microbiol, 157 (2012) 174-181.

[2] J.W. Costerton, P.S. Stewart, E.P. Greenberg, Bacterial Biofilms: A Common Cause of Persistent Infections, Science, 284 (1999) 1318-1322.

[3] L.G. Harris, R.G. Richards, Staphylococci and implant surfaces: a review, Injury, 37 Suppl 2 (2006) S3-14.

[4] K.F. Kong, C. Vuong, M. Otto, Staphylococcus quorum sensing in biofilm formation and infection, Int J Med Microbiol, 296 (2006) 133-139.

[5] C.R. Arciola, D. Campoccia, P. Speziale, L. Montanaro, J.W. Costerton, Biofilm formation in Staphylococcus implant infections. A review of molecular mechanisms and implications for biofilm-resistant materials, Biomaterials, 33 (2012) 5967-5982.

[6] T. Bjarnsholt, M. Alhede, M. Alhede, S.R. Eickhardt-Sorensen, C. Moser, M. Kuhl, P.O. Jensen, N. Hoiby, The in vivo biofilm, Trends Microbiol, 21 (2013) 466-474.

[7] A.K. Seth, M.R. Geringer, S.J. Hong, K.P. Leung, T.A. Mustoe, R.D. Galiano, In vivo modeling of biofilm-infected wounds: a review, J Surg Res, 178 (2012) 330-338.

[8] S. Esposito, S.M. Purrello, E. Bonnet, A. Novelli, F. Tripodi, R. Pascale, S. Unal, G. Milkovich, Central venous catheter-related biofilm infections: An up-to-date focus on meticillin-resistant Staphylococcus aureus, Journal of Global Antimicrobial Resistance, 1 (2013) 71-78.

[9] J.C. Middleton, A.J. Tipton, Synthetic biodegradable polymers as orthopedic devices, Biomaterials, 21 (2000) 2335-2346.

[10] S. Ramakrishna, J. Mayer, E. Wintermantel, K.W. Leong, Biomedical applications of polymer-composite materials: a review, Composites Science and Technology, 61 (2001) 1189-1224.

[11] B. Meng, J. Wang, N. Zhu, Q.Y. Meng, F.Z. Cui, Y.X. Xu, Study of biodegradable and self-expandable PLLA helical biliary stent in vivo and in vitro, Journal of materials science. Materials in medicine, 17 (2006) 611-617.

[12] H. Tamai, K. Igaki, E. Kyo, K. Kosuga, A. Kawashima, S. Matsui, H. Komori, T. Tsuji, S. Motohara, H. Uehata, Initial and 6-month results of biodegradable poly-l-lactic acid coronary stents in humans, Circulation, 102 (2000) 399-404.

[13] A. Colvin, C. Sharma, M. Parides, J. Glashow, What is the best femoral fixation of hamstring autografts in anterior cruciate ligament reconstruction?: a meta-analysis, Clin Orthop Relat Res, 469 (2011) 1075-1081.

[14] D.J. Beebe, G.A. Mensing, G.M. Walker, Physics and applications of microfluidics in biology, Annu Rev Biomed Eng, 4 (2002) 261-286.

[15] K.K. Jain, Biochips and Microarrays: Technology and Commercial Potential, Urch Publishing, 2000.

[16] A.D.S. H.A Stone, A.Ajdari, Engineering flows in small devices microfluidics towards lab-on-a-chip, Annual reviews in Fluid Mechanics, 36 (2004) 381-411.

[17] R. Mukhopadhyay, When microfluidic devices go bad, Anal Chem, 77 (2005) 429 A-432 A.

[18] M.D. Levenson, N.S. Viswanathan, R. Simpson, Improving resolution in photolithography with a phase-shifting mask, Electron Devices, IEEE Transactions on, 29 (1982) 1828-1836.

[19] D.C. Duffy, J.C. McDonald, O.J. Schueller, G.M. Whitesides, Rapid Prototyping of Microfluidic Systems in Poly(dimethylsiloxane), Anal Chem, 70 (1998) 4974-4984.

[20] F.J. Blanco, M. Agirregabiria, J. Garcia, J. Berganzo, M. Tijero, M.T. Arroyo, J.M. Ruano, I. Aramburu, K. Mayora, Novel three-dimensional embedded SU-8 microchannels fabricated using a low temperature full wafer adhesive bonding, J Micromech Microeng, 14 (2004) 1047-1056.

[21] L. Che-Hsin, L. Gwo-Bin, C. Bao-Wen, C. Guan-Liang, A new fabrication process for ultra-thick microfluidic microstructures utilizing SU-8 photoresist, J Micromech Microeng, 12 (2002) 590.

[22] A.A. Tseng, Recent developments in micromilling using focused ion beam technology, J Micromech Microeng, 14 (2004) R15.

[23] S. Schlautmann, H. Wensink, R. Schasfoort, M. Elwenspoek, A.v.d. Berg, Powder-blasting technology as an alternative tool for microfabrication of capillary

electrophoresis chips with integrated conductivity sensors, J Micromech Microeng, 11 (2001) 386.

[24] H. Becker, U. Heim, Hot embossing as a method for the fabrication of polymer high aspect ratio structures, Sensors and Actuators A: Physical, 83 (2000) 130-135.

[25] A.M. Morales, C.M. Lieber, A Laser Ablation Method for the Synthesis of Crystalline Semiconductor Nanowires, Science, 279 (1998) 208-211.

[26] K. Ikuta, K. Hirowatari, Real three dimensional micro fabrication using stereo lithography and metal molding, in: Micro Electro Mechanical Systems, 1993, MEMS '93, Proceedings An Investigation of Micro Structures, Sensors, Actuators, Machines and Systems. IEEE., 1993, pp. 42-47.

[27] D.A. Bartholomeusz, R.W. Boutte, J.D. Andrade, Xurography: rapid prototyping of microstructures using a cutting plotter, Journal of Microelectromechanical Systems, 14 (2005) 1364-1374.

[28] Y. Xia, G.M. Whitesides, Soft Lithography, Annual Review of Materials Science, 28 (1998) 153-184.

[29] A. Trampuz, A.F. Widmer, Infections associated with orthopedic implants, Curr Opin Infect Dis, 19 (2006) 349-356.

[30] J.S. Schultz, S. Mansouri, I.J. Goldstein, Affinity sensor: a new technique for developing implantable sensors for glucose and other metabolites, Diabetes Care, 5 (1982) 245-253.

[31] J. Zhou, A.V. Ellis, N.H. Voelcker, Recent developments in PDMS surface modification for microfluidic devices, Electrophoresis, 31 (2010) 2-16.

[32] S.K. Sia, G.M. Whitesides, Microfluidic devices fabricated in Poly(dimethylsiloxane) for biological studies, Electrophoresis, 24 (2003) 3563-3576.

[33] V. Perumal, U. Hashim, Chrome mask design for microfluidic fabrication, in: Advanced Materials Research, Trans Tech Publ, 2013, pp. 276-280.

[34] T. Desai, M. Ferrari, S.N. Bhatia, BioMEMS and Biomedical Nanotechnology: Volume III: Therapeutic Micro/Nanotechnology, Springer US, 2007.

[35] P. Lalanne, P. Chavel, Perspectives for Parallel Optical Interconnects, Springer Berlin Heidelberg, 2013.

[36] J. Narasimhan, I. Papautsky, Polymer embossing tools for rapid prototyping of plastic microfluidic devices, J Micromech Microeng, 14 (2004) 96-103.

[37] P. Vadgama, Surfaces and Interfaces for Biomaterials, Elsevier Science, 2005.

[38] Y. Xia, G.M. Whitesides, Soft Lithography, Angewandte Chemie International Edition, 37 (1998) 550-575.

[39] A. del Campo, C. Greiner, SU-8: a photoresist for high-aspect-ratio and 3D submicron lithography, J Micromech Microeng, 17 (2007) R81.

[40] K.E. Herold, A. Rasooly, Lab on a Chip Technology: Fabrication and microfluidics, Caister Academic Press, 2009.

[41] Z.L. Zhang, C. Crozatier, M. Le Berre, Y. Chen, In situ bio-functionalization and cell adhesion in microfluidic devices, Microelectronic Engineering, 78-79 (2005) 556-562.

[42] J.H. Koschwanez, R.H. Carlson, D.R. Meldrum, Thin PDMS Films Using Long Spin Times or Tert-Butyl Alcohol as a Solvent, Plos One, 4 (2009) e4572.

[43] F.J. Mergulhao, G.A. Monteiro, Analysis of factors affecting the periplasmic production of recombinant proteins in Escherichia coli, J Microbiol Biotechnol, 17 (2007) 1236-1241.

[44] K. Merrett, R.M. Cornelius, W.G. McClung, L.D. Unsworth, H. Sheardown, Surface analysis methods for characterizing polymeric biomaterials, J Biomater Sci Polym Ed, 13 (2002) 593-621.

[45] Y. Yuan, T.R. Lee, Contact angle and wetting properties, in: Surface science techniques, Springer, 2013, pp. 3-34.

[46] B. Janczuk, E. Chibowski, J. Bruque, M. Kerkeb, F.G. Caballero, On the consistency of surface free energy components as calculated from contact angles of different liquids: an application to the cholesterol surface, Journal of colloid and interface science, 159 (1993) 421-428.

[47] C.J. Van Oss, Interfacial forces in aqueous media, CRC press, 2006.

[48] L.C. Simoes, M. Simoes, M.J. Vieira, Adhesion and biofilm formation on polystyrene by drinking water-isolated bacteria, Antonie Van Leeuwenhoek, 98 (2010) 317-329.

[49] C.A. Schneider, W.S. Rasband, K.W. Eliceiri, NIH Image to ImageJ: 25 years of image analysis, Nat Meth, 9 (2012) 671-675.

[50] J.M. Moreira, J.D. Araujo, J.M. Miranda, M. Simoes, L.F. Melo, F.J. Mergulhao, The effects of surface properties on Escherichia coli adhesion are modulated by shear stress, Colloids Surf B Biointerfaces, 123 (2014) 1-7.

[51] J.S. Teodosio, M. Simoes, L.F. Melo, F.J. Mergulhao, Flow cell hydrodynamics and their effects on *E. coli* biofilm formation under different nutrient conditions and turbulent flow, Biofouling, 27 (2011) 1-11.

[52] M. Simoes, L.C. Simoes, S. Cleto, M.O. Pereira, M.J. Vieira, The effects of a biocide and a surfactant on the detachment of Pseudomonas fluorescens from glass surfaces, Int J Food Microbiol, 121 (2008) 335-341.

[53] A.D. Michelson, Preface, in: A.D. Michelson (Ed.) Platelets (Second Edition), Academic Press, Burlington, 2007, pp. xxi.

[54] L.S. Ronald, W. University of, Analysis of Pathoadaptive Mutations in Escherichia Coli, University of Washington, 2008.

[55] H.J. Busscher, H.C. van der Mei, Microbial adhesion in flow displacement systems, Clin Microbiol Rev, 19 (2006) 127-141.

[56] B.P. Leonard, A stable and accurate convective modelling procedure based on quadratic upstream interpolation, Comput. Methods Appl. Mech. Eng., 19 (1979) 59-98.

[57] R.I. Issa, Solution of the implicitly discutised fluid flow equations by operating-splitting, J. Comput Phys, 62 (1986) 40-65.

Chapter 4

Biological adhesion – Effect of surface properties

Abstract

Microchannels fabricated with different biocompatible polymers were utilized to determine the adhesion rate with *Escherichia coli* (E. *coli)* suspension. Different polymeric surfaces - namely: cellulose acetate (CA), polydimethylsiloxane (PDMS), polystyrene (PS), polyamide (PA), poly L-Lactide (PLLA) and polyethylene oxide (PEO) - were fabricated and implemented into the microchannel through the developed in-house method along with the xurographic technique. The adhesion rate for all the polymeric surfaces were compared for two different wall shear stresses namely 0.01 Pa and 0.02 Pa. Along with 6 polymeric surfaces, glass was used as a control surface. The surfaces were determined as hydrophilic or hydrophobic based on the surface contact angle obtained by the sessile drop method. Attempts were made to relate adhesion rate with wall shear stress, hydrophobicity and zeta potential. No significant trends were identified, suggesting that for the two shear stresses studied, adhesion is independent of the surface properties. Further studies are necessary, with a larger range of shear stresses. Adhesion on PDMS surface was studied for a range of shear stresses from 0.01 Pa to 2 Pa. Adhesion rate was small for very low shear stress and attained a maximum for 0.2Pa decreasing for larger wall shear stresses. Also adhesion rate obtained for 0.01 Pa and 0.02 Pa were compared with the macroscale study with parallel plate flow chamber. There was not a statistical significant difference between adhesion at different scales for the same wall shear stress. The computational fluid dynamics simulation was used to verify the shear stress in the region of interest in the microchannel. This work was developed to study the adhesion of living cells in polymeric surfaces inserted in microchannels through the technique detailed in chapter 3.

4.1 Introduction

There are a variety of biomedical applications, for example, arterial implants, catheters, blood pump systems or controlled drug delivery valves, in which chronic infections occur [1]. In these infections, the first step is the adhesion of microorganisms over a conditioning film (saliva, blood, urine etc.) covering the surface. Biofilm formation is the second step, which depends on the Brownian motion, gravitation, diffusion, convection or intrinsic movement of the microorganisms [2]. Biomedical applications use, sometimes, smart materials at small scales for novel functions [3]. Therefore, there is a need to understand the dynamics of biofilm development and development in small scale materials to prevent infections [4].

The adhesion of microorganisms to a surface is also an important study in food process industries and in many chemical and biomedical industrial processes. For over two decades, membrane biofouling in water treatment systems has been an intense research topic [5]. However, a complete understanding of the initial fouling mechanism is still lacking.

Several effects on cell adhesion have been studied: different surface materials [6], different bacteria [7], hydrophilicity and hydrophobicity of the surfaces [8], electrical charges of the bacteria [9], bacterial cell wall hydrophobicity [10, 11] and wall shear stresses [12, 13].

Many studies reported the adhesion on different surface materials. A recent one stated that adhesion is governed by a combination of physico-chemical-macromolecular and wall shear force effects [14]. Bacterial adhesion studies on glass slides were performed for shear rates ranging from 30 to 200 s^{-1} and it was reported that bacterial colonization starts at high wall shear rates and the subsequent monolayer develops at a low shear rate after 1200 hours of experiment [15].

In microchannels, the number of studies about adhesion in polymeric surfaces is scarce. Adhesion of L1210 cells on sulphonated and nonsulphonated micro polymeric surfaces [16] and cell adhesion on poly-methylmethacrylate (PMMA) were reported

on rough and smooth micro surfaces [17]. Very few adhesion studies have been carried out in surface modified PDMS microchannels [18-20].

Surface modification has paved way to reduce biofouling [21], in particular when applied to microfluidic devices. Sharma et al. [22] experimented two techniques, gas-phase modification and wet chemical modification, to develop a stable surface. Pinto et al. [23] modified the PDMS surface using an argon low-pressure plasma technique and reported that the surfaces became non-toxic and slightly haemolytic making them suitable for several biomedical applications.

The impact of electrostatic interactions, an often ignored effect, was studied by Loosdrecht et al. [24] to predict initial bacterial adhesion. Apart from the wall shear stress, the zeta potential effect was studied to understand the impact of electrostatic interactions on adhesion in different polymeric surfaces. A similar study was developed by Wang et al. [25] on different glycopolymer surfaces, reporting that lectin-carbohydrate interactions had much more significance on adhesion than electrostatic interactions. A higher adhesion was observed with *P. aeruginosa* than with *Escherichia coli* on stiffer glycopolymer surfaces in high ionic strength conditions.

Few adhesion studies were done on motile and non motile *E. coli,* according to the velocity of the suspension flow [26]. Experiments were carried out with microorganisms with and without the presence of flagella and appreciable differences were reported [27].

In this chapter, a study of *E. coli* adhesion to polymeric surfaces is presented. The experiments were performed at 37 °C and at different wall shear stress conditions. The objective was to find a relationship between wall shear stress and thermodynamic properties, namely hydrophobicity and Zeta potential. The polymeric surfaces were inserted in the microchannels through the technique detailed in Chapter 3 (section 3.2.4).

4.2 Materials and methods

4.2.1 Selection of polymers

A survey on different biocompatible biomedical polymers was carried out having in mind their limitations to be used in microfluidics. The polymers must be transparent after coated to the slides, they should be spincoatable to have uniform thickness and also be able to be retained in the substrate till the end of the experiment and even for more time [28, 29]. Several biomedical polymers usually used in biomedical applications were reviewed and their properties and applications listed. After eliminating the polymers that do not respect the three criteria, nine biocompatible polymers from different fields [30-32] were selected and manufactured.

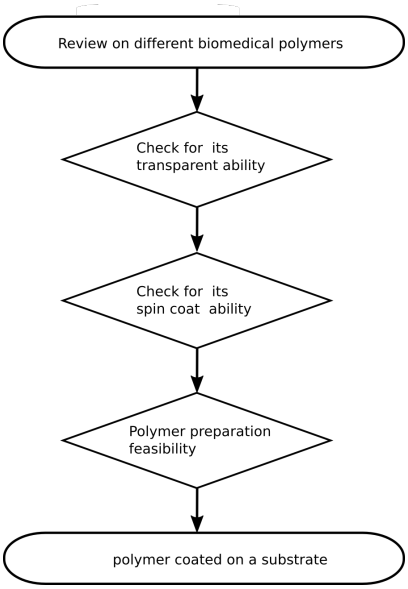

Figure 4.1. Flow chart describing the selection of polymers for the initial adhesion study.

The polymers selected were cataloged in terms of applications such as: urinary catheters, urinary bladder, tracheal, etc (Table 4.1).

The polymers were prepared and spincoated over a glass slide and durability tests were performed at the shear stresses of the assays [33], only five polymers were suitable to be used: cellulose acetate (CA), polyamide (PA), polydimethylsiloxane (PDMS), poly L-Lactide (PLLA) and polyethylene oxide (PEO).

Table 4.1 Polymers application

Polymer	Application	Selected references
Cellulose acetate (CA)	Orthopedic applications due to its strength and stiffness.	[34, 35]
Polyamide (PA)	Woven mesh implant (SupraFOIL, Supramesh, S. Jackson, Inc., Alexandria, VA)	[36]
Polydimethylsiloxane (PDMS)	Micro-transponder system for measuring intra ocular pressure, blood pressure and a system for stimulating nerve cells. PDMS based porous inorganic hybrid materials for good hepatite particle deposition to get a good bond with soft and hard body tissues.	[37, 38]
Poly L-Lactide (PLLA)	Endotine forehead fixation device, endotine midface (Coapt systems, Inc., Palo Alto, CA)	[36]
Polyethylene oxide (PEO)	Micro container for drug delivery applications. Different concentration ranges are used for delivering drug for rectal, ophthalmic, parenteral and percutaneous applications.	[38]
Polystyrene (PS) (commercially available Petridish)	Cell culturing.	[39]

4.2.2. Zeta potential and water contact angles for different polymers

Zeta potential was determined with a Nano Zeta sizer from Malvern Instruments by mixing the dried polymer particles in a solution. Zeta potential is the main index that provides information about the electrostatic repulsion between the polymer surface and the cell assay [40]. When the zeta potential is high, the repulsion force between similarly charged particles is strong and aggregation is avoided. When the zeta potential value is small, the repulsion between similarly charged particles is weak. The zeta potential was calculated using Helmholtz–Smoluchowski equation (1). The water contact angles and the hydrophobicity of the polymers listed in Table 4.1 were obtained as described in Chapter 3 (section 3.3).

$$\zeta = 4\pi\mu\eta / D \qquad (1)$$

4.2.4 Wall shear stress from CFD

Numerical simulations were made in Ansys Fluent CFD package (version 14.5) to obtain the wall shear stresses in the microchannels. A rectangular microchannel of

width 450 μm, height 100 μm and length of 5000 μm was the model created by Design Modeller 14.5. The schematic representation of the microchannel is shown in Figure 4.2. The numerical grid was constructed using Meshing 14.5. The grid was denser in the first half of the channel; 124,154 hexahedral cells uniformly distributed, in counterpart to 94,374 hexahedral cells in the second half. Results were obtained by solving the Navier-Stokes equations for laminar regime using the PISO algorithm, and the QUICK and PRESTO schemes. The no slip boundary condition was considered in all the walls.

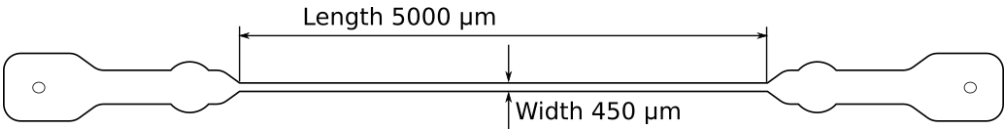

Figure 4.2. Straight microchannel with dimensions

In the simulations, a uniform velocity profile was set at the inlet and the relative pressure was set to zero at the outlet. The inlet velocity ranged between 2.5×10^{-4} and 1.45×10^{-3} m/s, corresponding to a flowrate between 1.13×10^{-11} and 4.34×10^{-12} m^3/s and a Reynolds number between 3.6×10^{-2} and 6.22×10^{-2}. For the fluid, the properties of water (density and viscosity) at 37 ºC were used. Simulations were made in transient mode, to assure convergence and to capture transient flow structures. For each case, 2s of physical time were simulated with a fixed time step of 10^{-4} s.

Two kinds of microchannels were used in this chapter. The microchannel that was used for studying the initial adhesion and the effect of the flow rate is represented in Figure 4.3 is the microchannel that is used for studying the initial adhesion based on the effect of flow rate. The other microchannel, which was used for studying the initial adhesion and the effect of the polymeric surface, is shown in chapter 3. Simulations with this microchannel were made to understand whether there are large changes in the WSS values before and after the lowered surface.

For a particular flowrate, the wall shear stress was obtained by numerical simulation. Figure 4.3 represents the wall shear stress along the rectangular microchannel. The wall shear stress is constant along all the flow direction. A detailed

representation of the viewing region in Figure 4.3 shows that the wall shear stress is constant in the region where adhesion will be measured.

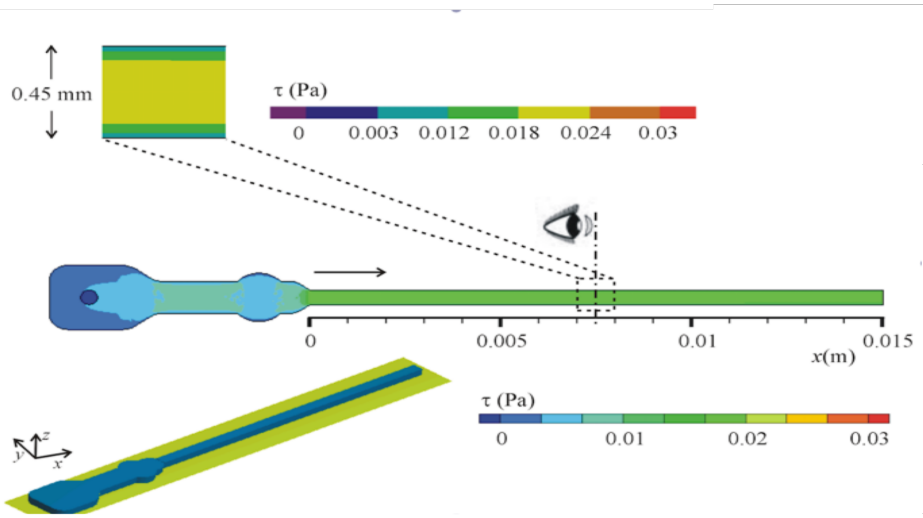

Figure 4.3. Wall shear stress in the microchannel obtained by numerical simulation

4.2.5. Experimental setup

The experimental setup for obtaining the adhesion rate in different polymeric surfaces is described in Chapter 3. A schematic representation of the microchannel with the polymeric surface is in Figure 4.4. The cell suspension enters the inlet port, with the help of a syringe pump, at a particular flowrate and, by consequence, a well-defined wall shear stress. The microscope was used to visualize the adhesion in the polymeric surface.

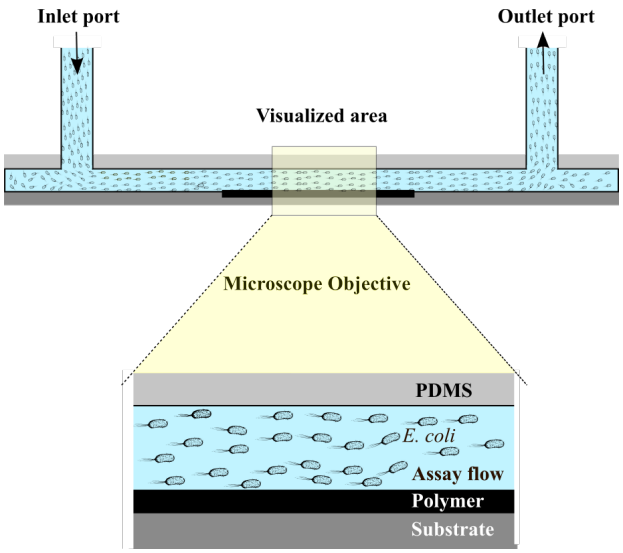

Figure 4.4. The microchannel with the polymeric surface and an enlarged view of the focusing area

4.3 Results and discussion

4.3.1 Contact angle

The contact angles were obtained with water, formamide and α-bromonaphtalene and the respective values are in Table 3.3 of Chapter 3. Vogler (1998) suggested that water contact angles in hydrophobic surfaces are greater than 65° and in hydrophilic surfaces lesser than 65° [41]. The PA, PDMS, PLLA and PS are hydrophobic materials since their contact angles are above 65° while CA, PEO and glass were hydrophilic materials (Table 3.3).

4.3.2. Initial adhesion on different surfaces

The initial adhesion in the seven selected surfaces was done. The *E. coli* suspension was pumped into the rectangular microchannel and the images recorded for 30 minutes. A brief picture of how the cells adhere to the surface (not yet processed with ImageJ) over time (15 mins interval gap) is shown in Figure 4.5 (b).

Initial	15th min	30th min
CA		
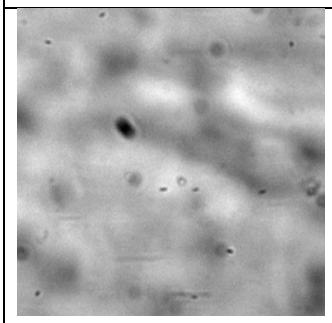	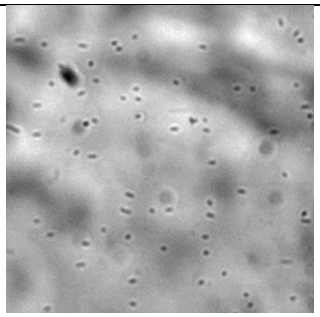	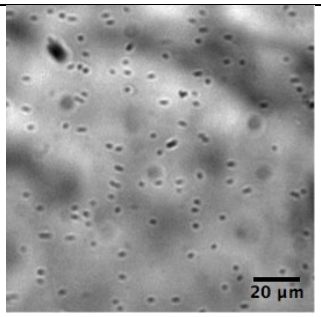
PA		
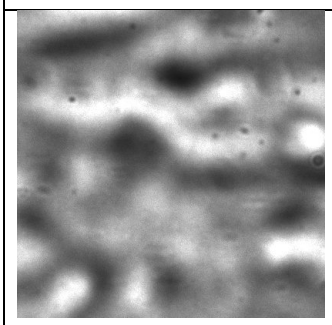	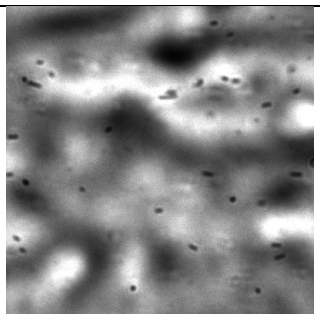	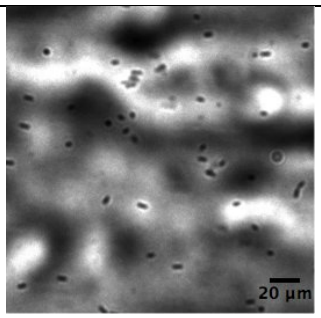
PDMS		
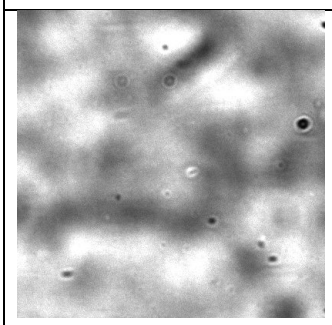	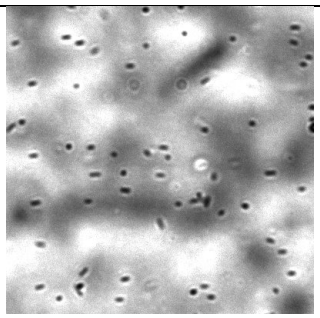	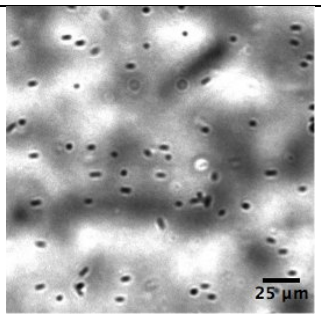

Figure 4.5 (a). Adhesion of *E.coli* at different time points on different surfaces (CA, PA, PDMS) of size 201.83 × 191.05 μm^2

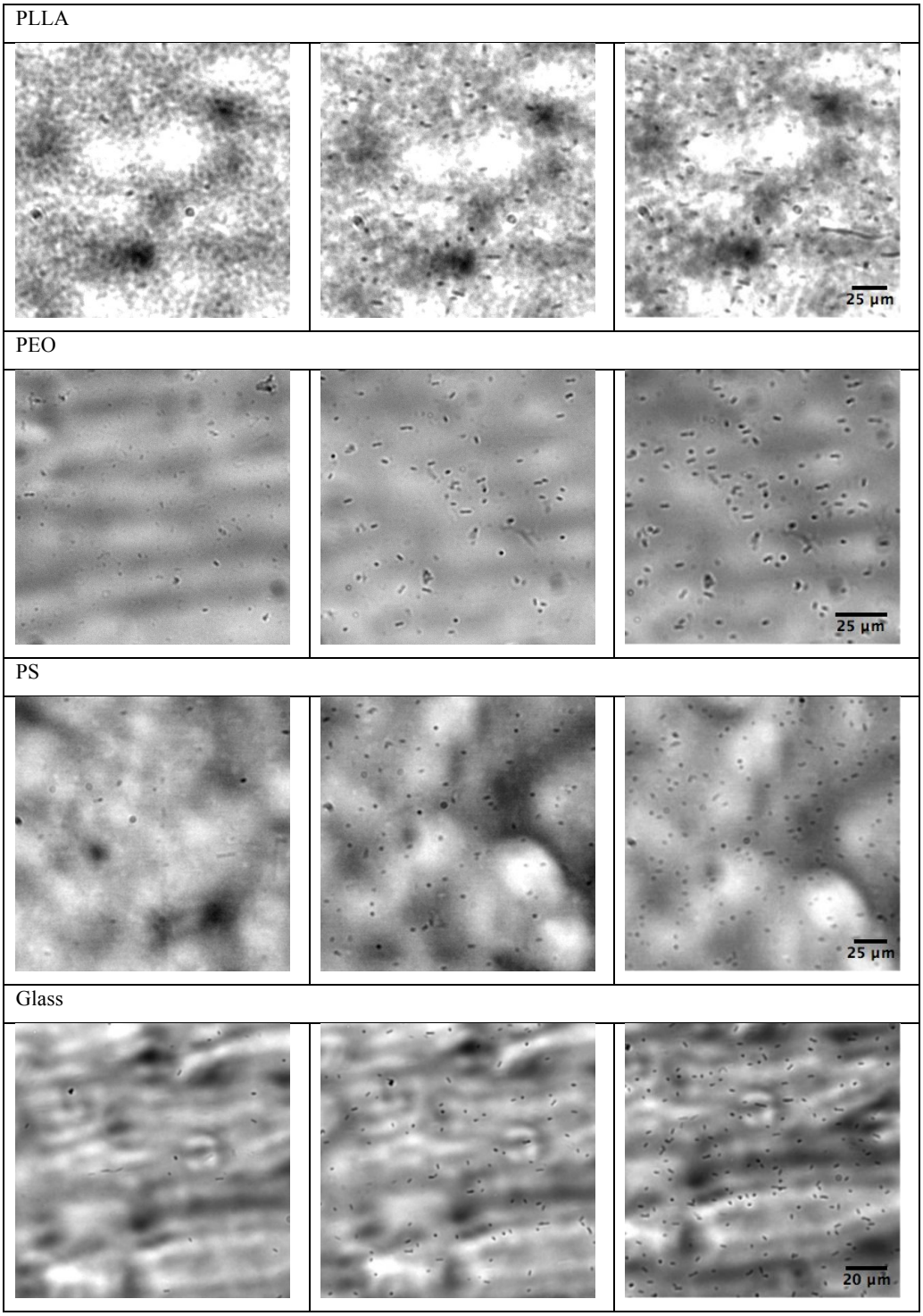

Figure 4.5 (b). Adhesion of *E.coli* at different time points on different surfaces (PLLA, PEO, PS, Glass) of size 201.83 × 191.05 μm^2

These are cropped oversized images of the captured microscopic images of size 201.83 × 191.05 μm^2, so that the bacteria can *be* easily observed over the surface. Analysing in sequence (initial, 15th min and 30th min), the images clearly bring to light that cells adhere at some particular rate in a given surface.

The initial adhesion, in the seven different surfaces, was quantified. For each polymeric surface, three trials were made to assure repeatability. Figure 4.6 shows the results obtained for a microchannel with a coated cellulose acetate surface**.** In Figure 4.7**,** the average of the three trials is plotted along time**.** Also represented are the standard deviation and a trend line to quantify the adhesion rate - 578.55 cells/ (s.cm^2). The adhesion of *E. coli* varies from surface to surface, and further results are presented in following sections.

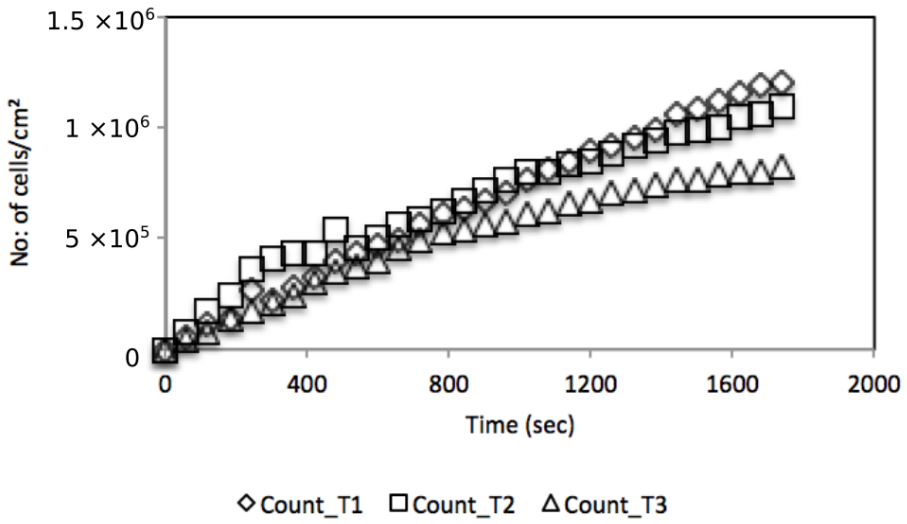

Figure 4.6. Adhesion experiments (three trials) made during 30 mins in a cellulose acetate coated microchannel.

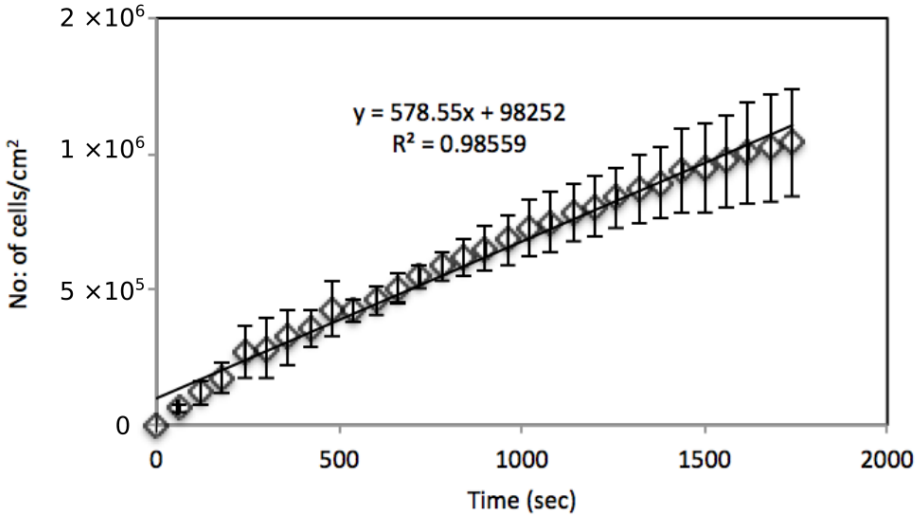

Figure 4.7. Average adhesion of *E. coli* on cellulose acetate along time; the adhesion rate is 578.55 nº of cells/(cm^2.s)

4.3.3. Effect of wall shear stress

The wall shear stress has different values according to the biomedical device and to the human body location. It ranges from 0.01 Pa to beyond 5 Pa as shown in Table 4.2.

Table 4.2. Wall shear stress in different locations of the human body and also in biomedical devices

Location	Shear stress
Femoral artery	0.3 – 0.5 Pa [43]
Branchial artery	0.4 – 0.5 Pa [43]
Carotid artery	1.1 – 1.3 Pa [44]
Infra-renal aorta	0.5 Pa [43]
Urinary catheter	0.01 Pa [45]
Bladder implant	0.02 – 0.1 Pa [46]
Central venous catheters	300 mL/min in a 18 mm catheter tube [47]
Endo tracheal tubes	0.15 – 0.5 Pa [48]
Vena cava, veins	0 – 0.1 Pa [49]
Descending aorta	0.6 Pa [49]
Veins	0.7 Pa [49]
Ascending Aorta, Arteries	1.1 Pa [49]
Venules	1.6 Pa [49]
Arterioles, critical shear stress for cancer cells detachment in microchannels	5.2 Pa [49], 2 – 5 Pa [50]

Biomedical devices with polymeric surfaces in contact with flowing biofluids includes: blood glucose monitors, insulin delivery devices, blood pressure monitors and microfluidic devices for detection of infectious diseases [42]. So the knowledge of initial adhesion over a large range of wall shear stress is important information to predict the vulnerability of the biomedical devices to biofilm contamination.

PDMS was selected to study the effect of shear stress on cell adhesion. PDMS is a versatile polymer with its biocompatibility, inertness, non-toxicity and non-flammable characteristics. It is widely used in applications ranging from contact lenses to biomedical devices and also in sensors [42]. The PDMS has many applications in the biomedical engineering field, where it endures wall shear stresses up to 70 Pa [51].
In the present study, a wall shear stress range from 0.01 to 2 Pa was selected, mainly due to two reasons:

- In a microchannel of 450 μm x 100 μm cross section, for wall shear stresses lower than 0.01 Pa, the flow is very small and the adhesion of *E. coli* too slow to be observed through the microscope;
- To obtain wall shear stresses above 2 Pa, the flow must be too high and the adhesion of *E. coli* is scarce.

In that range, a total of eleven wall shear stresses were selected as reported in Table 4.3. The adhesion rate was calculated for each wall shear stress and the values are listed in Table 4.3.

Figure 4.8 shows the average adhesion results and the respective standard deviations from three trials, for different wall shear stresses. The adhesion rate after attaining a peak near 0.2 Pa gradually falls down up to 0.4 Pa. Increasing the wall shear stress, the adhesion rate decreases, converging to almost zero. Included in Figure 4.8 are the wall shear stress ranges for different human circulatory settings. Several blood vessels, in particular cardiovascular vessels, have wall shear stresses less than 0.8 Pa [52].

Table 4.3. Wall shear stresses and correspondent adhesion rates for PDMS microchannels

Wall shear stress (Pa)	Adhesion rate (nº of cells/(cm^2.s))
0.0104	499.13
0.0208	838.5
0.154	1029.6
0.231	829.7
0.307	510.78
0.346	274.4
0.384	237.88
0.484	288.33
0.75	207.1
1	199.46
2	111.71

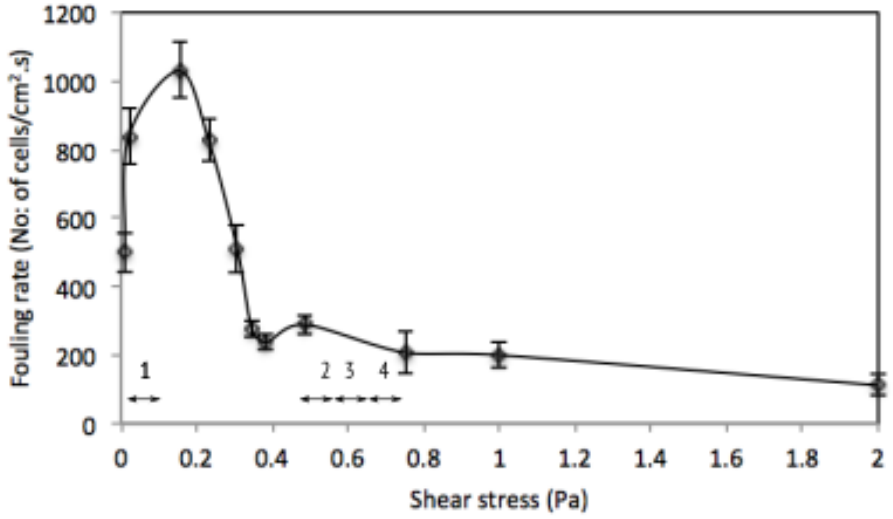

Figure 4.8. Fouling rate in a PDMS surface versus wall shear stress applied. Ranges of wall shear stress in human circulatory settings: 1) vena cava, aorta, veins urinary catheter, bladder implant; 2) venules, infra-renal aorta [43] ; 3) arteries; 4) capillaries.

It should be stressed that the adhesion for low wall shear stresses grows linearly along the 30 minutes duration of the experiment (Figure 4.9 for 0.0208 Pa) while for high values (Figure 4.10 and Figure 4.11 for 2 Pa) it is linear during a short initial period remaining almost constant after that, so the trendline was fitted for first initial 200 s for the example shown in Figure 4.11.

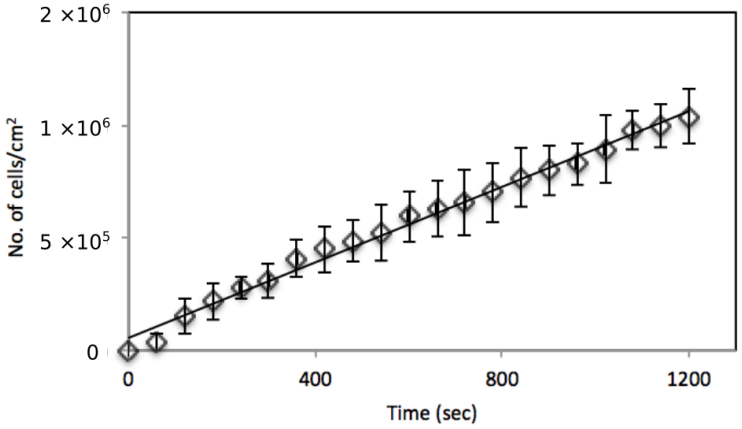

Figure 4.9. *E. coli* bacteria adhesion along experiment for a low wall shear stress (0.0208 Pa). Linear trend during 1200 s.

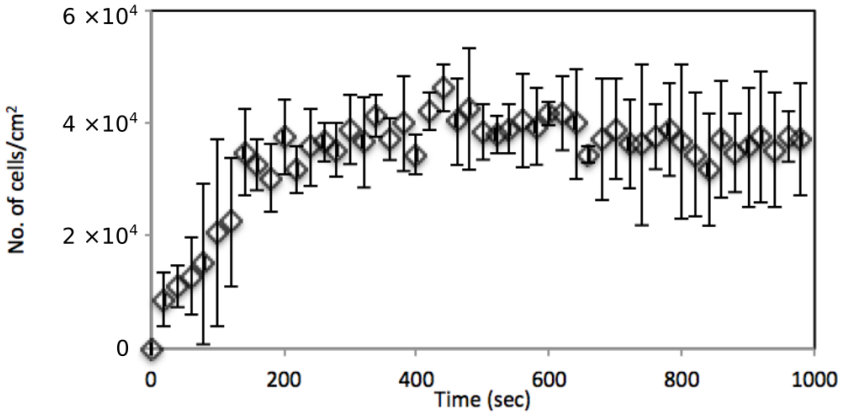

Figure 4.10. *E. coli* bacteria adhesion along experiment for a high wall shear stress (2 Pa). The adhesion stops after 200 s.

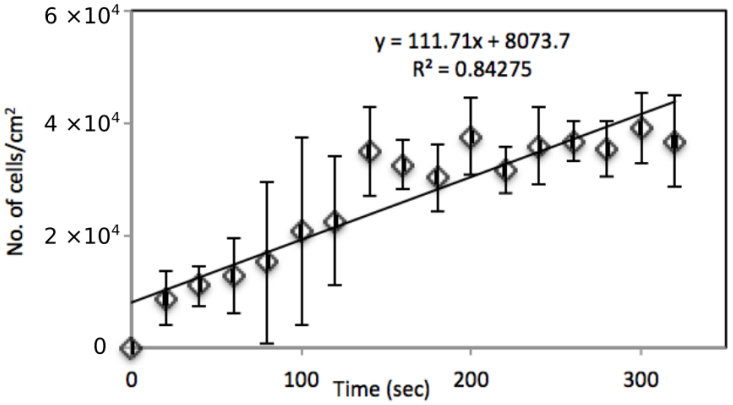

Figure 4.11. Trendline fitted up to 200 s for the plot in Figure 4.10

4.3.4 Contact angle effect on adhesion

The contact angle effect on cell adhesion is plotted in Figure 4.12 for two different wall shear stresses, 0.01 Pa and 0.02 Pa. The adhesion rates for PA (69.4^0), PDMS (113.6^0) and glass (16.4^0) at 0.02 Pa are higher than at 0.01 Pa while the adhesion in PLLA (88.03^0) is more or less independent of the wall shear stress applied. A different trend can be observed for CA (65.2^0), PEO (55.5^0) and PS (80.8^0); the adhesion rate is higher for 0.01 Pa than for 0.02 Pa. The diversity of results explains why certain materials are chosen for specific applications.

With these different trends there is no clear effect of the contact angle on the cell adhesion. This effect needs to be further studied with more wall shear stresses and different surfaces.

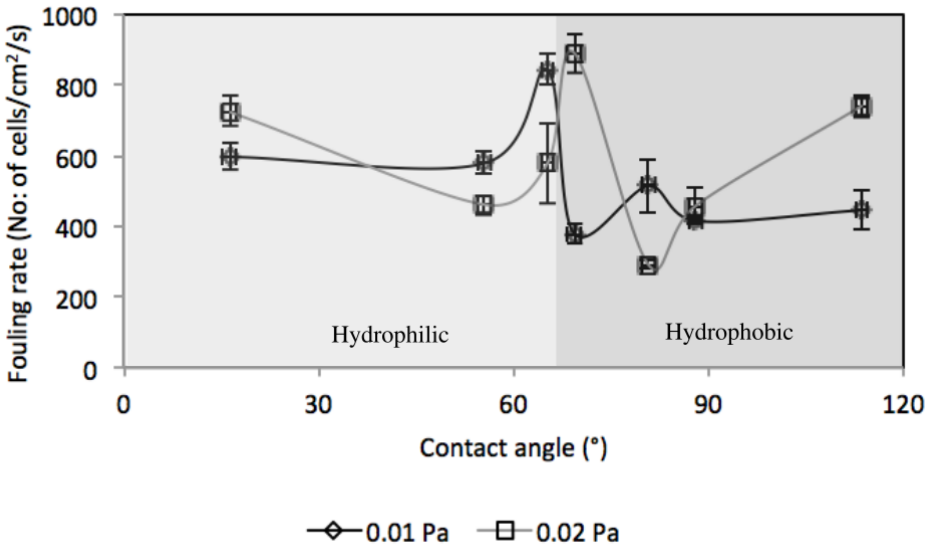

Figure 4.12. *E. coli* bacteria fouling rates on different polymers at two wall shear stresses (0.02 and 0.01 Pa) versus contact angle

4.3.5. Effect of hydrophobicity on adhesion

The hydrophobicity values of the surfaces calculated in Chapter 3 are reproduced in Table 4.4. The negative values are more hydrophilic in nature.

According to the table, PLLA (- 65.32 mJ/m^2) is the most hydrophilic material, while glass is the most hydrophilic (27.99 mJ/m^2). When the hydrophobicity is high, the cells should have difficulty to adhere to the surface. However, the results in Figure 4.13 do not show this trend. A detail study is needed for further clarification.

Table 4.4. Hydrophobicity for different surfaces along with adhesion rates for 0.01 Pa and 0.02 Pa.

Surface	Hydrophobicity (mJ/m^2)	0.01 Pa cells/(cm^{2}s)	0.02Pa cells/(cm^{2}s)
GLASS	27.99	595.9	762.2
PEO	0.34	578.9	474.4
CA	-36.04	837.6	570.4
PA	-37.58	379.5	891.4
PS	-49.56	514.4	290.3
PDMS	-61.81	446	741
PLLA	-65.31	419.2	457.8

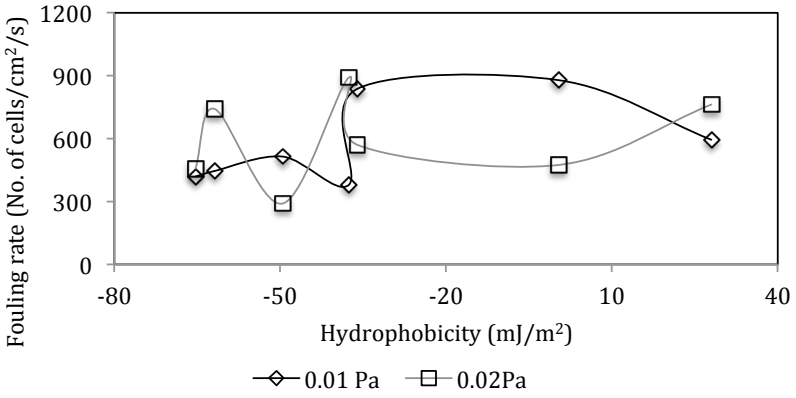

Figure 4.13. *E. coli* bacteria fouling rate versus hydrophobicity of the surface

4.3.6. Effect of zeta potential on adhesion

The zeta potential values obtained for all the polymer surfaces are negative as shows Table 4.5. The *E. coli* is a Gram-negative bacterium with negative charge. Therefore both have negative charges (*E. coli* and polymer surface) favoring the repulsion instead the adhesion. On seeing the results in Figure 4.14, where the adhesion level is high, adhesion rate does not seem to have any solid relation with the zeta potential values. Proper further insight into this topic is required to understand adhesion rate in terms of zeta potential.

Table 4.5 Zeta potential values for each polymeric surface

Polymeric surfaces	Zeta potential (mV)
CA	-23.4
PA	-28.0
PDMS	-29.3
PLLA	-27.9
PEO	-11.0
PS	-29.6
Glass	-37.0

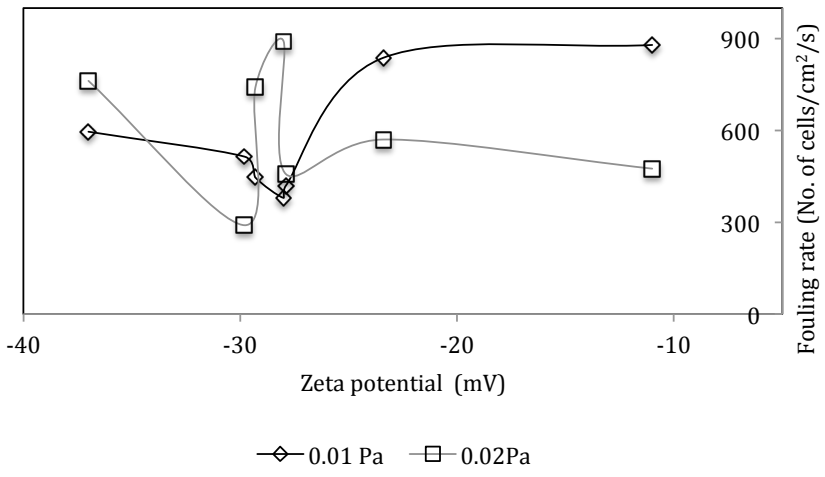

Figure 4.14. *E. coli* bacteria fouling rate versus zeta potential

4.3.7 Adhesion rate in micro and macro scales.

The adhesion rates in the microchannel were compared with those obtained in a macroscale parallel plate flow chamber (PPFC- the LEPABE group of FEUP has this equipment). The microscopic slides were coated with the polymers and the adhesion rates were analyzed in the PPFC at the same wall shear stress (microchannel) through different flowrates. The volumetric scale-up factor, between PPFC and microchannel, is about 50000x, while the aspect ratio is higher in the microchannel. The average wall shear stress chosen for the comparison was 0.02 Pa. As already referred, approximate shear stress values can be found in the human body at different locations like: urethra [53], uterus [54] and veins [55].

In Figure 4.15, the adhesion rates obtained in the microchannel and in the PPFC are compared. It is observed that, when similar wall shear stresses are used in both scales, similar adhesion rates are obtained whatever the surface. This similarity is an advantage, since it allows the choice of the scale experiment depending on the expertise and equipment available. Micro flow systems can be used taking advantage of lower hold-up volumes or macro flow systems can be selected in order to obtain a higher biofilm mass, which can be used for further biochemical analysis [33].

The highest adhesion rate is in PA for both scales and the lowest in PLLA also for both scales. The highest adhesion rate was expected to be found in a hydrophobic surface and the lowest in a hydrophilic surface (glass [56]). However the results do not follow this trend as explained before.

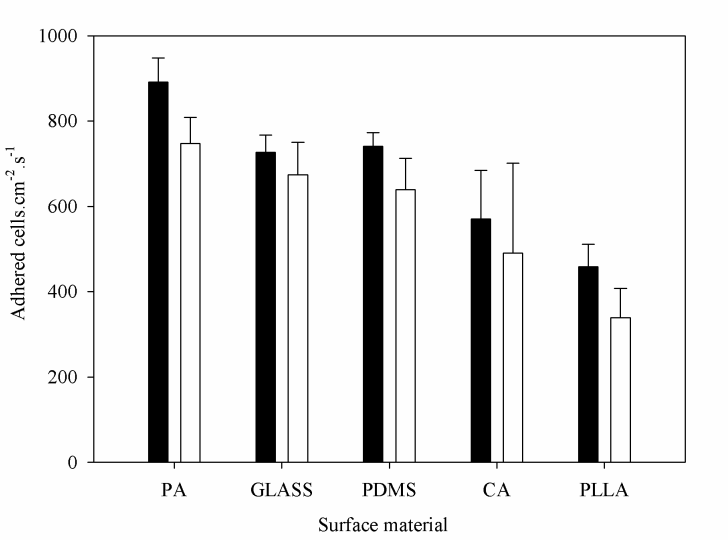

Figure 4.15. *E. coli* bacteria adhesion rates on PA, glass, PDMS, CA and PLLA obtained in the microchannel (black bars) and in the PPFC (white bars). Error bars shown for each surface represent the standard deviation from three independent experiments [33]

4.4. Conclusions and future work.

The adhesion study performed in a PDMS surface for wall shear stresses ranging from 0.01 Pa to 2 Pa shows a consistent trend. After attaining a peak near 0.2 Pa, the adhesion rate gradually falls down up to 0.4 Pa. For higher shear stress values, the adhesion rate decreases, converging to almost zero. This data can be used to understand as how the PDMS surface would get fouled while operating in an implant or in any micro medical device.

A consistent correlation between bacterial adhesion rates and material surface properties (hydrophobicity and zeta potential) was not found. Further studies should be performed to better understand the adhesion on a thermodynamic scale. The polarity of the surfaces should also be considered to get an insight into the adhesion phenomenon. Also a database should be created for each biomaterial.

The biofouling rate comparison between micro and macro flow systems showed interesting results. The observed similarity between the adhesion rates is an added

advantage, as it allows the choice of the scale experiment depending on the expertise and equipment available on the lab.

References.

[1] T. Bjarnsholt, The role of bacterial biofilms in chronic infections, APMIS, 121 (2013) 1-58.

[2] R. Bos, H.C. van der Mei, H.J. Busscher, Physico-chemistry of initial microbial adhesive interactions - its mechanisms and methods for study, Fems Microbiol Rev, 23 (1999) 179-230.

[3] F. Greco, V. Mattoli, Introduction to Active Smart Materials for Biomedical Applications, in: G. Ciofani, A. Menciassi (Eds.) Piezoelectric Nanomaterials for Biomedical Applications, Springer Berlin Heidelberg, 2012, pp. 1-27.

[4] G.A. Truskey., F. Yuan., D.F. Katz, Transport Phenomena in Biological Systems, 2004.

[5] H.S. Vrouwenvelder, J.A.M. van Paassen, H.C. Folmer, J.A.M.H. Hofman, M.M. Nederlof, D. van der Kooij, Biofouling of membranes for drinking water production, Desalination, 118 (1998) 157-166.

[6] U. Hersel, C. Dahmen, H. Kessler, RGD modified polymers: biomaterials for stimulated cell adhesion and beyond, Biomaterials, 24 (2003) 4385-4415.

[7] J.H. Lee, G. Khang, J.W. Lee, H.B. Lee, Interaction of Different Types of Cells on Polymer Surfaces with Wettability Gradient, Journal of Colloid and Interface Science, 205 (1998) 323-330.

[8] T. Horbett, J. Waldburger, B. Ratner, A. Hoffman, Cell adhesion to a series of hydrophili–hydrophobic copolymers studies with a spinning disc apparatus, Journal of biomedical materials research, 22 (1988) 383-404.

[9] M.A. Lopes, F.J. Monteiro, J.D. Santos, A.P. Serro, B. Saramago, Hydrophobicity, surface tension, and zeta potential measurements of glass-reinforced hydroxyapatite composites, Journal of Biomedical Materials Research, 45 (1999) 370-375.

[10] M.C. van Loosdrecht, J. Lyklema, W. Norde, G. Schraa, A.J. Zehnder, The role of bacterial cell wall hydrophobicity in adhesion, Appl Environ Microbiol, 53 (1987) 1893-1897.

[11] R. Oliveira, J. Azeredo, P. Teixeira, A. Fonseca, The role of hydrophobicity in bacterial adhesion, (2001).

[12] J.E. Duddridge, C. Kent, J. Laws, Effect of surface shear stress on the attachment of Pseudomonas fluorescens to stainless steel under defined flow conditions, Biotechnology and bioengineering, 24 (1982) 153-164.

[13] P.F. Davies, A. Robotewskyj, M.L. Griem, Quantitative studies of endothelial cell adhesion. Directional remodeling of focal adhesion sites in response to flow forces., J Clin Invest, 93 (1994) 2031-2038.

[14] M.G. Katsikogianni, Y.F. Missirlis, Bacterial adhesion onto materials with specific surface chemistries under flow conditions, Journal of materials science. Materials in medicine, 21 (2010) 963-968.

[15] T. Paris, S. Skali-Lami, J.C. Block, Effect of wall shear rate on biofilm deposition and grazing in drinking water flow chambers, Biotechnology and bioengineering, 97 (2007) 1550-1561.

[16] J. Dobkowski, R. Kolos, J. Kamiński, H.M. Kowalczyńska, Cell adhesion to polymeric surfaces: experimental study and simple theoretical approach.
, J Biomed Mater Res, 47 (1999) 234-242.

[17] M. Lampin, R. Warocquier-Clérout, C. Legris, M. Degrange, M.F. Sigot-Luizard, Correlation between substratum roughness and wettability, cell adhesion, and cell migration, Journal of Biomedical Materials Research, 36 (1997) 99-108.

[18] H. Makamba, J.H. Kim, K. Lim, N. Park, J.H. Hahn, Surface modification of poly (dimethylsiloxane) microchannels, Electrophoresis, 24 (2003) 3607-3619.

[19] H. Lu, L.Y. Koo, W.M. Wang, D.A. Lauffenburger, L.G. Griffith, K.F. Jensen, Microfluidic Shear Devices for Quantitative Analysis of Cell Adhesion, Anal Chem, 76 (2004) 5257-5264.

[20] Z.L. Zhang, C. Crozatier, M. Le Berre, Y. Chen, In situ bio-functionalization and cell adhesion in microfluidic devices, Microelectronic Engineering, 78-79 (2005) 556-562.

[21] J. Zhou, D.A. Khodakov, A.V. Ellis, N.H. Voelcker, Surface modification for PDMS-based microfluidic devices, Electrophoresis, 33 (2012) 89-104.

[22] M.D. V. Sharma, S.M. Shivaprasad, S.C. Jain, Surface characterization of plasma-treated and PEG-grafted PDMS for micro fluidic applications, Vacuum, 81 (2007) 1094-1100.

[23] S. Pinto, P. Alves, C.M. Matos, A.C. Santos, L.R. Rodrigues, J.A. Teixeira, M.H. Gil, Poly(dimethyl siloxane) surface modification by low pressure plasma to improve its characteristics towards biomedical applications, Colloids and Surfaces B: Biointerfaces, 81 (2010) 20-26.

[24] v.L.M. C., L. J., N. W., S. G., Z.A. J, Electrophoretic mobility and hydrophobicity as a measured to predict the initial steps of bacterial adhesion., Appl. Environ. Microbiol., 53 (1987) 1898-1901.

[25] Y. Wang, R. Narain, Y. Liu, Study of Bacterial Adhesion on Different Glycopolymer Surfaces by Quartz Crystal Microbalance with Dissipation, Langmuir, 30 (2014) 7377-7387.

[26] J.W. McClaine, R.M. Ford, Characterizing the adhesion of motile and nonmotile Escherichia coli to a glass surface using a parallel-plate flow chamber, Biotechnology and bioengineering, 78 (2002) 179-189.

[27] T.A. Camesano, B.E. Logan, Influence of fluid velocity and cell concentration on the transport of motile and nonmotile bacteria in porous media, Environ Sci Technol, 32 (1998) 1699-1708.

[28] B.D. Ulery, L.S. Nair, C.T. Laurencin, Biomedical Applications of Biodegradable Polymers, J Polym Sci B Polym Phys, 49 (2011) 832-864.

[29] J.-P. Simon, G. Fabry, An overview of implant materials, Acta Orthop Belg, 57 (1991) 1-5.

[30] H. Chen, L. Yuan, W. Song, Z. Wu, D. Li, Biocompatible polymer materials: Role of protein–surface interactions, Progress in Polymer Science, 33 (2008) 1059-1087.

[31] M.I. Shtil′man, Polymeric biomaterials, VSP, 2003.

[32] B.D. Ratner, Biomaterials science: an introduction to materials in medicine, Academic press, 2004.

[33] J.M.R. Moreira, J. Ponmozhi, J.B.L.M. Campos, J.M. Miranda, F.J. Mergulhão, Micro- and macro-flow systems to study Escherichia coli adhesion to biomedical materials, Chemical Engineering Science, 126 (2015) 440-445.

[34] R.L. Reis, A.M. Cunha, Characterization of two biodegradable polymers of potential application within the biomaterials field, J Mater Sci: Mater Med, 6 (1995) 786-792.

[35] O. Pillai, R. Panchagnula, Polymers in drug delivery, Current Opinion in Chemical Biology, 5 (2001) 447-451.

[36] A.S. Breitbart, V.J. Ablaza, Implant materials, Grabb and Smith's Plastic Surgery, 5th Ed. Philadelphia: Lippincott-Raven, (1997) 39-46.

[37] W. Mokwa, U. Schnakenberg, Micro-transponder systems for medical applications, Instrumentation and Measurement, IEEE Transactions on, 50 (2001) 1551-1555.

[38] T. Yabuta, E.P. Bescher, J.D. Mackenzie, K. Tsuru, S. Hayakawa, A. Osaka, Synthesis of PDMS-Based Porous Materials for Biomedical Applications, Journal of Sol-Gel Science and Technology, 26 (2003) 1219-1222.

[39] E. Biazar, M. Heidari, A. Asefnejad, N. Montazeri, The relationship between cellular adhesion and surface roughness in polystyrene modified by microwave plasma radiation, Int J Nanomedicine, 6 (2011) 631-639.

[40] K. Mahrag Tur, H.-S. Ch'ng, Evaluation of possible mechanism(s) of bioadhesion, International Journal of Pharmaceutics, 160 (1998) 61-74.

[41] E.A. Vogler, Structure and reactivity of water at biomaterial surfaces, Advances in Colloid and Interface Science, 74 (1998) 69-117.

[42] M. Dou, D.C. Dominguez, X. Li, J. Sanchez, G. Scott, A versatile PDMS/paper hybrid microfluidic platform for sensitive infectious disease diagnosis, Anal Chem, 86 (2014) 7978-7986.

[43] R.S. Reneman, A.P. Hoeks, Wall shear stress as measured in vivo: consequences for the design of the arterial system, Med Biol Eng Comput, 46 (2008) 499-507.

[44] C. Cheng, F. Helderman, D. Tempel, D. Segers, B. Hierck, R. Poelmann, A. van Tol, D.J. Duncker, D. Robbers-Visser, N.T. Ursem, R. van Haperen, J.J. Wentzel, F. Gijsen, A.F. van der Steen, R. de Crom, R. Krams, Large variations in absolute wall shear stress levels within one species and between species, Atherosclerosis, 195 (2007) 225-235.

[45] D.P. Bakker, A. van der Plaats, G.J. Verkerke, H.J. Busscher, H.C. van der Mei, Comparison of Velocity Profiles for Different Flow Chamber Designs Used in Studies of Microbial Adhesion to Surfaces, Applied and Environmental Microbiology, 69 (2003) 6280-6287.

[46] S. Saha, Biomedical Engineering: I Recent Developments: Proceedings of the First Southern Biomedical Engineering Conference, Elsevier, 2013.

[47] G. Mareels, R. Kaminsky, S. Eloot, P.R. Verdonck, Particle Image Velocimetry–Validated, Computational Fluid Dynamics–Based Design to Reduce Shear Stress and Residence Time in Central Venous Hemodialysis Catheters, ASAIO Journal, 53 (2007) 438-446.

[48] W.J. Muller, S. Gerjarusek, P.W. Scherer, Studies of wall shear and mass transfer in a large scale model of neonatal high-frequency jet ventilation, Ann Biomed Eng, 18 (1990) 69-88.

[49] C.A. Reinhart-King, Mechanical and Chemical Signaling in Angiogenesis, Springer, 2013.

[50] C. Couzon, A. Duperray, C. Verdier, Critical stresses for cancer cell detachment in microchannels, Eur Biophys J, 38 (2009) 1035-1047.

[51] S. Varma, A cell-based sensor of fluid shear stress for microfluidics, in, Massachusetts Institute of Technology, 2013.

[52] M. Zamir, Shear forces and blood vessel radii in the cardiovascular system, The Journal of General Physiology, 69 (1977) 449-461.

[53] P. Aprikian, G. Interlandi, B.A. Kidd, I. Le Trong, V. Tchesnokova, O. Ykovenko, M.J. Whitfield, E. Bullitt, R.E. Stenkamp, W.E. Thomas, E. Sokurenko, The bacterial fimbrial tip acts as a mechanical force sensor, PLoS Biol, 9 (2011).

[54] E.A. Nauman, C.M. Ott, E. Sander, D.L. Tucker, D. Pierson, J.W. Wilson, C.A. Nickerson, Novel quantitative biosystem for modeling physiological fluid shear stress on cells, Applied and Environmental Microbiology, 73 (2007) 699-705.

[55] J.M. Ross, B.R. Alevriadou, L.V. McIntire, Rheology, in: Loscalzo J, A.I. Schafer (Eds.) Thrombosis and Hemorrhage, Williams & Wilkins, Baltimore, MD, 1998, pp. 405-421.

[56] V. Kochkodan, S. Tsarenko, N. Potapchenko, V. Kosinova, V. Goncharuk, Adhesion of microorganisms to polymer membranes: a photobactericidal effect of surface treatment with TiO2, Desalination, 220 (2008) 380-385.

Chapter 5

Biological fouling-channel geometry effect

Abstract

Fouling is unavoidable is any system and is capable of easily clogging in all Micro Electro- Mechanical Systems (MEMS), Lab on Chip Devices (LOC) and Point of Care Systems (POC) and could not operate with the same efficiency. Three different microchannel geometry designs were drafted and fabricated to have the adhesion study with *E. coli* suspension: 1- three different constriction lengths of 5000 μm, 2000 μm, 500 μm, 2- Multiple constrictions, 3- converging microchannel. The adhesion was monitored through out the 30 minute duration and the whole length of the microchannel is visualized at the end of 30 minute to quantify the adhesion and compare the change in adhesion before, after and in the constriction zones at 0.2 Pa and 1 Pa i.e, low and high shear stress respectively. The numerical simulation supported the results obtained for adhesion. High velocity and high shear stress were observed in the constrictions. The real wall shear stress is approximately 50% above the nominal wall shear stress. The wall shear stress in the constriction is approximately 40 times the wall shear stress in the upstream channel.

5.1. Introduction

Fouling is expected in many microfluidic applications such as Micro Electro-Mechanical Systems (MEMS), Lab on Chip Devices (LOC) and Point of Care Systems (POC). Fouling starts with the initial adhesion of organic or inorganic matter to the surface. Under fouling conditions, the microfluidic devices do not operate efficiently. Studies on fouling in macro heat exchangers with different flow conditions were done since 1999 to reduce this phenomenon in the design stage itself [1]. In this stage, it is necessary to understand which geometrical shape of the

microchannel is more or less favorably to fouling. So, in this chapter, fouling in microfluidic devices with different microchannel constrictions is monitored to understand the initial adhesion mechanisms in different locations.

Moreover, it is also important to understand how cells behave and how the formation of biofilms can hinder the normal functions of the device. This knowledge is important to know how long a system can work without maintenance or when substitution is indispensable. Microfluidic devices are useful to study cell adhesion in a controllable dynamic environment simulating *in vivo* conditions. The main conclusions in microchannels can be extrapolated, adopting similarity rules, to larger scale devices.

A microfluidic system can be designed to provide information about fouling rates on specific materials, antibiotics minimum dosage [2], quorum sensing [3] or on the relation between shear stress and biofouling [4, 5]. Some devices have been designed with the specific intention of studying biofilm related problems. Meyer et al. [6] developed a platform for monitoring the biofilm formation by measuring its optical density, which has the potential to be used as a standalone biochip for testing cleaning methods. Ghodssi et al. [7] developed microfluidic systems for optical and surface acoustic waves based detection and quantification of biofilms. Kim et al. [8] developed a device to determine the minimum concentration of antibiotics for biofilm eradication using generated antibiotics gradients. Zhang et al. [9] developed a procedure to bio functionalize a micro channel wall with antibodies to promote cell adhesion. Valiei et al. [10] used a microfluidic device to study the development of streamers and their role on biofilm growth. They found that the formation and morphology of the streamers depended on the flow rate. Rusconi et al. [11] observed the formation of streamers in microfluidic devices with curved-section channels. They proposed a relation between streamers development and secondary flows in the corners. These are examples on how microfluidics can be used for detailed observation of biofilm evolution and also situations in which fluid dynamics is relevant for biofilms formation.

Biomimetic design approach has been proposed for developing optimized geometries [12-15]. Networks following Murray's law are known to have a constant shear rate in all the branches. Barber et al. [13] proposed the application of the

Murray's law statement of constant wall shear stress, to constant depth rectangular cross section channels made by standard planar microfabrication techniques like photolithography. This design, when utilized in systems with fouling, reduces the risk of the appearance of critical points and the subsequent clogging of the channel. Emerson and Barber [15] extended this analysis to non-Newtonian fluids, concluding that the optimal design for a power law fluid requires detailed numerical simulations, since a simple analytical approach is not possible. As described in chapter 4, the cell adhesion over a surface was studied by several authors along the years from 1970's: experimentally [16, 17], numerically, considering just a single spherical cell adhered to a surface [18], and also theoretically [19].

Very few papers were published about cell adhesion in microchannels and only some of them describe the methods to reduce fouling in microchannels. Hang Lu et al. [20] studied cell attachment and detachment in a 25 x 500 μm microchannel. They applied relatively high shear stresses (160 Pa) using a multi-shear device and constant flow rate. Fuhr et al. [21] studied the reduction of cells and microparticles adhesion through an electric field created by ultra-microelectrodes fabricated by electron-beam lithography on silicon wafers, to create bio-repellent surfaces. They proposed two experimental techniques: one passing the erythrocyte cell suspension through the microchannel that had the electrode array for several hours; the second by growing fibroblasts under constant electric field. They showed that there was no cell adhesion on the substrate with amplitudes between 0.5 and 2 volt for both experiments performed. In another cell adhesion study in a microchannel [22], a method was described to measure the adhesion forces of a bacteria possessing different types of pili's. Polymer stencils that function as scaffolds to control cell adhesion inside microchannels were used to measure biofilm formation both in static and flow conditions [23]. Vijay et al. [3] tried to predict a physical model of the biofilm grown in a microchannel with *Pseudomonas aeruginosa*. A similar initial adhesion study was done by Velraeds et al. [24] with different uropathogenic bacteria, fouling during 4 h a silicone rubber surface, to understand urinary tract infection in hospitals. Liu et al. [25] investigated the effects of environment, micro geometry and flow on bacterial adhesion. They showed that, the adhesion is influenced by cell culture time, microchannel geometry and cell suspension flowrate. According to the study, the adhesion increases in complex geometries.

In this chapter, a study about the effect of microchannel constrictions on cell adhesion is presented. It is known that some spots in channel networks can be critical points prone to fouling and clogging. In this study, initial adhesion in constrictions, multiple constrictions and channels with variable cross sections are analysed and adhesion rates are related to local wall shear stresses and flow patterns.

5.2. Materials and Methods

5.2.1. Microchannel designs

Three different constrictions were used with different constriction lengths as shown in Figure 5.1 and Table 5.1. The constriction lengths (L_c) are 5000 μm, 2000 μm and 500 μm with entrance length (L_e) of 5000 μm for all the channels. The design was used to identify areas of higher adhesion: before, after or in the constriction at a pre-tested, high adhesion over a short period of time at particular shear stress. The second geometry, Figure 5.2, is a converging channel followed by a sudden expansion. The third design, is a channel with multiple constrictions within a short span of 5000 μm distance.

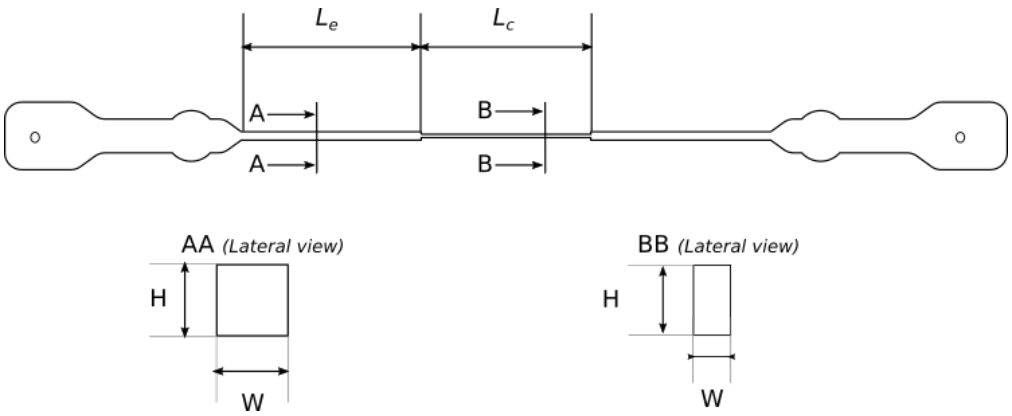

Figure 5.1. Sudden constriction channel design (not to scale)

Table 5.1. Dimensions of the channels with a sudden contraction

Constriction	AA		BB		L_e (μm)	L_c (μm)
	H (μm)	W (μm)	H (μm)	W (μm)		
A	94.4	88.5	94.4	8.54	5000	5000
B	94.4	86.4	94.4	10.5	5000	2000
C	94.4	92.6	94.4	13.6	5000	500

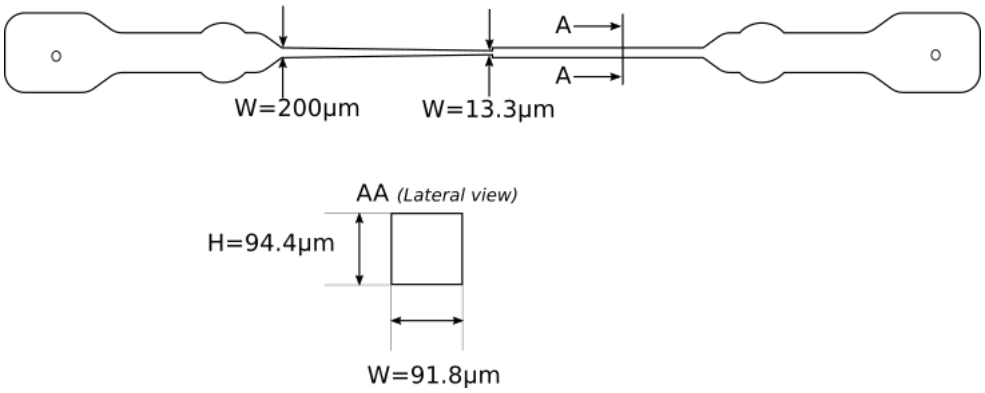

Figure 5.2. Converging channel design (not to scale)

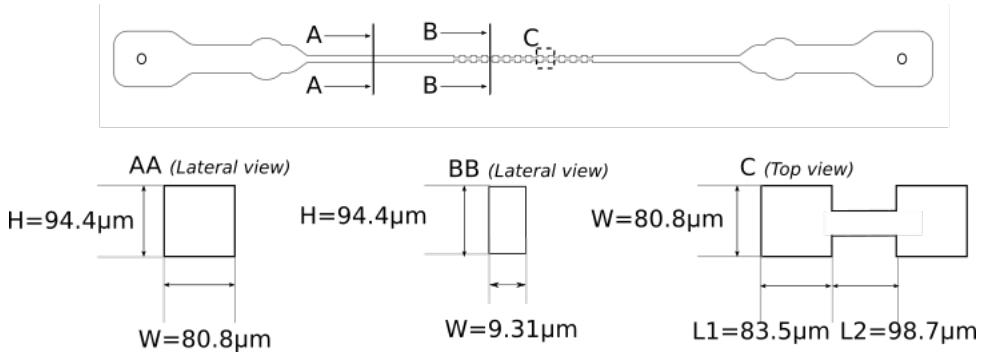

Figure 5.3. Multiple sudden constriction channel design (not to scale)

The cell suspension preparation was discussed in detail in chapter 3 and chapter 4, while the experimental set up (Figure 5.5) was described in detail in chapter 3 and will be briefly explained in section 5.2.4.

5.2.2 Flow conditions

In this study, the flow is laminar, viscous forces dominate, and so Reynolds number is small. Depending on the channel dimensions, measured after fabrication, the flow rate will be set through the constant pre-established value of the shear stress at the wall. The shear stress at the wall, τ_w, is directly proportional to the flow rate Q in the microchannel, to the fluid viscosity μ (the cell suspension has physical properties similar to water, a Newtonian incompressible fluid) and inversely proportional to the width and to the square height of the channel.

$$\tau_w = \mu \frac{6Q}{wh^2} \quad (1)$$

Equation 1 is an approximation, valid when *w* is significantly larger than *h*. The values obtained by this equation were used as the base to design the experiments and will be referred as "nominal wall shear stress". More accurate values, obtained by computational fluid dynamics, will also be presented.The flow regime was determined by calculating the Reynolds number based on the width and height of the microchannel:

$$\mathrm{Re} = \frac{\rho Q}{(W+H)\mu} \quad (2)$$

The shear stress values selected for the different microchannels are presented in Table 5.2, along with the flow rates (calculated from equation 1), channel width and Reynolds number (always less than 1). The shear stresses values will be compared with data from the numerical simulations.

Cell adhesion was obtained for four different nominal shear stresses. Nominal shear stresses are evaluated in region of interest (in the middle of the microchannel length) in all the five different channels with different types of constrictions, as tabulated in Table 5.2. These varied types of microchannels were designed for the purpose of studying the minimal fouling areas in different zones (especially near constrictions) of the microchannel with shear stresses ranging from 0.1 to 1 Pa. These shear stresses were selected for the study, because the adhesion rate, in these conditions, is high as shown in

Table 5.3 (conclusions from chapter 4, section 4.3.3).

Table 5.2 Shear stress at the region of interest and flow rates values employed in studies with different microchannels

Nominal wall shear stress (Pa)	Geometry	Flow rate (m^3/s)	Upstream channel width (μm)	Reynolds number
0.1	constriction	1.71×10^{-11}	79.7	0.31
0.2	constriction	3.42×10^{-11}	79.7	0.62
	converging microchannel	8.58×10^{-11}	200	0.62
	multiple constrictions	3.47×10^{-11}	80.8	0.62
0.3	constriction	5.13×10^{-11}	79.7	0.92
1	constriction	1.71×10^{-10}	79.7	3.08
	converging microchannel	4.29×10^{-10}	200	3.08
	multiple constrictions	1.73×10^{-10}	80.8	3.08

A list of adhesion rates corresponding at different wall shear stresses, from chapter 4, are listed in

Table 5.3 for an easy understanding of shear stress relation to adhesion rate. In this range of wall shear stress, the adhesion rate decreases as the wall shear stress increase.

Table 5.3 Adhesion rates and respective shear stresses (from chapter 4)

Wall shear stress (Pa)	Adhesion rate (nº cells/ $cm^2.s$)
0.154	1029.6
0.231	829.7
0.307	510.78
1	199.46

5.2.3 Numerical simulations

The flow in the microchannels was simulated to determine the wall shear stresses. A section of the microchannel, around the visualization region, was selected for simulation domain (Figure 5.4).

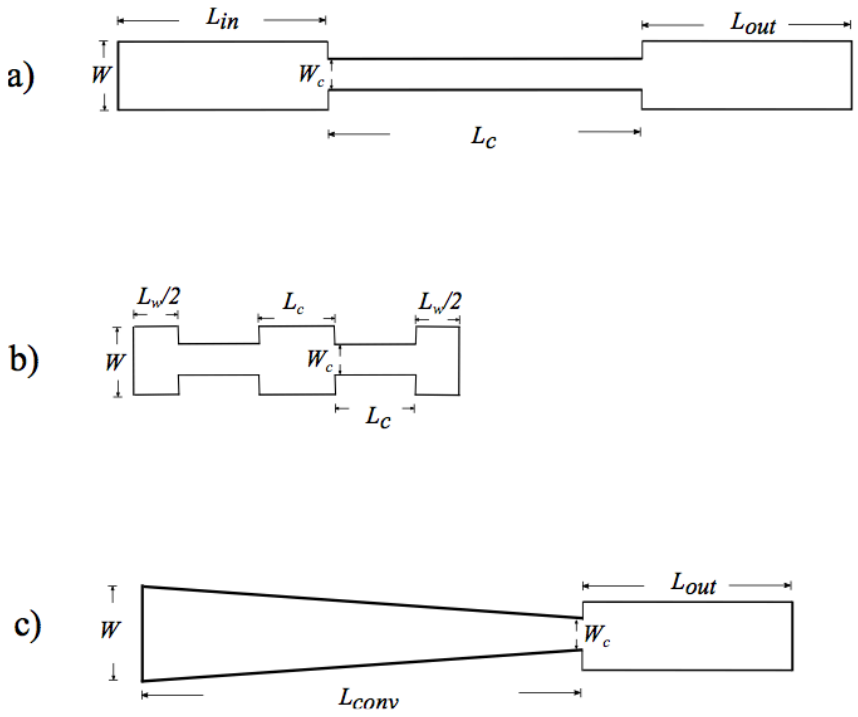

Figure 5.4. 2D representation of the numerical domains: (a) constriction geometry; (b) multiple constrictions; (c) converging microchannel.

Numerical simulations were made in Ansys Fluent CFD package (version 14.5). Models of the microchannels were built in Design Modeler 14.5 and were discretized into a grid by Meshing 14.5. Results in the laminar regime were obtained by solving the Navier– Stokes equations. The velocity–pressure coupled equations were solved by PISO algorithm (Issa 1986), QUICK scheme (Leonard 1979) [26] was used for the discretization of the momentum equations. The simulation is carried out with the same method as described in the previous chapter.

5.2.4 Experimental set-up

The experimental set-up was the same described as in Chapters 3 and 4. The *E. coli* suspension was used to fill the syringe and the syringe pump controlled the flow rate. The working temperature was monitored with the RTD sensor throughout the experiment. Figure 3.8 in Chapter 3 and Figure 4.2 in Chapter 4 describe pictorially the set-up.

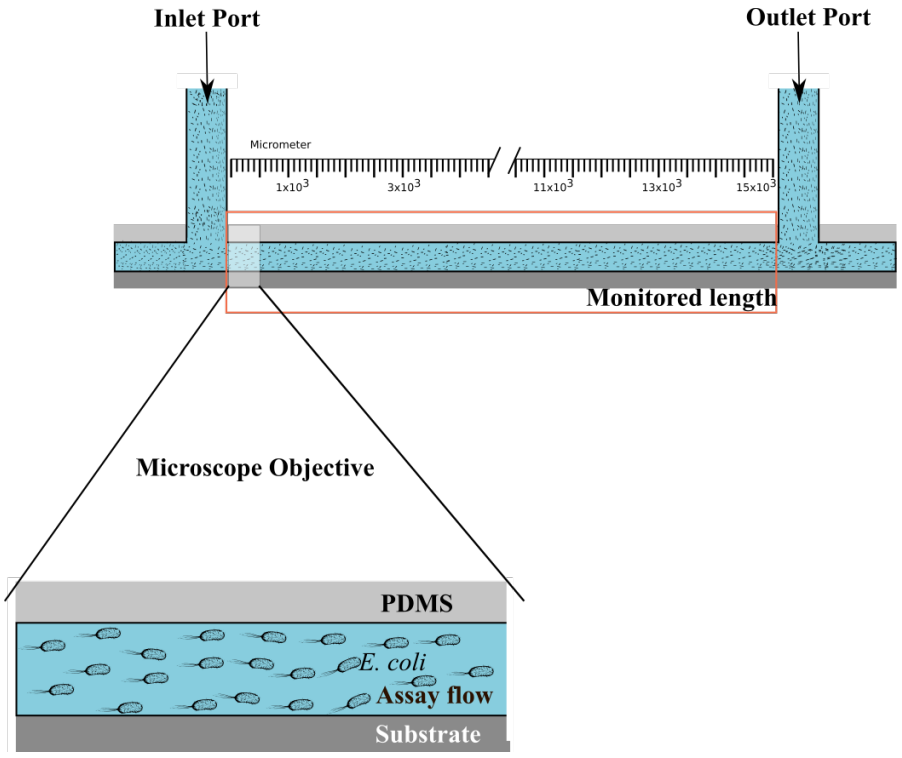

Figure 5.5. Schematic representation of monitoring the whole length of the microchannel with the microscope objective for every 500 µm interval.

The adhesion study was performed for 30 mins following the same procedure described in Chapter 4. Additionally for this chapter at the end of the experiment, i.e. after 30 mins of adhesion study, the whole length of the microchannel was observed with the microscope. Images were captured for every 500 µm interval length of the microchannel by moving the microscope objective as shown in the Figure 5.5 throughout the whole length of the microchannel.

5.3 Results and Discussion

5.3.1. Constrictions

5.3.1.1. Wall shear stress effect

The adhesion along the channel constrictions was monitored for all the microchannel designs shown in Figure 5.1, 5.2 and 5.3 Unlike the straight rectangular channels where adhesion was uniform along all its length (Chapter 3 - section 3.9.4), adhesion is not uniform along the channels with constrictions.

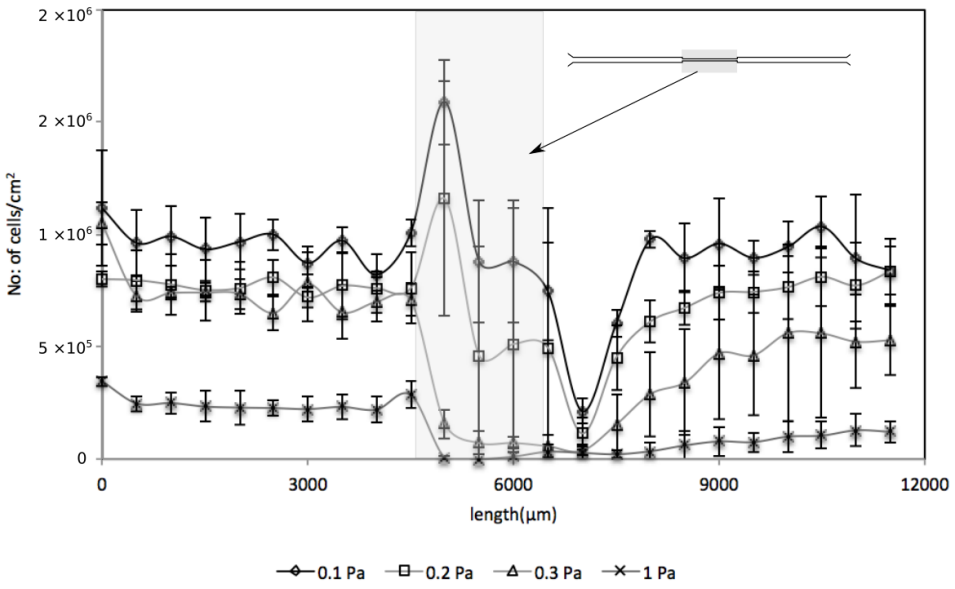

Figure 5.6. Adhesion along the 2000 μm constriction microchannel at different shear stresses

The effect of shear stress was studied for a microchannel with a 2000 μm constriction (Table 5.1). Four wall shear stress values were studied; 0.1, 0.2, 0.3 Pa and 1 Pa. In Figure 5.6, the x- axis refers to the length of the microchannel (in μm) and the y-axis to the number of cells adhered per square centimeter.

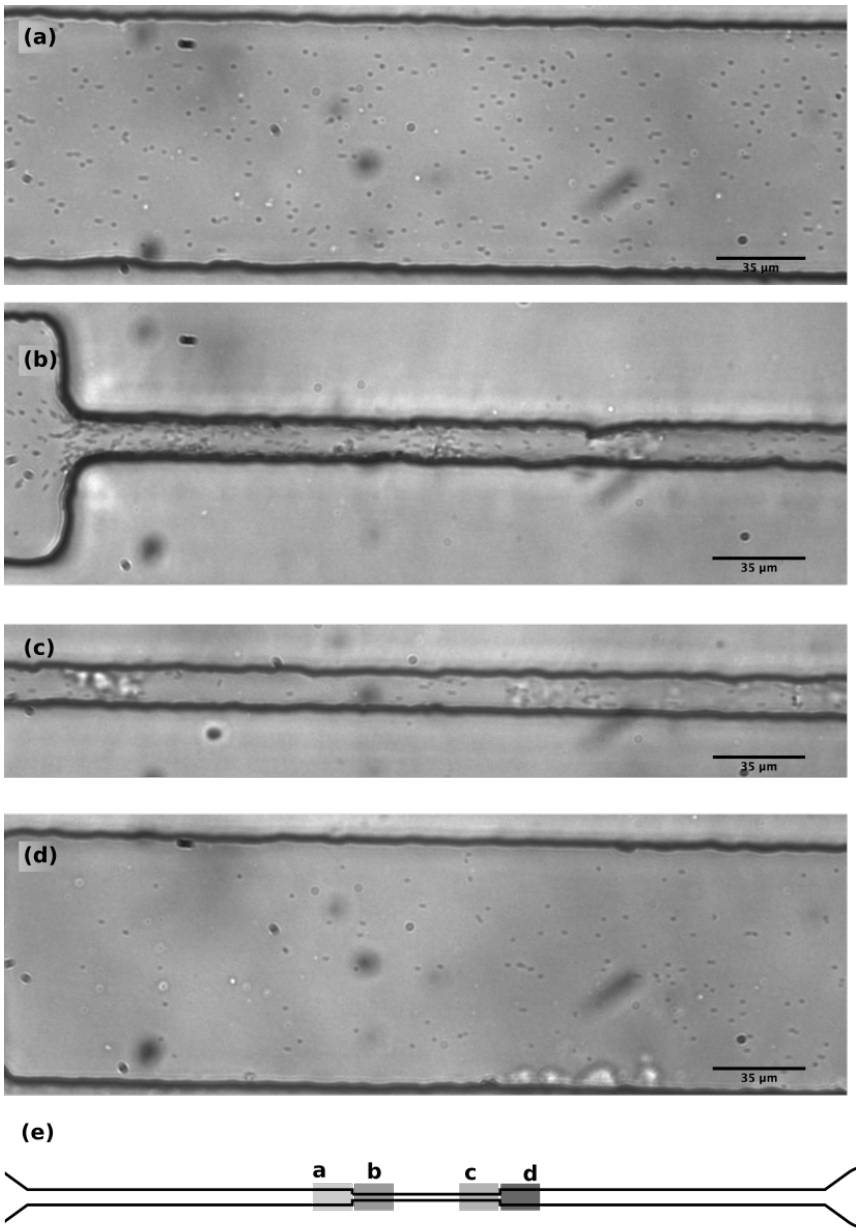

Figure 5.7. Microscopic image of 2000 µm constriction at different spots along its length for 0.2 Pa shear stress: (a) before the constriction (uniform adhesion); (b) start of the constriction (sudden contraction - sudden increased adhesion); (c) end of the constriction (decreased adhesion); (d) after the constriction (sudden expansion – highly decreased adhesion); (e) location of a,b,c and d adhesion zones along the 2000 µm constriction microchannel.

The adhesion gradually decreased as the wall shear stress increases from 0.1 Pa to 1 Pa. This was clearly noticeable in the upstream, constriction and downstream regions of the microchannel. For the shear stress of 1 Pa, the adhesion is very low, as expected by observation of the adhesion rates in

Table 5.3

In the upstream region adhesion is more or less uniform for all the shear stresses. In the downstream region, adhesion behaviour depends on the wall shear stress: except for 1 Pa, after the sudden expansion in the downstream region, the adhesion ascents gradually to a level more or less equal to the upstream adhesion one. For 1 Pa, the adhesion does not recover to the upstream adhesion level.

The coloured region in Figure 5.6 signalizes the constriction. When the contraction starts, a sudden rise of adhesion is notorious for 0.1 and 0.2 Pa followed by an accentuated decrease. The initial shoot up is not observed for 0.3 and 1 Pa. This behaviour shows that the intensity level of the wall shear stress changes the nature of adhesion in this geometry in a span of 2000 μm.

The microscopic images presented in Figure 5.7 show the adhesion in different regions along the 2000 μm constriction microchannel for 0.02 Pa. These image show evidence to: uniform adhesion upstream the constriction, Figure 5.7 (a); sudden adhesion increase at the beginning of the constriction, Figure 5.7 (b); and gradual decrease along the constrictions, Figure 5.7 c). The end of the constriction and the region downstream just after the constriction (Figure 5.7 (c) and (d)) are depleted of cells.

5.3.1.2. Effect of the constriction length

To understand the effect of different constrictions lengths, channels with constrictions of length 500, 2000 and 5000 μm were studied. A 0.2 Pa shear stress was selected to perform this study because, according to the shear stresses study presented in chapter 4, the adhesion rate is considerable for this case.

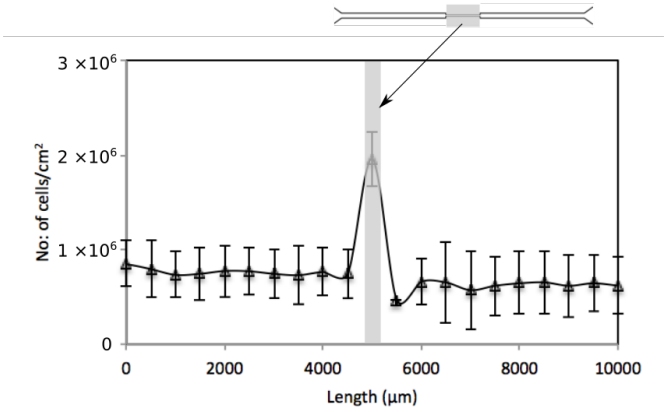

Figure 5.8. Average adhesion along the length of the microchannel with 500 µm constriction for 0.2 Pa

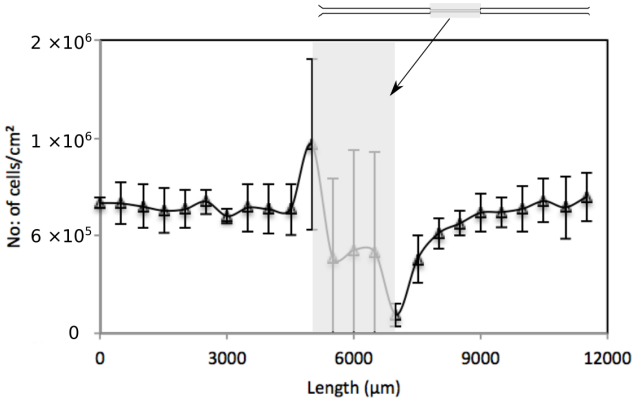

Figure 5.9. Average adhesion along the length of the microchannel with 2000 µm constriction for 0.2 Pa

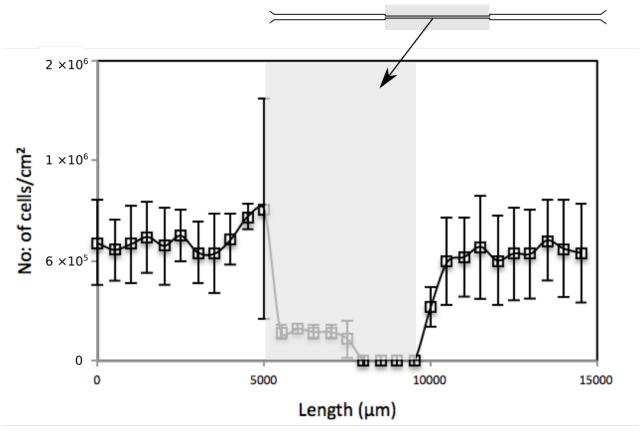

Figure 5.10. Average adhesion along the length of the microchannel with 5000 µm constriction for 0.2 Pa

Once more, Figure 5.8, 5.9 and 5.10 show that the upstream adhesion is uniform. The adhesion downstream starts recovering after the constriction and attains uniformity before the end of the microchannel. The adhesion level of *E. coli* downstream, after the recovery length, is similar to the adhesion level upstream the constriction. The major difference between the three experiments lies in the constriction zone. But, as the wall shear stress is the same, the adhesion pattern maintains: a high adhesion at the beginning and a decrease until the end of the constriction. The extension of this reduction depends on the constriction length. For a long constriction, adhesion is almost zero at the end of the constriction. This last conclusion can be utilized in appropriate applications in order to prevent cell adhesion.

To illustrate the above results, two microscopic images are presented in Figure 5.11. It can be observed that there are no cells adhering in the last 2000 μm of the constriction, Figure 5.11 (a), and just 6 cells adhered in the sudden expansion region after the constriction, Figure 5.11 (b). This last value is lower than those observed in the other constriction lengths (2000 μm and 500 μm). The location of Figure 5.11 a and b is shown in Figure 5.11 c.

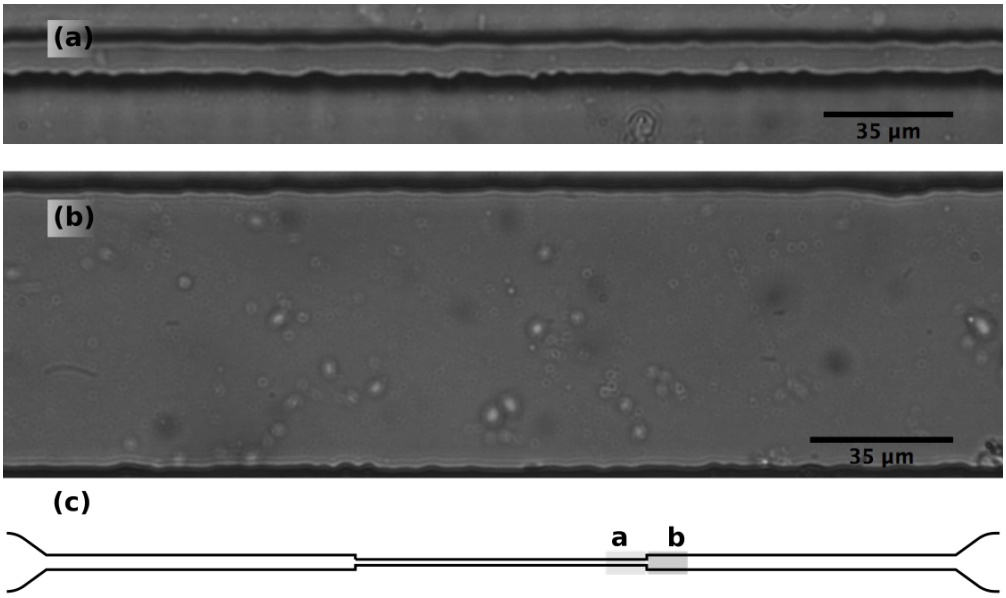

Figure 5.11. Microscopic images: (a) no adhesion zone; and (b) lower adhesion zone (depleted region) for 5000 μm constriction microchannel length at 0.2 Pa; (c) location of a and b adhesion zones.

5.3.2 Multiple constrictions

From the results presented until now, it is evident that the constrictions are playing a role in adhesion. It was observed that the adhesion level changes with the length of the constrictions and the intensity of the adhesion recovery, after the constrictions with different lengths, is also different. So, multiple constrictions were studied to check for the interaction effect between consecutive constrictions. The geometry shown in Figure 5.3 was used and the effect of two inlet wall shear stresses, low (0.2 Pa) and high (1 Pa), was studied.

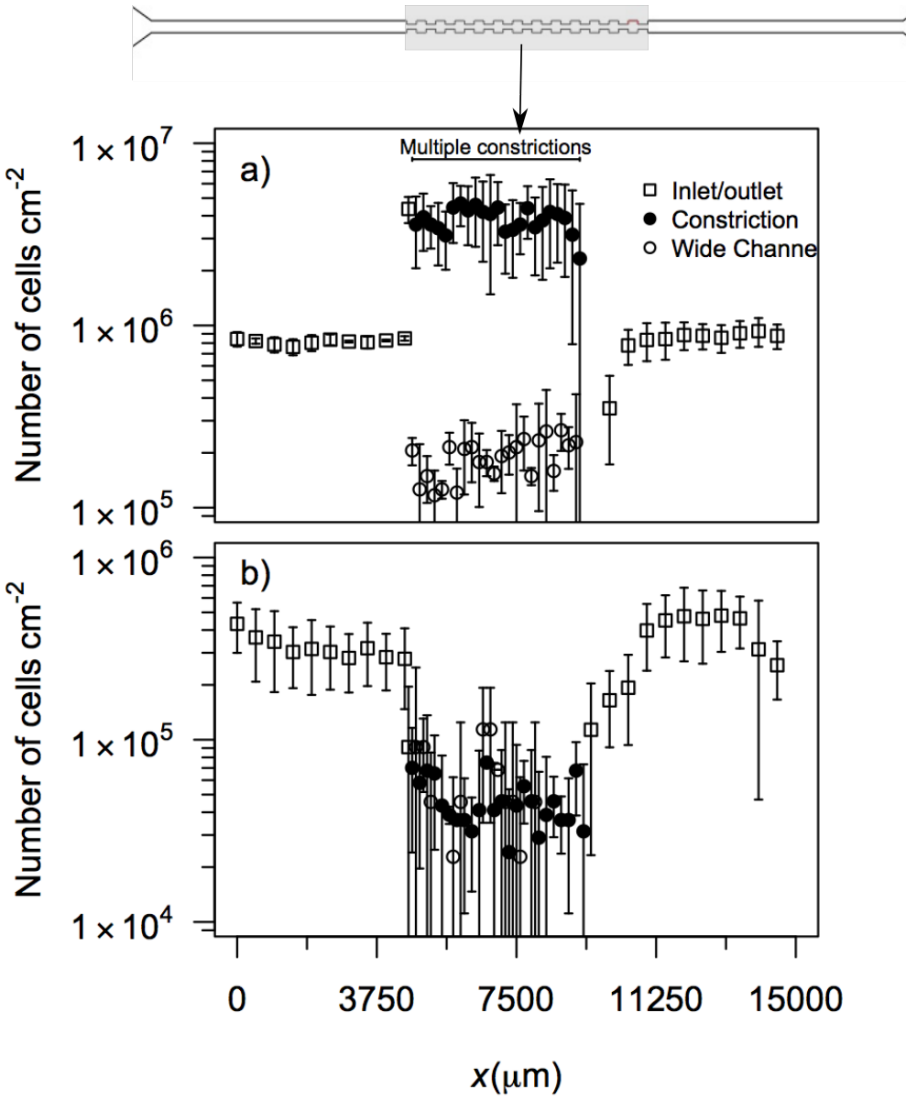

Figure 5.12. Adhesion along the length of the microchannel with multiple constrictions: (a) τ_w= 0.2 Pa; (b) τ_w = 1 Pa.

The adhesion results in the multiple constrictions are plotted in Figure 5.12. The microchannel length is comprised of consecutive wide and narrow sub-channels. For 0.2 Pa, the adhesion in the narrow sub-channels is one order of magnitude higher than the adhesion in the wide channels. For 1Pa, the adhesion is smaller than for the 0.2 Pa and the difference between adhesion in narrow and wide channels is small.

The microscopic images add more evidence to these conclusions. It is evident that for 0.2 Pa more cells adhere in the narrow channels and less in the wide channels (Figure 5.13). For 1 Pa, less cells in narrow channels and more in wide channels (Figure 5.14) are observed. Thus, in multiple sudden constriction zones, the capture and adhesion can be modified, in a pre-defined way using different geometries and different wall shear stresses.

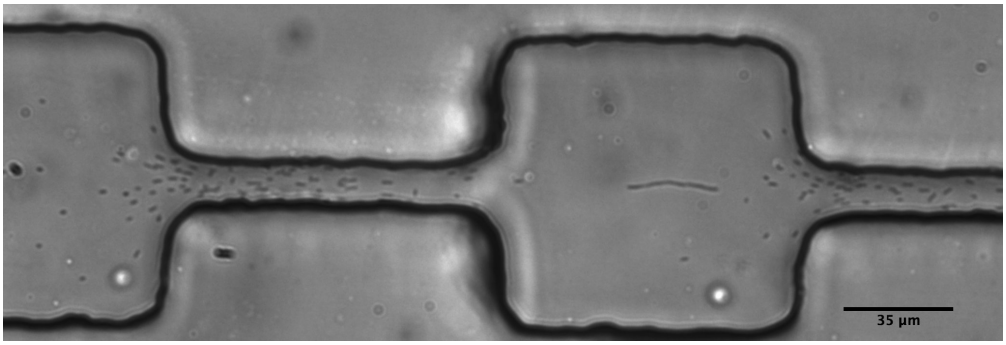

Figure 5.13. Adhesion in a multiple constriction channel for 0.2 Pa.

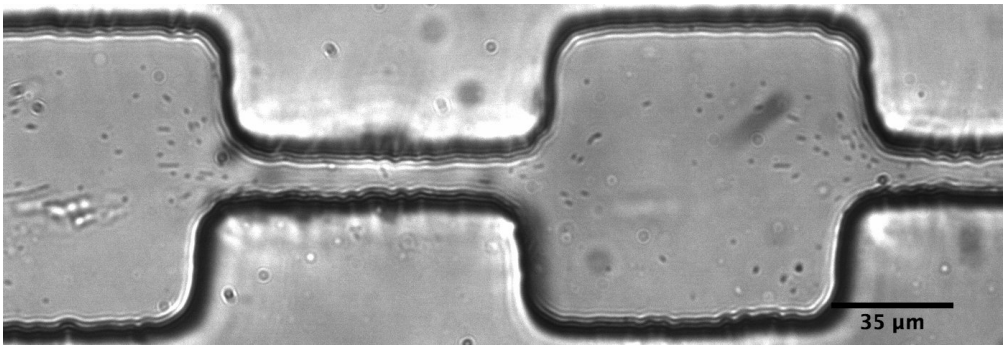

Figure 5.14. Adhesion in a multiple constriction channel for 1 Pa.

5.3.3. Converging microchannel

The converging microchannel (Figure 5.2) was also investigated for low and high wall shear stresses along the channel length. In Figure 5.15, a converging channel is shown. For 0.2 Pa at the starting of the microchannel flow regime, Figure 5.15 a, there is a small gradual decrease in adhesion as the width of the channel decreases and just before the beginning of the sudden expansion, adhesion has a small decrease and then a gradual increase until the end of the channel.

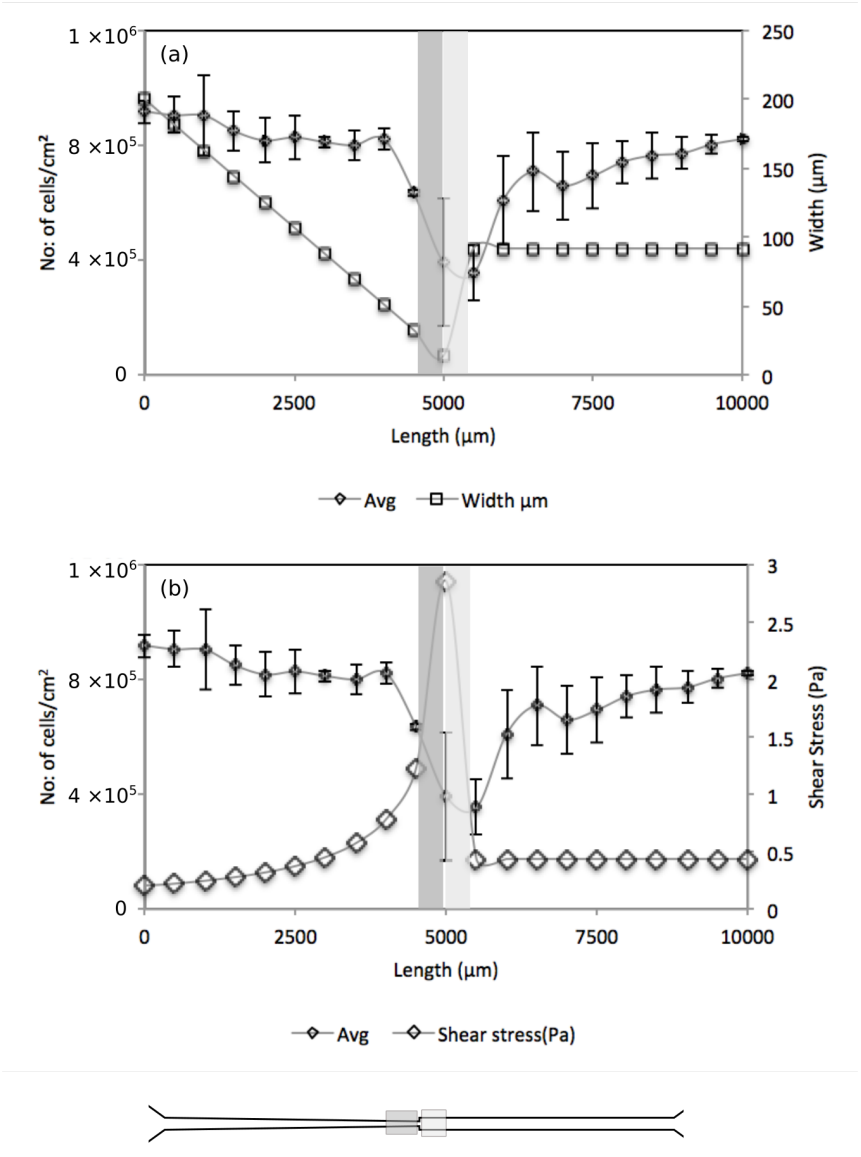

Figure 5.15. Converging microchannel for 0.2 Pa: (a) Adhesion with respective channel width at each location along the length; (c) Adhesion with wall shear stress at each location along the length

In Figure 5.15a the adhesion along the length is represented in simultaneous with the width of the microchannel. The adhesion decreases as long as the width decreases and, in the sudden expansion region, it takes some length to attain the uniform adhesion value. In Figure 5.15 b, the adhesion is represented in simultaneous with the wall shear stress at each location along the length. In very high adhesion regions, the wall shear stress is low and vice-versa. This behaviour was justified in the previous chapter (Chapter 4).

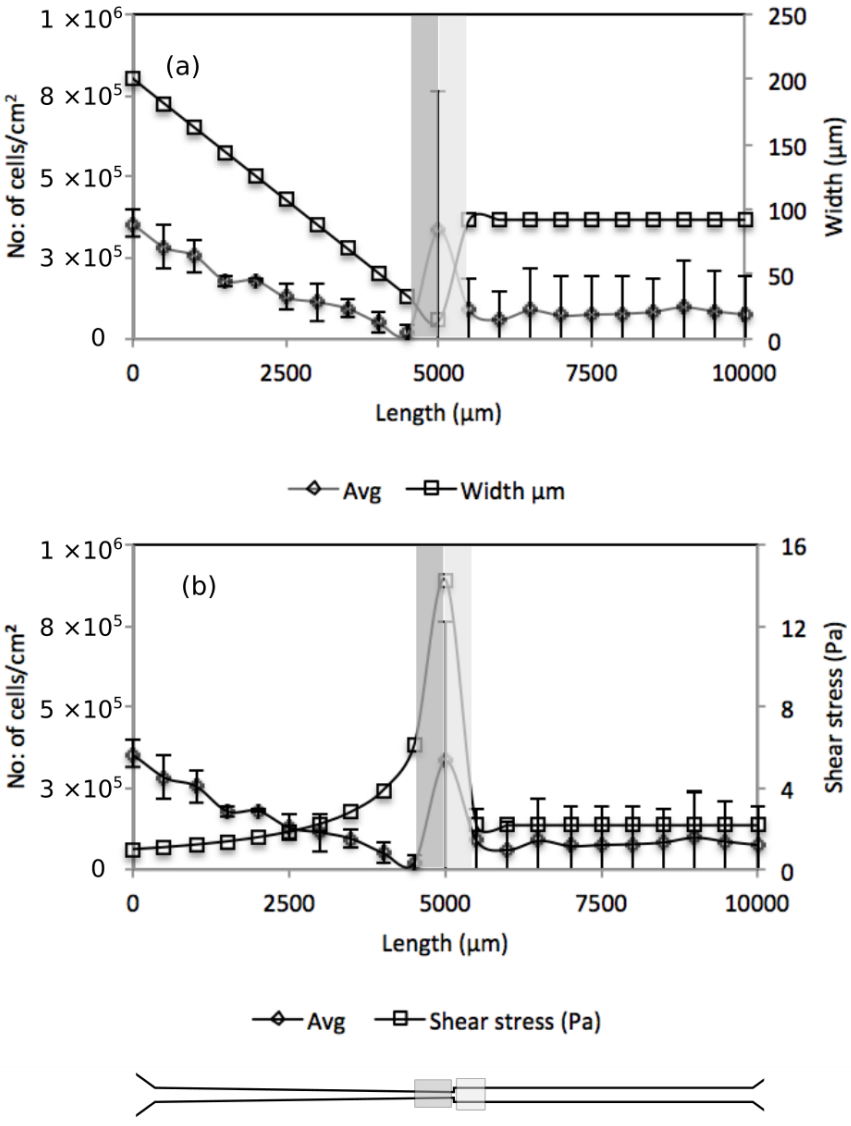

Figure 5.16. Converging microchannel for 1 Pa: (a). Adhesion along the length of the converging microchannel for 1 Pa at the inlet, (b) Adhesion with respective channel width at each location along the length, (c) Adhesion with wall shear stress at each location along the length.

Figure 5.16 a and b shows the experimental data for wall shear stress 1 Pa at the inlet. As the width of the channel decreases, the adhesion also decreases and its level is very low at the end of the converging channel. Contrasting to 0.2 Pa experiments, the adhesion in the sudden expansion region recovers in a short length and maintains the same low rate in the downstream region. These differences can be clearly seen in the images of Figure 5.17 and Figure 5.18.The upstream adhesion decreases slowly until the sudden expansion zone for 0.2 Pa experiments (Figure 5.17 a) and the downstream adhesion, after the convergence, has a gradual increase until the end of the microchannel (Figure 5.17 b).

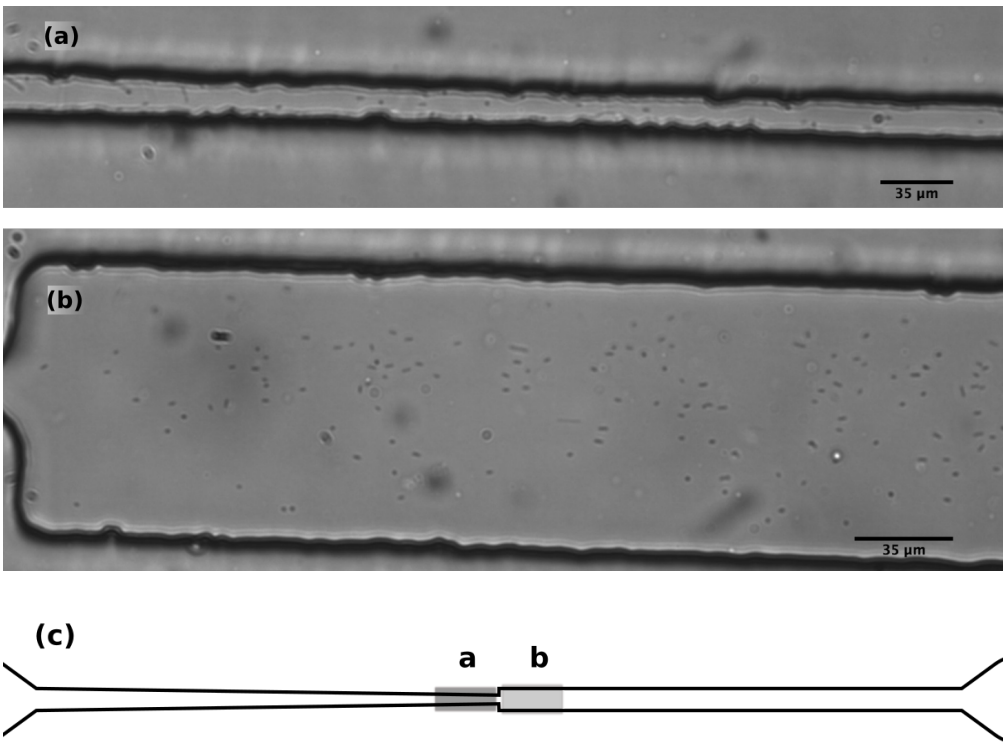

Figure 5.17. Microscopic image for the converging microchannel at 0.2 Pa: (a) End of the converging region; (b) Beginning of the expansion region after the convergent; (c) Location of a and b on zones along the converging microchannel

For the 1 Pa experiments, the upstream adhesion dropped to a greater extent but at the end of the converging channel (Figure 5.18 a) a significant number of cells appear to block the passage. This phenomenon does not occur in the multiple sudden constrictions or in the three different constriction microchannels analysed, where high

shear stresses induce low or null adhesion. Downstream the convergence region the adherence does not increase (Figure 5.18 b).

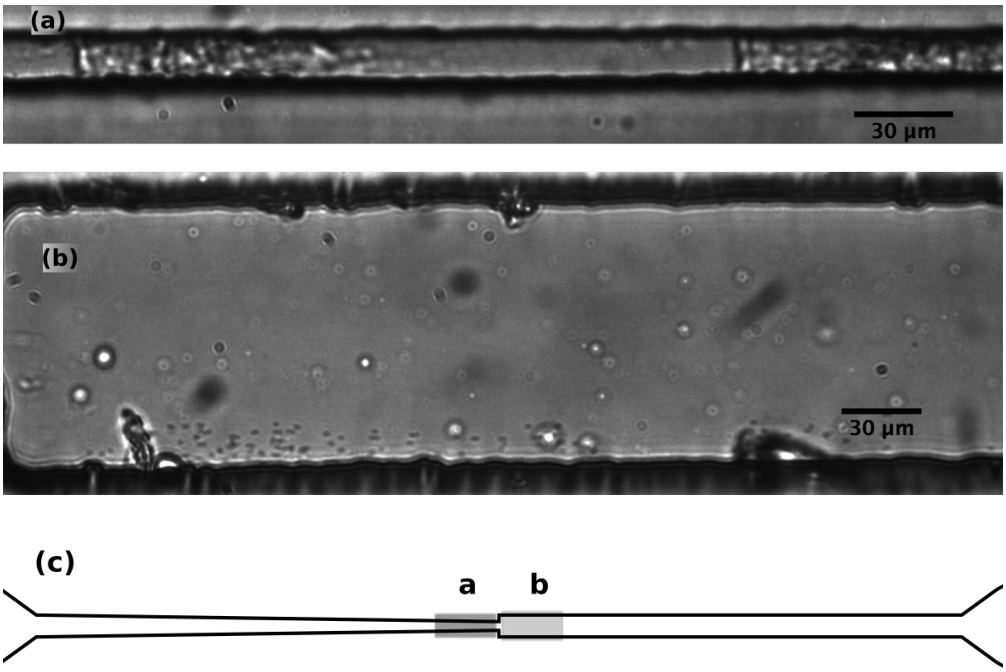

Figure 5.18. Microscopic image for the converging microchannel at 1 Pa: (a) End of the converging region; (b) Beginning of the expansion region after the convergent). (c) Location of a and b zones along the converging microchannel

5.4 CFD

An example of the flow in a constriction is represented in Figure 5.19 and Figure 5.20. The flow is in the laminar regime, with Reynolds number lower than 1 in all cases. The flow is characterized low lengths of development and symmetry between the flow entering and leaving the constriction. High velocity and high shear stress is observed in the constriction. Since the lengths of flow development are much shorter that 500 µm no significant difference is observed as the constriction length increases. Similar conclusions can be taken, even for the larger flow rates studied.

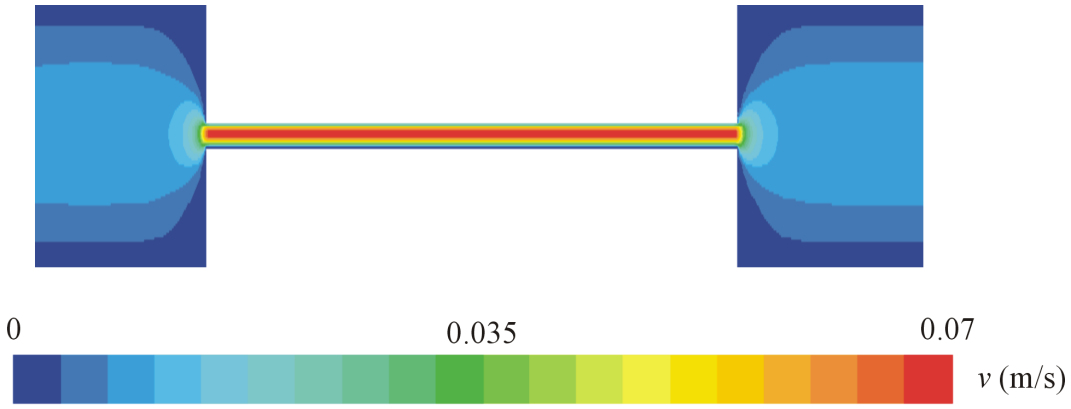

Figure 5.19. Magnitude of the velocity in a 500 μm long constriction. The flow rate is 3.42×10^{-11} m^3s^{-1}. The constriction width is 10 μm and the channel depth is 100 μm.

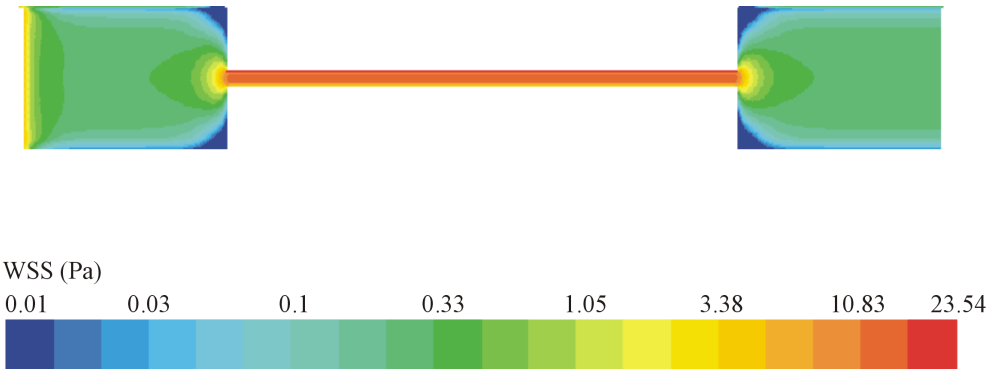

Figure 5.20. Wall shear stress in a 500 μm long constriction. The flow rate is 3.42×10^{-11} m^3s^{-1}. The constriction width is 10 μm and the channel depth is 100 μm. The nominal wall shear stress in the upstream channel is 0.2 Pa. The wall shear stress calculated by the numerical method in the upstream channel is 0.31 Pa. The wall shear stress in the constriction is 19.2 Pa.

Table 5.4 shows the wall shear stress for different flow rates in two locations in the channel, the upstream channel and the constriction. A significant correction must be introduced in the nominal wall shear stress. The real wall shear stress is approximately 50% above the nominal wall shear stress. The wall shear stress in the constriction is approximately 40 times the wall shear stress in the upstream channel.

Table 5.4. Wall shear stresses in a microchannel with a 500 μm long constriction. The constriction width is 10 μm and the channel depth is 100 μm.

Q (m^3s^{-1})	τ (Pa)		τ_c (Pa)
	Nominal	Numerical	
1.71×10^{-11}	0.1	0.155	6.8
3.42×10^{-11}	0.2	0.31	13.65
5.13×10^{-11}	0.3	0.465	20.5
1.71×10^{-10}	1	1.55	68.1

Figures 5.21 and 5.22 show the results obtained for the converging microchannel. As can be observed velocity and shear rate increase significantly along the channel, as was already predicted by the theoretical approach.

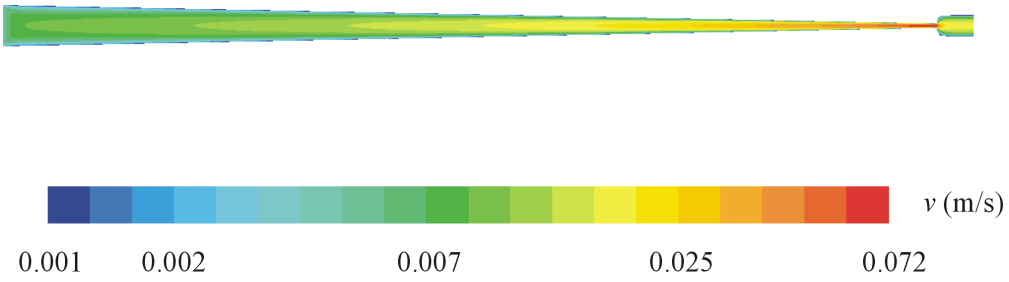

Figure 5.21. Magnitude of the velocity in a converging channel. The flow rate is 8.58×10^{-11}. m^3s^{-1}

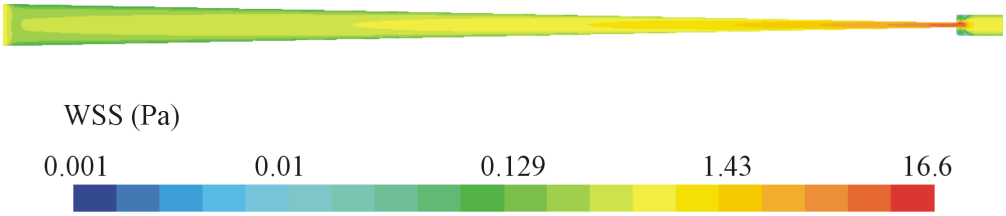

Figure 5.22. Wall shear stress in the converging channel. The flow rate is 8.58×10^{-11}. m^3s^{-1}

Figures 5.23 and Figure 5.24 show the results obtained for the multiple constrictions microchannel. As can be observed, the flow is fully developed in the constrictions but the wide channels have a length insufficient to reach developed flow. For this reason the wall shear stress along the centreline of the wide sections is higher than in a longer channel with the same width.

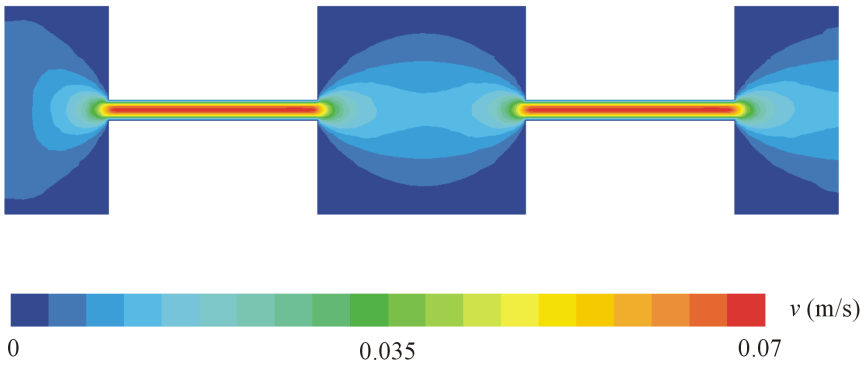

Figure 5.23. Velocity magnitude in a section of a multiple constrictions microchannel. The flow rate is 3.42×10^{-11} m^3s^{-1}. The constriction width is 10 μm and the channel depth is 100 μm. max is 13.8

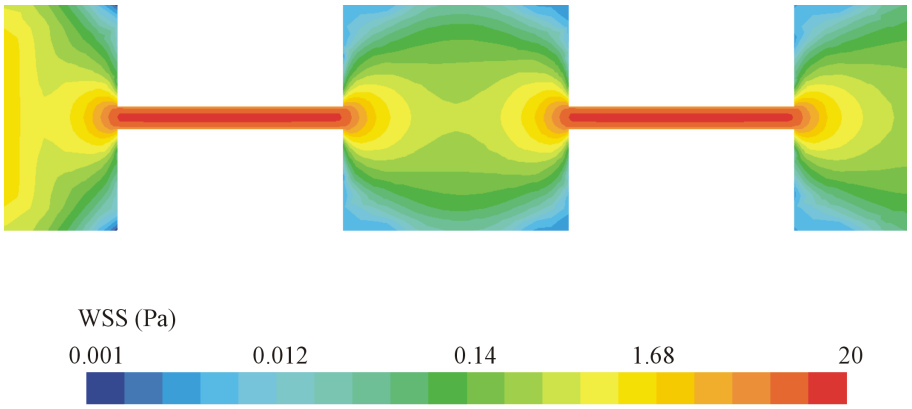

Figure 5.24. Velocity magnitude in a section of a multiple constrictions microchannel. The flow rate is 3.42×10^{-11} m^3s^{-1}. The constriction width is 10 μm and the channel depth is 100 μm.

5.5 Influence of wall shear stress on adhesion rates

The plot for local wall shear stress in different microchannels is plotted with their corresponding adhesion rates in Figure 5.25. This plot is the extension of Figure 4.7. in chapter 4 where adhesion rate in a PDMS surface is plotted for different wall shear stress The Adhesion rate is calculated at different locations along the length of the microchannels. The plot 1, 2, 3, 4 mentioned in Figure 5.25 is adapted from Figure

5.6, Figure 5.10, Figure 5.12 respectively for the presenting the points A to I to calculate the adhesion rates at those locations for a period of 30 minutes.

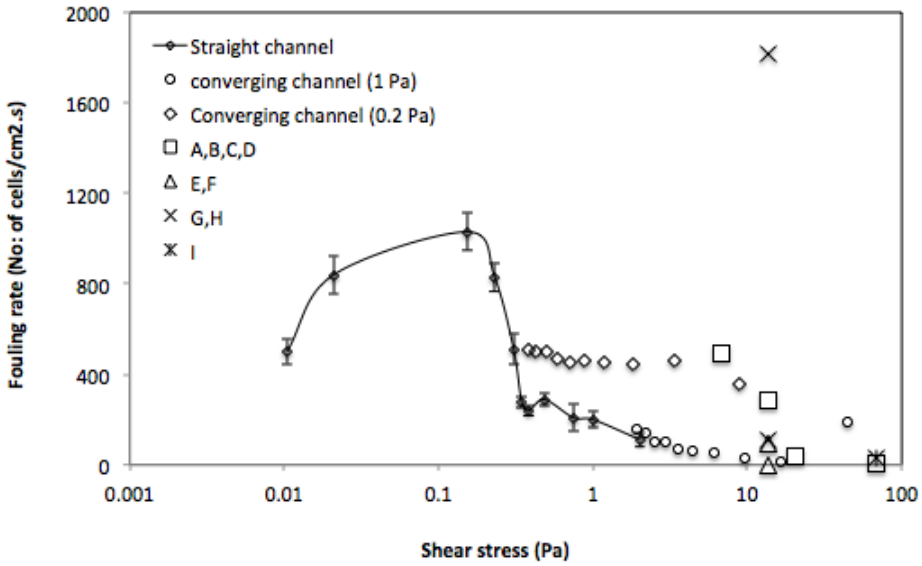

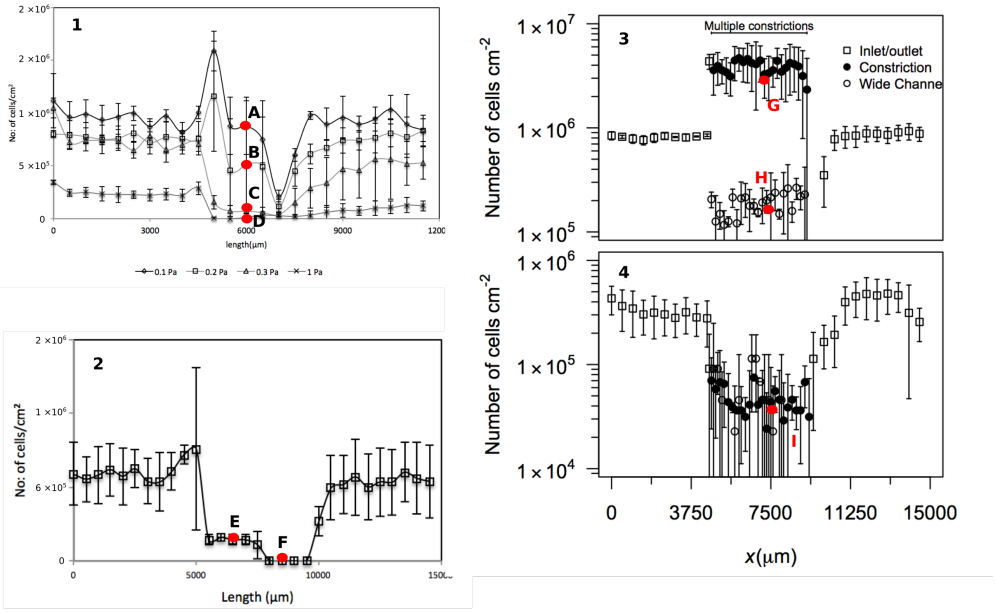

Figure 5.25. Fouling rates at different locations as mentioned in 1,2,3,4 plots (location of A to I points) with their local wall shear stress. 1- 2000 µm constriction microchannel; 2- 5000 µm constriction for a nominal shear stress of 0.2 Pa; 3 and 4 – multiple constrictions.

The values of adhesion rates with their local wall shear stress for the corresponding nominal wall shear stress is tabulated for all the location points in Figure 5.25 are tabulated in Table 5.

Table 5.5. Adhesion rates with local and nominal wall shear stress for the points mentioned in Figure 5.25.

Point	Nominal WSS	Local WSS	Adhesion rate (No. of cells/cm²/s)
A	0.1	6.8	488.61
B	0.2	13.65	284.65
C	0.3	20.5	39.63
D	1	68.1	5.99
E	0.2	13.65	95.49
F	0.2	13.65	0
G	0.2	13.65	1815.99
H	0.2	13.65	111.6
I	1	68.1	25.32

The results in Figure 5.25 show that local adhesion rates in constriction deviate significantly from the curve obtained for a straight channel suggesting that other factors other than local wall shear stress is influencing cell adhesion. The following factors may have a role in adhesion and further research is necessary:

- Mass transport effects when the fluid suddenly accelerates;
- Wall effects when the size of the channel becomes similar to the size of the cells;
- 3D flow effect

5.6. Conclusions

In this chapter, an adhesion study in microchannels with different geometries was performed. The relationship between wall shear stress and cross sectional area of the channel was explored. The results show that adhesion in all of the three sets of microchannel geometry designs analysed follow a similar adhesion pattern. However, an independent investigation should always be carried out to explore singularities of each geometry design. Manipulating the geometry, and by consequence the wall shear stress, it is possible to control cell adhesion, an event with great potential for many biomedical applications. Using a microchannel with multiple constrictions, it is also possible to work on both, high and low wall shear stress ranges, and to monitor the adhesion phenomenon in these two situations. Depending on the application, this

work can be extended to different bacterial cell based assays at a pre-required temperature, which also plays an important role in cell adhesion. The cell deformation and alignment along different constrictions during the flow will be an interesting future prospective study, as it would help to understand the development and behaviour of many unwanted diseased cells in the human body.

References

[1] B. Thonon, S. Grandgeorge, C. Jallut, Effect of geometry and flow conditions on particulate fouling in plate heat exchangers, Heat Transfer Eng, 20 (1999) 12-24.

[2] P. Sun, Y. Liu, J. Sha, Z. Zhang, Q. Tu, P. Chen, J. Wang, High-throughput microfluidic system for long-term bacterial colony monitoring and antibiotic testing in zero-flow environments, Biosensors and Bioelectronics, 26 (2011) 1993-1999.

[3] V. Janakiraman, D. Englert, A. Jayaraman, H. Baskaran, Modeling growth and quorum sensing in biofilms grown in microfluidic chambers, Annals of biomedical engineering, 37 (2009) 1206-1216.

[4] J.S. Salek MM1, Martinuzzi RJ., The influence of flow cell geometry related shear stresses on the distribution, structure and susceptibility of Pseudomonas aeruginosa 01 biofilms., Biofouling, 25 (2009) 711-725.

[5] C.C. Chan, P.R. Berube, E.R. Hall, Relationship between types of surface shear stress profiles and membrane fouling, Water Res, 45 (2011) 6403-6416.

[6] M.T. Meyer, V. Roy, W.E. Bentley, R. Ghodssi, Development and validation of a microfluidic reactor for biofilm monitoring via optical methods, J Micromech Microeng, 21 (2011) 054023.

[7] R. Ghodssi, M.T. Meyer, Y.W. Kim, Microsystems for sensing and characterization of bacterial biofilms, in: Sensors, 2013 IEEE, IEEE, 2013, pp. 1-6.

[8] K.P. Kim, Y.-G. Kim, C.-H. Choi, H.-E. Kim, S.-H. Lee, W.-S. Chang, C.-S. Lee, In situ monitoring of antibiotic susceptibility of bacterial biofilms in a microfluidic device, Lab Chip, 10 (2010) 3296-3299.
[9] Z.L. Zhang, C. Crozatier, M. Le Berre, Y. Chen, In situ bio-functionalization and cell adhesion in microfluidic devices, Microelectronic Engineering, 78-79 (2005) 556-562.

[10] A. Valiei, A. Kumar, P.P. Mukherjee, Y. Liu, T. Thundat, A web of streamers: biofilm formation in a porous microfluidic device, Lab Chip, 12 (2012) 5133-5137.

[11] R. Rusconi, S. Lecuyer, L. Guglielmini, H.A. Stone, Laminar flow around corners triggers the formation of biofilm streamers, Journal of The Royal Society Interface, 7 (2010) 1293-1299.

[12] M.S. Razavi, E. Shirani, M. Salimpour, Development of a general method for obtaining the geometry of microfluidic networks, AIP Advances, 4 (2014) 017109.

[13] R.W. Barber, D.R. Emerson, Optimal design of microfluidic networks using biologically inspired principles, Microfluid Nanofluid, 4 (2008) 179-191.
[14] R.W. Barber, D.R. Emerson, Biomimetic design of artificial micro-vasculatures for tissue engineering, Altern Lab Anim, 38 (2010) 67-79.

[15] D.R. Emerson, R.W. Barber, Designing Efficient Microvascular Networks Using Conventional Microfabrication Techniques, in: ASME 2009 Second International Conference on Micro/Nanoscale Heat and Mass Transfer, American Society of Mechanical Engineers, 2009, pp. 159-167.

[16] M.B. Lawrence, C.W. Smith, S.G. Eskin, L.V. McIntire, Effect of venous shear stress on CD18-mediated neutrophil adhesion to cultured endothelium, Blood, 75 (1990) 227-237.

[17] M.B. Lawrence, T.A. Springer, Leukocytes roll on a selectin at physiologic flow rates: Distinction from and prerequisite for adhesion through integrins, Cell, 65 (1991) 859-873.
[18] D.A. Hammer, S.M. Apte, Simulation of cell rolling and adhesion on surfaces in shear flow: general results and analysis of selectin-mediated neutrophil adhesion, Biophys J, 63 (1992) 35-57.

[19] D.P. Gaver, S.M. Kute, A Theoretical Model Study of the Influence of Fluid Stresses on a Cell Adhering to a Microchannel Wall, Biophysical Journal, 75 (1998) 721-733.

[20] H. Lu, L.Y. Koo, W.M. Wang, D.A. Lauffenburger, L.G. Griffith, K.F. Jensen, Microfluidic shear devices for quantitative analysis of cell adhesion, Anal Chem, 76 (2004) 5257-5264.

[21] G. Fuhr, A. Voigt, T. Muller, B. Wagner, K. Reimer, T. Lisec, Electric-Field-Mediated Inhibition of Cell and Microparticle Adhesion - a New Way to Create Bio-Repellent Surfaces, Sensor Actuat B-Chem, 27 (1995) 468-470.

[22] L. De La Fuente, E. Montanes, Y. Meng, Y. Li, T.J. Burr, H.C. Hoch, M. Wu, Assessing adhesion forces of type I and type IV pili of Xylella fastidiosa bacteria by use of a microfluidic flow chamber, Appl Environ Microbiol, 73 (2007) 2690-2696.

[23] Y.J. Eun, D.B. Weibel, Fabrication of microbial biofilm arrays by geometric control of cell adhesion, Langmuir, 25 (2009) 4643-4654.

[24] M.M.C. Velraeds, B. Van De Belt-Gritter, H.C. Van Der Mei, G. Reid, H.J. Busscher, Interference in Initial Adhesion of Uropathogenic Bacteria and Yeasts to Silicone Rubber by A Lactobacillus Acidophilus Biosurfactant, Journal of Medical Microbiology, 47 (1998) 1081-1085.

[25] Y. Liu, J.-C. Wang, L. Ren, Q. Tu, W.-M. Liu, X.-Q. Wang, R. Liu, Y.-R. Zhang, J.-Y. Wang, Microfluidics-based assay on the effects of microenvironmental

geometry and aqueous flow on bacterial adhesion behaviors, Journal of Pharmaceutical Analysis, 1 (2011) 175-183.

[26] B.P. Leonard, A stable and accurate convective modelling procedure based on quadratic upstream interpolation, Computer methods in applied mechanics and engineering, 19 (1979) 59-98.

Chapter 6

Biological fouling and cleaning in microchannels: The antibiotic effect

Abstract

Fouling is a major problem recently acknowledged in microfluidic devices used in biomedical field. The major problems encountered in miniaturized biomedical devices can be reduced and handled with appropriate cleaning strategies. Cleaning at the very early stage will increase the life of microfluidic devices. The present study assesses the cleaning rate of two antibiotics (ampicillin and ciprofloxacin) in citrate buffer. Rectangular polydimethylsiloxane microchannels were fouled for 150 minutes at normal body temperature. The fouling rate was found to be constant for all the trial attempts. The cleaning rate differed for the control (citrate buffer) and the two antibiotics tested. The fouling and cleaning process over time was visualized by microscopy and cell viability was assessed by colony plating. Ampicillin treatment was able to remove 50.9% of adhered cells whereas ciprofloxacin removed around 56.3%.

6.1 Introduction

The different implants in humans such as catheters, stents or nasolaryngeal tubes need to be replaced due to infection that causes inflammation and pain[1]. Bjarnsholt et al. [1] has tabulated in detail the different imaging techniques of biofilm aggregates that can be used to identify infections. In reality, cells adhere and develop as biofilms by adapting themselves to *in vivo* and *in vitro* environments [2]. Numerous studies based on infections associated with different foreign bodies are reported as follows. Engelsman et al. [3] have reported bacterial infections in monofilament and

multifilament meshes that are used in abdominal wall repair; Jacobsen et al. [4] studied catheter associated infections caused by *E. coli* and *Proteus mirabilis*. An *in vivo* study on the adhesion of *staphylococcus* to orthopaedic metals was made by Sheehan et al. [5] where it was reported that, sometimes, the antibiotic treatment is unable to eliminate the biofilm because this contains a polymer matrix (with polysaccharides, DNA and proteins) that helps its own sustention on the substrate surface. Antibiotic penetration inside this matrix is sometimes prevented and so bacteria residing in the inner layers of the biofilm remain viable, whereas only those forming the top layer are affected. Niles et al. [6] reported a detailed review on antibiotic resistance of different bacterial biofilms. They have listed strategies to increase biofilm susceptibility to antibiotics. Shlaes and Spellberg [7] have reviewed the medical need for new therapies together with the challenges for new antibacterial development and the complications in the clinical utility of newly developed drugs.

Although both, *in vitro* and *in vivo* model systems, have been developed to study biofilm formation, bacterial adhesion studies in microchannels are rare. A detailed review on different biofilm model systems (*in vitro and in vivo*) was reported by Coenye and Nelis [8]. Non-destructive and real-time biofilm monitoring systems are particularly suited for this task since adhesion can be readily imaged by microscopy. This latest technique was adopted in our microfluidic system to understand initial adhesion and detachment. A review on visualization of adherent microorganisms using different techniques throws light on recent advancements [9]. Similar to the current study, Peng Sun et al. [10] have studied a long-term bacterial colony monitoring with high-throughput and antibiotic testing on the bacterial colony in zero-flow environments with a microfluidic system. They observed that tetracycline and erythromycin treatments cause significant morphological changes in *E. coli*. Detachment of various cells from four types of modified microchannel surfaces with a pre-defined range of wall shear stresses was investigated using lab-on-a-chip systems by Zhang et al. [11].

There is also an increased usage of microfluidic devices in the biomedical field for research studies, for testing and treatment. Microchannels are particularly suitable for wall shear stress dependent experiments as they can operate in a wide range of

conditions. The biofilm forms in any place where there is moisture and nutrients. Considering microfluidic devices and any implants, *in vivo* biofilms develop in due course of time starting with the adhesion of a single cell. Bjarnsholt [12] has explained the biofilm formation with the paradigm 'united we stand – divided we fall' in a simplistic way making it clear that when the cells are alone in a site, they would not flourish as a biofilm due to many external agents, but if they form a community and stand united in a single place as a biofilm, it is difficult for the external agents to eliminate all the cells. Thus to efficiently control biofilm development, it is often more effective to attack the biofilm at its early stages of development, as cells are more likely to be susceptible to the antibiotic effect. This concept is used in the current chapter.

In this chapter two antibiotics, ampicillin and ciprofloxacin [13], were dissolved in citrate buffer and used as cleaning agents. The rationale for choosing these antibiotics is that they are prescribed to treat gonorrhoea, pneumonia, bronchitis, typhoid fever, and many other diseases. *E. coli* is responsible for up to 70% to 80% of the urinary tract infections (UTI) [14]. Most commonly ampicillin is prescribed for urine infection and ciprofloxacin is prescribed for complicated UTIs [15]. The susceptibility to ciprofloxacin is usually higher when compared to ampicillin [16]. Ampicillin inactivates the repair and synthesis of the *E. coli* wall [17]. Ciprofloxacin inhibits DNA gyrase and topoisomerase, which are responsible for *E. coli* division[18].

6.2 Materials and Methods

6.2.1 Experimental

Microchannels

A Y-shaped microchannel was used for the experiments described in this chapter. The soft lithography technique was used to obtain the microchannels, as described in chapter 3, section 3.2.2. The schematic of the Y channel is shown in Figure 6.1. The width of the microchannel is 450 μm and the height 100 μm. Two inlets were employed, with one inlet for the cell assay and the other for the antibiotic. The outlet

was used to collect the sample for cell viability tests. The inlet port A was connected to a syringe containing the *E. coli* suspension and the inlet port B to a syringe containing the cleaning solution.

In the beginning of the experiment, the inlet B was closed and the syringe pump with cells was operated at a flowrate of 1.95 µL/min generating a wall shear stress of 0.03 Pa. The fouling experiment was imaged for 150 minutes, after which the inlet port A was closed. Then, the syringe pump containing the antibiotic was operated for remaining an additional 150 minutes to evaluate the cleaning of the imaged area. Although the microchannel has a longer upstream section, only a small section can be imaged with the microscope. Both the fouling rate and the cleaning rate for the whole microchannel were determined from the number of cells adhered on the surface along time through the Image J software. The observation window location is shown on Figure. 6.1.

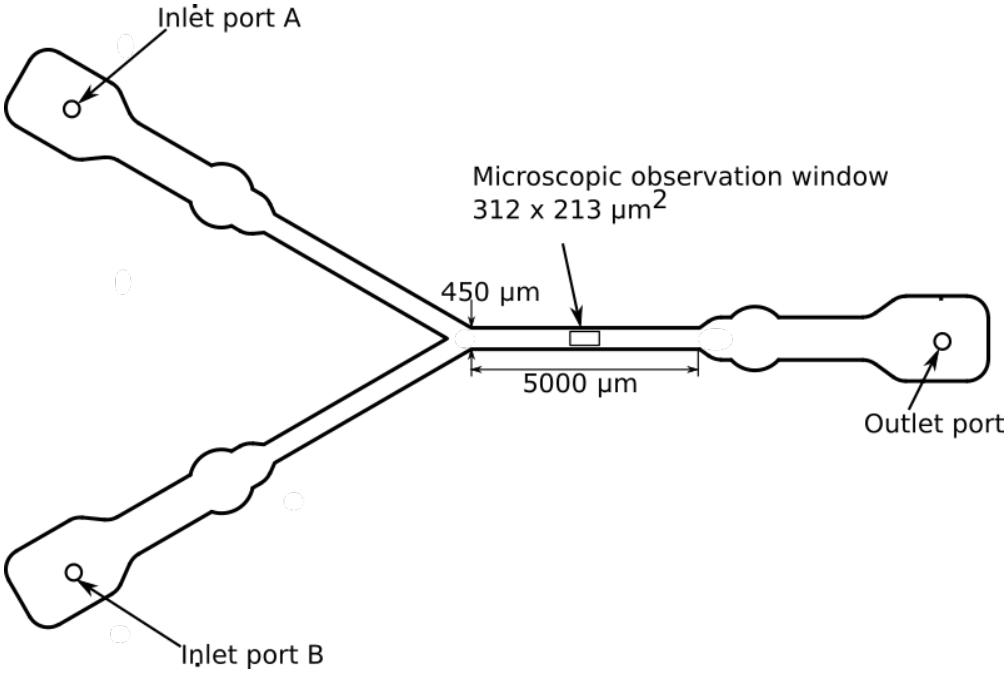

Figure 6.1. Schematic representation of the Y channel used for determining the fouling and cleaning rates.

6.2.1.1 Antibiotic preparation

The antibiotics were prepared as described by Gomes et al. [16] but higher concentrations were used in order to obtain a faster kinetic profile. For this work, ampicillin and ciprofloxacin solutions were obtained by diluting the chemicals in citrate buffer to a final concentration of 1.6 μg/ml for ampicillin and 1000 μg/ml for ciprofloxacin. The composition of citrate buffer was 0.05 mol L^{-1} with a pH of 5.0.

6.2.1.2 Microscopic visualization

The microchannels were fouled with *E. coli* cells by continuously feeding the cell suspension to the microchannel with a syringe pump (Cetoni, neMESYS syringe pump). The initial adhesion experiment was carried out at 37 °C to represent the normal body temperature. The cell suspension was prepared in citrate buffer at a concentration of $7.6x10^7$ cell.mL^{-1}. A section of the microchannel was imaged for 2.5 hours during fouling as shown in Figure 6.1. The cells were counted for each captured image with image J software.

Cell adhesion to the surface of the microchannel was recorded by imaging a small cross-section of surface area 312 × 233 μm^2 using a Leica microscope (DMI 5000M, Leica Microsystems GmbH). In this study, a magnification of 40X was used to visualize the *E. coli* cells. With this particular magnification, the counting of the adhered cells, either manually as with image analysis software (Image J), was performed. Adhesion was captured at time intervals of 30 mins for 150 mins and detachment phenomenon was also similarly captured at the same time interval of 30 mins for 150 mins.

6.2.2 CFU plate counting method

The CFU (Colony-forming unit) plate counting method is a technique where the viable bacteria are enumerated by counting the number of colony forming units on a

plate. The colony is formed from a group of *E. coli* cells and not from individual cells under constant maintained conditions such as nutrient, temperature of 37 ºC is maintained and 24 hour of incubation time. The microscopic slide containing the channel was resuspended in NaCl, which has molar concentration of 0.145 M and pH of between 5-7. A dilution of the sample is done to a proper bacterial concentration in order to originate 20 – 200 colony forming units per plate on solid growth medium Plate Count Agar (PCA; Merck, Portugal). 100 µL samples were taken to assess cultivability, by planting the dilutions in agar plates. Plates were incubated at 37 ºC for 24 hours. The real viable cell count was deduced with its dilution factor. The final values were expressed in percentage of cell viability. The cells were counted with programmable MATLAB, Image J and CellProfiler free software. Three independent trials were made with mean variations of 6 - 18 %.

6.3 Results and discussion

6.3.1 Fouling and cleaning analysis

Preliminary experiments were conducted in a 450 µm wide microchannel where fouling curves were obtained for wall shear stresses ranging from 0.01 Pa to 2 Pa. The image in Figure 6.2 is a tiff image obtained at the 150^{th} min. The Image J software was used and the cell number was evaluated as described in chapter 3 section 3.5. For clarity, a single cell is highlighted in the image (Figure 6.2). The total number of cells in the image (Figure 6.2) is 1.5×10^6 cells/cm^2.

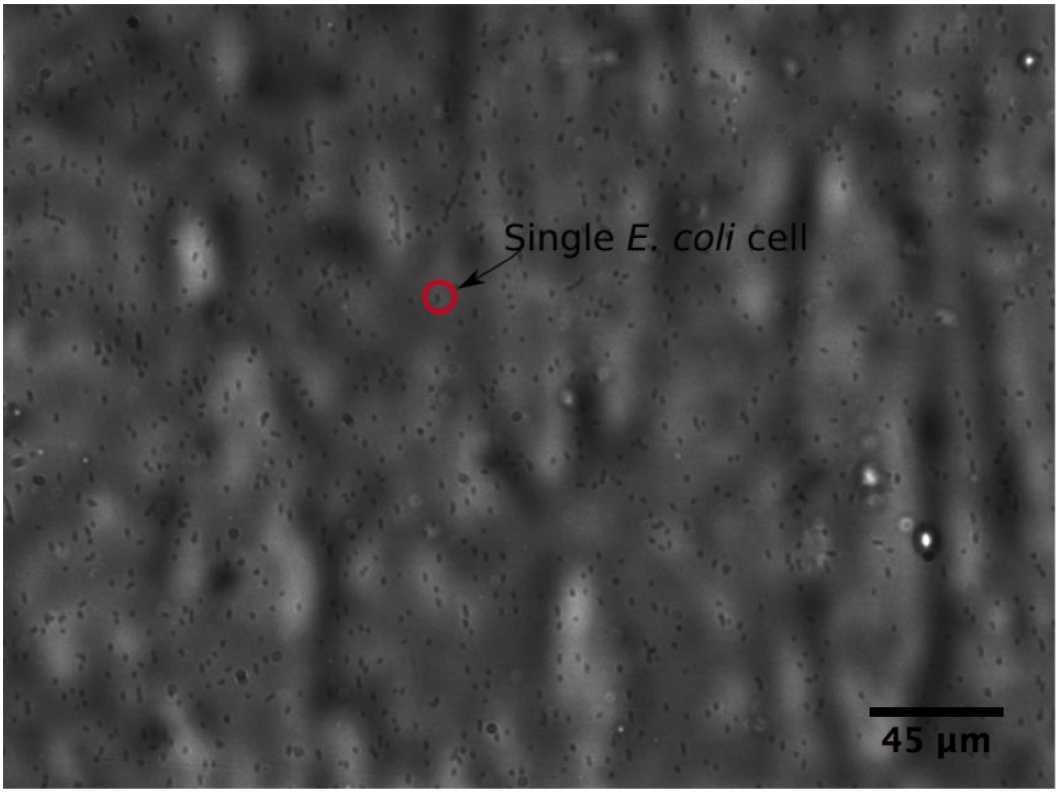

Figure 6.2 Visualization of the fouled microchannel with *E. coli* bacteria after 2.5 hours from the beginning of fouling.

The adhesion and removal of *E. coli* with ciprofloxacin at different times is shown in Figure 6.3 and Figure 6.4, with the corresponding cell count per unit area. At t=0 already some cells are observed adhered to the surface (1.6×10^5 No. of cells/cm^2) but this number increases up to 8 fold during the fouling period. At t = 150 min, the antibiotic ciprofloxacin was introduced and substantial cell removal occurs after the 150 minutes of cleaning time. The cell number decreased by 56.3%.

Time (min)	Image	No.cells/cm^2
0	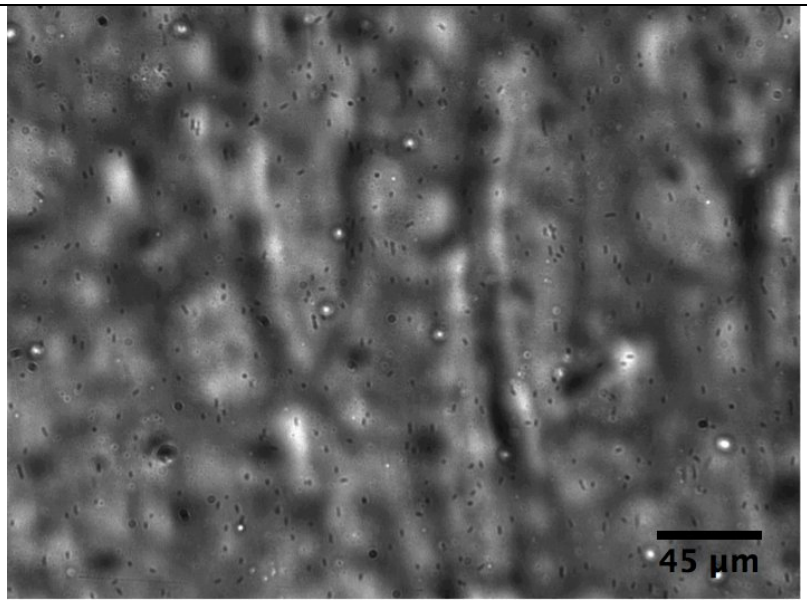	1.6×10^5
60	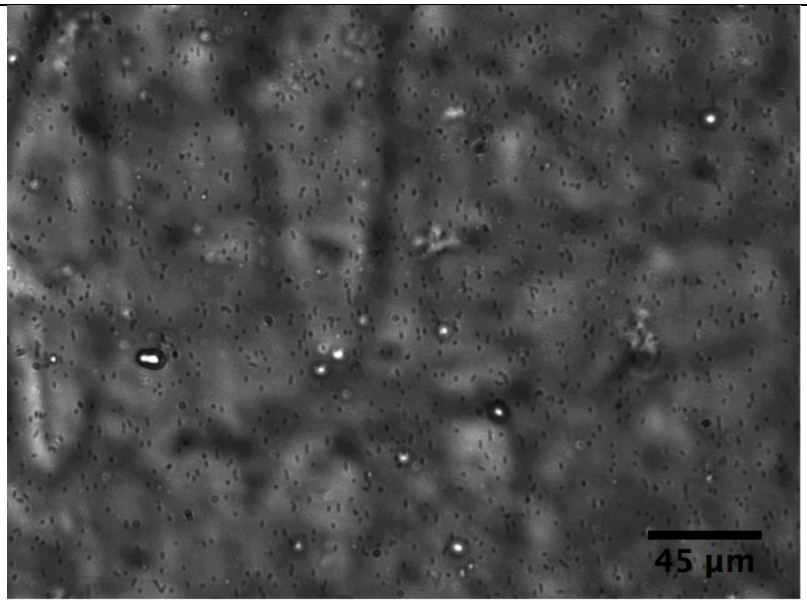	9.8×10^5

Figure 6.3. Microscopic images of the Y –shaped microchannel shown in Figure 6.1 at different times when ciprofloxacin antibiotic was used, with corresponding cell count by Image J software.

240	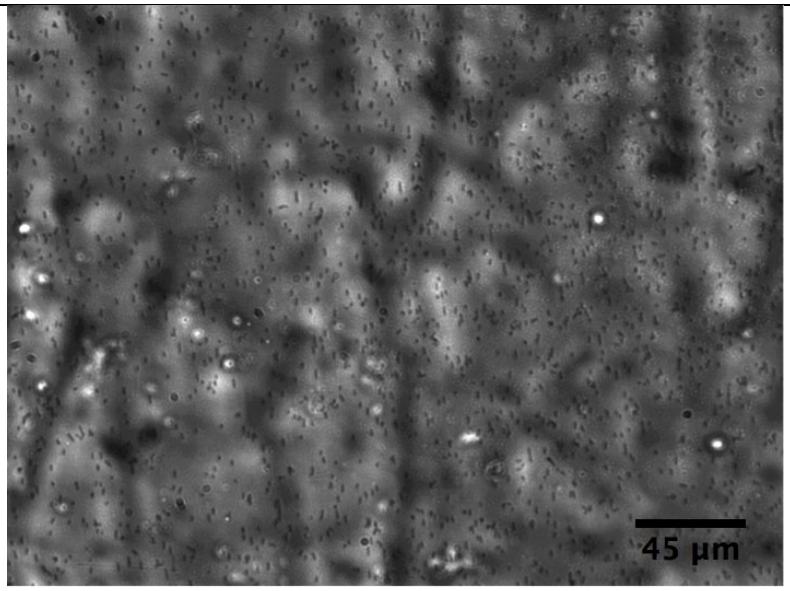	9.6×10^5
300	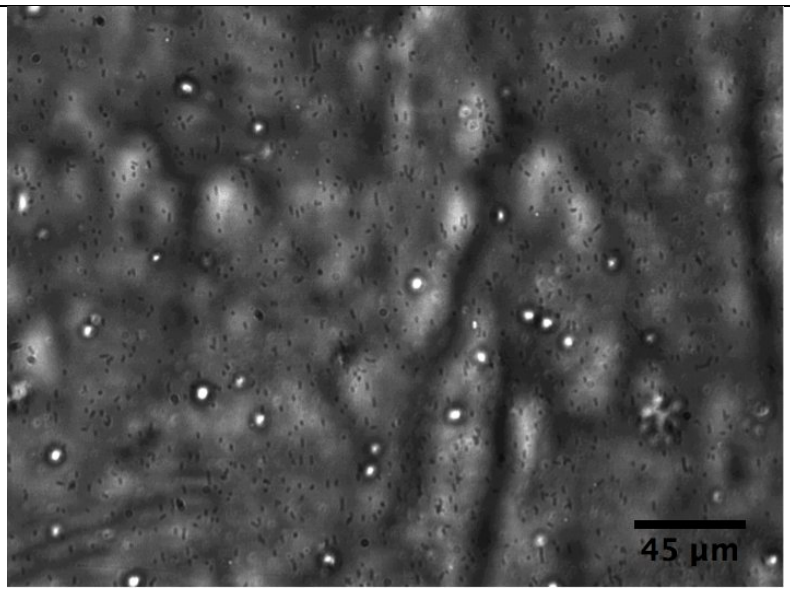	7.5×10^5

Figure 6.4. Continuation of Microscopic images of the Y –shaped microchannel shown in Figure 6.1 at different times when ciprofloxacin antibiotic was used, with corresponding cell count by Image J software.

In order to ascertain if the cell removal observed in the previous experiment was partially due to the wall shear stress effect and not only to the antibiotic effect, a control experiment was performed in which the fouling period was maintained and no antibiotic was introduced in the cleaning phase (only citrate buffer was flowing at the same flow rate). The results of this study are shown in Figure 6.5. This assay

demonstrates that the wall shear stress alone (without the antibiotic addition) is responsible for 6.5 % of cell removal at the end of 150th minute, an insignificant reduction. Here the plot shows fouling and cleaning obtained at a constant wall shear stress of 0.03 Pa. Three independent trials were made to assure repeatability. The images were recorded automatically or manually at 30 min intervals for 5 hours of experiment.

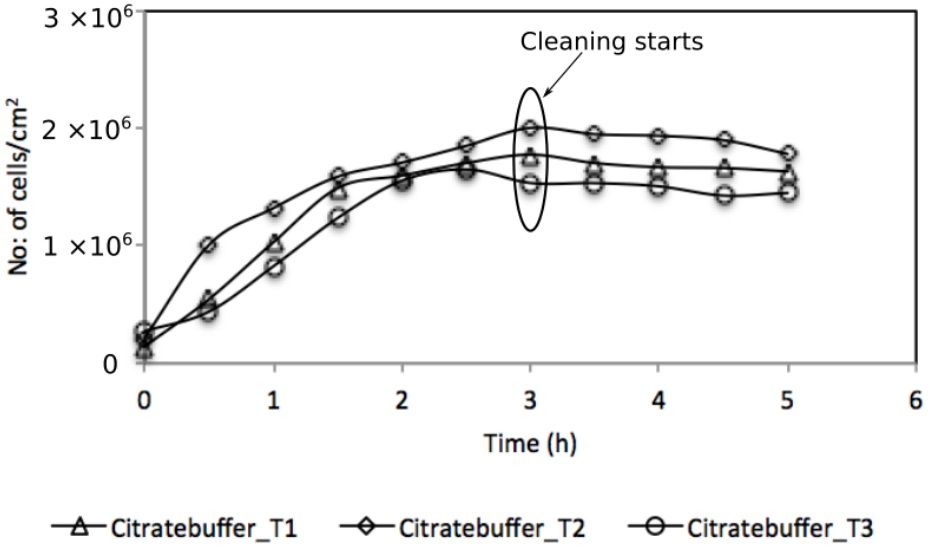

Figure 6.5. Plot showing cell adhesion and cleaning with citrate buffer alone. Experiments were conducted at a wall shear stress of 0.03 Pa.

Figure 6.6 shows that ampicillin has faster cell removal kinetics, although the final results obtained with both antibiotics were not statistically different. Ampicillin accounted to 51% of cell removal and ciprofloxacin around 45%. From the experimental setup that was used on this work it is not clear if these detached cells were viable or non-viable. Little modification in the collecting procedure while the removal of the cell takes place during the cleaning process is missed in the experimental set up, so it was not possible to be analysed for the percentage of dead and live cells with the current experimental set up.

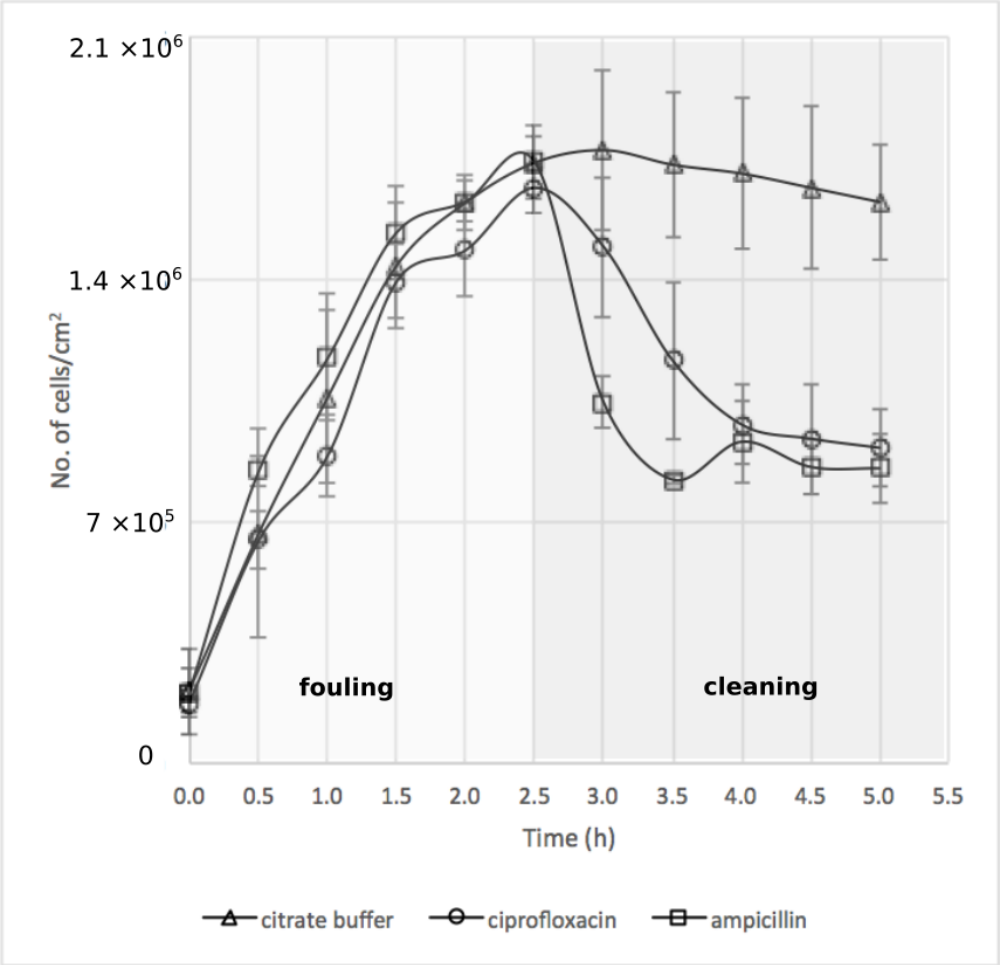

Figure 6.6. Plot showing the number of adhered cells per unit area. Results are an average of three independent experiments. Standard deviation between the individual assays is indicated with error bars.

6.3.2 Cell viability analysis.

After analysing the cell removal, the viability of the cells that remained attached was assessed by plate counting with CFU plate counting method as explained in section 6.2.2 of this chapter. There is a significant difference between cell killing and removal performances. For ciprofloxacin, the percentage of dead cells still adhered was 7% while 45 % of cells were removed. For ampicillin, 14% of adhered cells were dead while 51% of cells were removed (Figure 6.7). The experimental protocol that was used did not allow for the evaluation of the killing efficiency of the removed cells (only cells that remained attached were analysed) and therefore it is possible that the

overall killing efficiency of these antibiotics is much higher than reported. This may explain the apparently higher killing efficiency observed for ampicillin in this work which is not consistent with previous works using this strain and antibiotics [16].

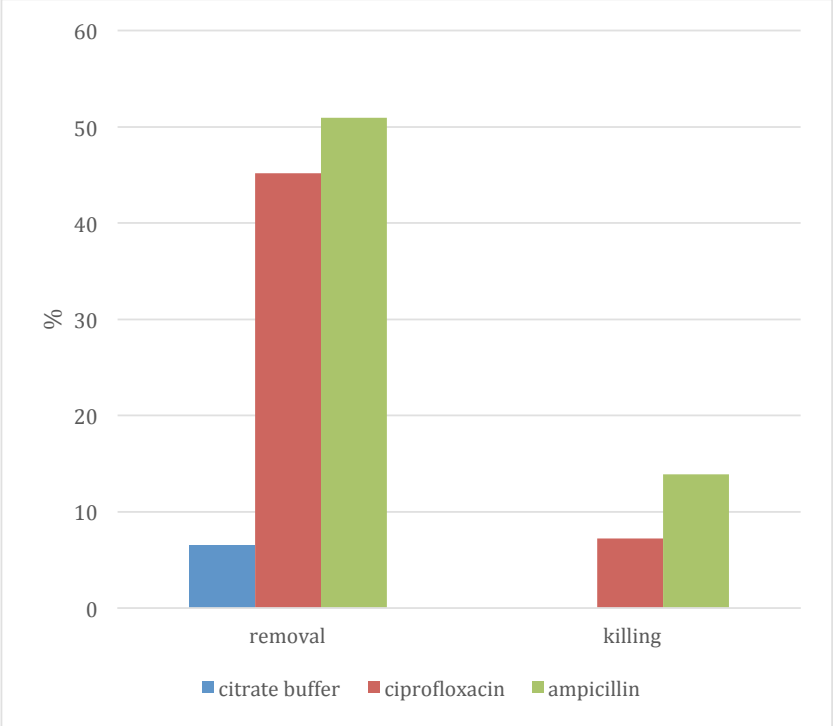

Figure 6.7. Plot showing percentage of cell removal in microchannel and number of cells killed (by CFU plate count method) at the end of 2.5 hours in microchannel.

6.4 Conclusions and future work

This work has shown that biofilm development can be slowed down considerably when the system is subjected to early cleaning procedures. This is due to the fact that 50% of the adhered cells were removed and were therefore precluded to continue their development into a growing biofilm. Using antibiotics as cleaning agents under these conditions is however not advisable since the percentage of killed cells remaining attached is very low. Thus, the development of resistant phenotypes is potentiated which is likely to render the cleaning procedure ineffective.

A detailed study on the removed cells is needed. This is for understanding whether dead cells alone detach from the surface or if both viable and non-viable cells are equally removed. The dynamics of cell detachment under different conditions can be further studied with different temperature range, with different antibiotics and a combination of antibiotics. The cleaning can be attempted at even higher shear stresses or antibiotic concentrations. The use of high wall shear stress can be utilized in cleaning biomedical microfluidic devices but, as far as implants are considered, other factors apart from shear stresses may have to be considered. Bjarnsholt et al. [1] has argued that *in vivo* and *in vitro* biofilms are not the same and the activity of tissue cells and the immune system further complicated this analysis.

References

[1] T. Bjarnsholt, M. Alhede, M. Alhede, S.R. Eickhardt-Sorensen, C. Moser, M. Kuhl, P.O. Jensen, N. Hoiby, The in vivo biofilm, Trends Microbiol, 21 (2013) 466-474.

[2] P. Stoodley, L. Hall-Stoodley, B. Costerton, P. DeMeo, M. Shirtliff, E. Gawalt, S. Kathju, 5 - Biofilms, Biomaterials, and Device-Related Infections, in: K.M. Ebnesajjad (Ed.) Handbook of Polymer Applications in Medicine and Medical Devices, William Andrew Publishing, Oxford, 2013, pp. 77-101.

[3] A.F. Engelsman, G.M. van Dam, H.C. van der Mei, H.J. Busscher, R.J. Ploeg, In Vivo Evaluation of Bacterial Infection Involving Morphologically Different Surgical Meshes, Annals of Surgery, 251 (2010) 133-137 110.1097/SLA.1090b1013e3181b1061d1099a.

[4] S.M. Jacobsen, D.J. Stickler, H.L. Mobley, M.E. Shirtliff, Complicated catheter-associated urinary tract infections due to Escherichia coli and Proteus mirabilis, Clin Microbiol Rev, 21 (2008) 26-59.

[5] E. Sheehan, J. McKenna, K.J. Mulhall, P. Marks, D. McCormack, Adhesion of Staphylococcus to orthopaedic metals, an in vivo study, Journal of Orthopaedic Research, 22 (2004) 39-43.

[6] N. Høiby, T. Bjarnsholt, M. Givskov, S. Molin, O. Ciofu, Antibiotic resistance of bacterial biofilms, International Journal of Antimicrobial Agents, 35 (2010) 322-332.

[7] D.M. Shlaes, B. Spellberg, Overcoming the challenges to developing new antibiotics, Curr Opin Pharmacol, 12 (2012) 522-526.

[8] T. Coenye, H.J. Nelis, In vitro and in vivo model systems to study microbial biofilm formation, Journal of Microbiological Methods, 83 (2010) 89-105.

[9] C. Hannig, M. Follo, E. Hellwig, A. Al-Ahmad, Visualization of adherent micro-organisms using different techniques, Journal of Medical Microbiology, 59 (2010) 1-7.

[10] P. Sun, Y. Liu, J. Sha, Z. Zhang, Q. Tu, P. Chen, J. Wang, High-throughput microfluidic system for long-term bacterial colony monitoring and antibiotic testing in zero-flow environments, Biosensors and Bioelectronics, 26 (2011) 1993-1999.

[11] X. Zhang, P. Jones, S. Haswell, Attachment and detachment of living cells on modified microchannel surfaces in a microfluidic-based lab-on-a-chip system, Chemical Engineering Journal, 135 (2008) S82-S88.

[12] T. Bjarnsholt, The role of bacterial biofilms in chronic infections, APMIS, 121 (2013) 1-58.

[13] S. Krcmery, K.G. Naber, Ciprofloxacin once versus twice daily in the treatment of complicated urinary tract infections, International Journal of Antimicrobial Agents, 11 (1999) 133-138.

[14] J.C. Nickel, Urinary Tract Infections and Resistant Bacteria, in: Highlights of a Symposium at the Combined Meeting of the 25th International Congress of Chemotherapy (ICC) and the 17th European Congress of Clinical Microbiology and

Infectious Diseases (ECCMID), Reviews in Urology, Munich, Germany, 2007, pp. 78-80.

[15] D. Boy, M. Well, M. Kinzig-Schippers, F. Sorgel, D. Ankel-Fuchs, K.G. Naber, Urinary bactericidal activity, urinary excretion and plasma concentrations of gatifloxacin (400 mg) versus ciprofloxacin (500 mg) in healthy volunteers after a single oral dose, International Journal of Antimicrobial Agents, 23 (2004) S6-S16.

[16] L.C. Gomes, L.N. Silva, M. Simoes, L.F. Melo, F.J. Mergulhao, Escherichia coli adhesion, biofilm development and antibiotic susceptibility on biomedical materials, Journal of biomedical materials research. Part A, 103 (2015) 1414-1423.

[17] G.N. Rolinson, A.C. Macdonald, D.A. Wilson, Bactericidal action of beta-lactam antibiotics on Escherichia coli with particular reference to ampicillin and amoxycillin, 1977.

[18] M. LeBel, Ciprofloxacin: Chemistry, Mechanism of Action, Resistance, Antimicrobial Spectrum, Pharmacokinetics, Clinical Trials, and Adverse Reactions, Pharmacotherapy: The Journal of Human Pharmacology and Drug Therapy, 8 (1988) 3-30.

CHAPTER 7

Conclusions

The main objective of this thesis was the investigation of initial adhesion in microchannels to understand biofilm formation in biomedical devices and lab-on-chips. For this purpose, several aspects of cell adhesion in microfluidic devices were explored:

- The effect of wall shear stress on adhesion in a rectangular microdevice. This effect was assessed and compared in different size scales ;
- The effect of different polymeric surfaces on adhesion;
- The effect of the geometry in different geometrical configurations;
- Fouling and cleaning of microchannels to understand the killing and cleaning behavior of two antibiotics.

The main difficulty of studying adhesion in microchannel is the construction of the microdevice. Most of the research groups perform adhesion studies in macro devices. Microdevices, in spite of their advantages, are usually considered too expensive and they cannot be reused [1]. The fabrication process developed in this thesis has shown to be suitable for research work, circumventing some of the drawbacks. Low cost xurography method was used to make simple rectangular microchannels for biofouling study. Applying xurography, different microchannel geometries were easily prepared in short development cycles. A new fabricating technique was developed and validated to include a polymeric surface in a microfluidic chip, in order to understand adhesion on different polymers, which are used in diversified biomedical applications.

Applying the developed technique of microchannel fabrication, six different polymeric surfaces (Polyamide, Cellulose acetate, Polydimethylsiloxane, Poly L-Lactide, Polyethylene oxide, Polystyrene) along with glass were fabricated and placed in a microchannel to study the effect of different surfaces in the biofouling. The adhesion in identical surfaces was studied, at scaled hydrodynamic conditions, in a

macroscale device. According to the results, the adhesion is independent of the scale, if microchannels with at least with 100 μm of depth are used. Microchannels are then a good option to perform these studies, provided that expertise, equipment and resources are available.

The surfaces were tested for surface contact angle, zeta potential and adhesion phenomenon. A general correlation between material surface properties (hydrophobicity and zeta potential) and *E. coli* adhesion rates was not found. The cell adhesion studies showed, however, the way to determine the adhesion rate in the surface employed in any microsystem device. Knowing the adhesion rate may be helpful to decide when medical disposables need replacement.

To study the effect of wall shear stress on biofouling, wall shear stresses, which exist in the human body, from blood vessels and capillaries to urinary catheters, were selected (0.01 to 2 Pa). Adhesion changes significantly as wall shear stress increases. High adhesion rates are observed in the low wall shear stress region, 0.01 to 0.3 Pa. As the wall shear stress increases, up to 0.5 Pa, the adhesion rate decreases abruptly. At 2 Pa the adhesion rate is extremely low.

Fouling is inevitable in microsystems, especially in constrictions as it is clearly evident in many lab-on-chip devices, biosensors, and point of care diagnostic devices. Constrictions were appended to different microchannel geometries and studied for adhesion phenomenon in the range of wall shear stress from 0.2 to 1 Pa. In the three sets of microchannel geometries with constrictions studied, the adhesion pattern was similar. The results showed also that the cell adhesion can be controlled (rate and place of deposition) by manipulating the geometry of the microchannel and, by consequence the wall shear stress, with implications in different biomedical applications.

Apart from microsystems, there are different types of implants, made with different materials for the human body, which are susceptible to infections. Two common antibiotics, ampicillin and ciprofloxacin, were selected and tested against *E. coli*. The cleaning rate differed for the two antibiotics tested. Ampicillin removed to 51% of cells and ciprofloxacin around 45%. The percentage of dead cells remaining adhered

to the microchannel was 14% and 7% for ampicillin and ciprofloxacin respectively. In summary, the biofilm development can be considerably slowed down, when the microfluidic system is subjected to early cleaning procedures.

These findings will be synthesized to answer, fully or partially, to the research questions highlighted in the first chapter,

a. The results obtained showed that adhesion phenomenon decreases when the WSS increases, except in a particular range of low WSS;
b. When similar wall shear stresses are used in both scales, macro and micro, similar adhesion rates were obtained whatever the surface is;
c. Almost 50% of adhered cells were removed with antibiotics at a low wall shear stress of 0.03 Pa and were therefore precluded to continue their development into a growing biofilm.

This work can be used as a strategic cue for avoiding, reducing or delaying adhesion by varying the material of the surface, geometry, wall shear stress and cleaning agents, according to the requirements of different applications. The work done investigating the initial step of adhesion on a clean surface will contribute to future findings.

References

[1] P.M. Valencia, O.C. Farokhzad, R. Karnik, R. Langer, Microfluidic technologies for accelerating the clinical translation of nanoparticles, Nature nanotechnology, 7 (2012) 623-629.

CHAPTER 8

Future work

Microfluidics was given importance from 1980's as the demand for microsystems increased due to the onset of new fabrication techniques. The scope related to fouling research will never slow down, as there are always innovations in fields related to chemical, biological, mechanical and electronics engineering, like Micro Electro-Mechanical Systems (MEMS), Lab on Chip Devices (LOC), Point of Care Systems (POC). Just like computers, cars, mobile phones were invented, people never thought of having it for their own personal use., ,microsystems and microfluidics will find space to entry in almost all walks of life to make it easier. All the applications will have fouling as a major daunting problem. As till now, fouling will affect sensitivity, durability and reproducibilityof the equipment bothering.

The experimental results obtained in this investigation concerning biofouling in microchannels touched different effects - wall shear stress, surface properties of the surface and geometry provided valuable data and understanding that can be used as standard for future works. The results of cleaning of biofouled microchannel using ampicillin and ciprofloxacin can be used as a first step to make a deeper and broad develop cleaning strategies.study.

Follow-up biofouling works in microchannels should be performed:

- Studies with different microorganisms to find their adhesion behaviour, like was done for *E. coli*. This would help to understand how different diseases causing by cells adhesion to the substrate start and develop at different conditions.
- The microfabrication work needs to be concentrated in the way to incorporate more polymeric surfaces for the biofouling studies. New techniques have to be

developed to have a polymeric surface through the entire length of the microchannel.

- Further work must be carried out to deeply understand the similarity between the biofouling results in micro and macro scales. The comparison should be extended to different surfaces, wall shear stresses and temperatures.
- Three types of geometries were studied in chapter 5 and to draw a general conclusion was difficult to state. So, new microchannel geometries have to be studied using a large range of wall shear stress to understand cell adhesion. Multiple parallel microchannels of uniform width and also with different width and different depth should be carried to the research, to improve the knowledge on biofouling: the study based on different geometric effects.
- The cleaning of microchannels study has to be extended to understand the roles of the wall shear stress and of the antibiotics in the detachment process. This work has to be extended to different antibiotics and the antibiotic cleaning effect should be analysed must be tested in different surfaces, important variables in cleaning and disinfection.
- The biofouling should be studied changing the depth of the microchannel. This would develop to an interesting study about how the aspect ratio of the microchannel could be changed according to the aspect ratio of the microorganism.
- Further, the alignment of the cells that are adhered in a straight microchannel needs to be studied with respect to different wall shear stresses, to investigate the growth factor of aligned cells in a new implant embedded in the body. This type of study will help in understanding the diseased cell growth and alignment.